THICKNESS DEPENDENT PHYSICAL AGING AND SUPERCRITICAL CARBON DIOXIDE CONDITIONING EFFECTS ON CROSSLINKABLE POLYIMIDE MEMBRANES FOR NATURAL GAS PURIFICATION

A Dissertation
Presented to
The Academic Faculty

By

Adam Michal Kratochvil

In Partial Fulfillment
Of the Requirements for the Degree
Doctor of Philosophy in
Chemical & Biomolecular Engineering

Georgia Institute of Technology

August 2008

THICKNESS DEPENDENT PHYSICAL AGING AND SUPERCRITICAL CARBON DIOXIDE CONDITIONING EFFECTS ON CROSSLINKABLE POLYIMIDE MEMBRANES FOR NATURAL GAS PURIFICATION

Approved by:

Dr. William J Koros, Advisor
School of Chemical & Biomolecular Engineering
Georgia Institute of Technology

Dr. J. Carson Meredith
School of Chemical & Biomolecular Engineering
Georgia Institute of Technology

Dr. Charles A Eckert
School of Chemical & Biomolecular Engineering
Georgia Institute of Technology

Dr. Haskell W Beckham
School of Polymer, Textile, & Fiber Engineering
Georgia Institute of Technology

Dr. Clifford L Henderson
School of Chemical & Biomolecular Engineering
Georgia Institute of Technology

Date Approved: April 10, 2008

DEDICATION

To Kelly And My Family

Thank You For Your Prayer, Encouragement, And Patience

ACKNOWLEDGEMENTS

I would like to thank Dr. William Koros for all of his time, advisement, and encouragement throughout the many years I have been a part of his research group. He has an incredible ability to recognize and develop the potential within students, and I am forever grateful for the opportunity to return to school under his tutelage to pursue a career in research. His excitement and approach to these projects made them enjoyable, and I appreciate that he never made these years feel like "work".

One of the great things about exploring science at a university is the breadth of knowledge of the people. I'd like to thank the members of my committee, Dr. Haskell Beckham, Dr. Cliff Henderson, Dr. Carson Meredith, and Dr. Charles Eckert, for their time and insight on numerous problems over the years.

To everyone in the Koros group, past and present, you have been wonderful to work with and I've greatly enjoyed our time together. I appreciate all of your help over the last five years. So many people have helped out with late night valve turning and weekend pump refills that I can't even remember who to thank…so thank you all. Thank you to Dr. De Vu, Dr. Shilpa Damle-Mogri, Dr. Ted Moore, and Dr. John Perry for teaching me the tricks of the trade. Also, part of what made this work so much fun was the conversation and discussion with my office mates whom I'd like to acknowledge, Dr. Raymond Chafin, Dr. Shu Shu, Dr. John Perry, and (the future Dr.) Ryan Adams. Finally, behind the scenes, Michelle Martin is instrumental in making this group function, and I greatly appreciate all her help over the years.

I'd like to acknowledge and thank the students in other research groups who have helped me obtain the various measurements needed for this thesis. Matija Crne for help with fluorescence spectroscopy, Sunghyun Nam for help with in-situ IR, and Carsten Sievers for help with solid-state NMR.

I don’t think words can express how thankful I am to my family for everything they have provided to allow me to reach this point. Whether it was words of encouragement, a lunchtime conversation, or a plane ticket to visit, they have always been supportive of my time back at school, and I’m forever grateful for them.

None of this would have been possible without the unwavering support, encouragement, and understanding of my wife, Kelly. She endured many weekend trips to the lab, late nights of work, missed vacations and holidays, and the general annoyance of failing experiments. I’m still amazed how she willingly came to school with me at night and on weekends, and always with a smile. Thank you.

All praise be to the Father, from whom all blessings flow.

TABLE OF CONTENTS

LIST OF TABLES

LIST OF FIGURES

SUMMARY

Membrane separations are rapidly growing alternatives to traditionally expensive gas separation processes. For natural gas purification, membranes are used to remove carbon dioxide to prevent pipeline corrosion and increase the heating value of the natural gas. The robust chemical and physical properties of polyimide membranes make them ideal for the numerous components and high pressures associated with natural gas production. Typically, the performance of membranes changes over time as a result of physical aging of the polymer. Previous work shows that the thin selective layer of an asymmetric hollow fiber membrane, the morphology of choice for gas separations, ages differently than a thick dense film of the same material. Also, carbon dioxide, which is highly soluble in most polymers, can actively swell and plasticize polymer membranes at higher pressures. In this work, free acid groups present in the model polyimide are covalently crosslinked to stabilize the matrix against plasticization.

Physical aging of two different crosslinked derivatives are compared to the free acid polyimide through gas permeation, gas sorption, and refractive index measurements. Thick (~50 μm) and thin (~650 nm) films are examined to determine the effects of sample dimension on physical aging. The crosslinking mechanism employs diol substituents to form ester linkages through the free acid group. However, the annealing treatment, above the glass transition temperature, used to "reset" the thermal history of the films is found to form a new crosslinked polymer. Characterization of this new crosslinking mechanism reveals a high-temperature decarboxylation of the free acid creates free-radical phenyl groups which form covalent crosslinks through other portions of the polymer structure. Since ester crosslinks may be vulnerable to hydrolysis in

aggressive gas feed streams, this new mechanism of crosslinking may create a more robust membrane for aggressive separations.

In addition to the physical aging study, supercritical carbon dioxide conditioning of the two glycol crosslinked polyimides is compared to the free acid polymer. In this case, the free acid polymer is not crosslinked since the esterification crosslinking reaction occurs at much lower temperature than the decarboxylation mechanism. The free acid polymer displays an atypical permeation response under supercritical carbon dioxide conditions which suggests a structural reorganization of the polymer occurs. The crosslinked polymers do not exhibit this type of response. Mixed gas permeation confirms a substantial decrease in the productivity of the free acid polyimide and reveals the enhanced stability of the crosslinked polyimides following the supercritical carbon dioxide conditioning.

Finally, examination of structurally similar fluorine-containing polyimides following approximately 18 years of aging allows the study of polymer structure on physical aging. A 6FDA-based polyimide is compared to a BPDA-based polyimide to understand the effects of bulky, CF_3 groups on physical aging, and polyimides with diamine isomers reveal the effects of structural symmetry on physical aging.

1.0 INTRODUCTION

1.1 Polymer Membranes for Gas Separations

Polymer membranes have been in use for nearly four decades performing a wide variety of separations through reverse osmosis, gas permeation, and vapor permeation processes. These membrane separation processes offer attractive alternatives to many conventional approaches which tend to be energy intensive and much more complex. Glassy polymers have been the preferred medium of membranes in these areas due to their ease of manufacture, low cost, and durability while maintaining their separation efficiency over long periods of time.

One of the fastest growing areas of membrane use is in gas separations which rely almost entirely on traditional, thermal-based applications such as cryogenic distillation and chemical absorption. These processes tend to have high capital and operating costs, large equipment footprints, and in some cases use chemicals that can be detrimental to the environment. The current major membrane applications in the gas separations sector includes nitrogen purification, carbon dioxide removal from natural gas, hydrogen recovery, and air and natural gas dehydration. The membrane market for these separations has increased from $20 million in 1986 to $150 million in 2000, and is projected to reach $760 million in 2020 [1, 2]. As material development of robust glassy polymers progresses, membranes will continue to assume a larger role in the separation of aggressive feed streams. In fact, membrane system sales for the removal of carbon dioxide from natural gas are expected to more than triple from $30 million/year in 2000 to $100 million/year in 2020 [3].

1.2 Natural Gas Purification

The United States produces about 20 trillion scf/year of natural gas which generates more than $100 billion annually in sales [4]. According to the most recent International Energy Outlook, natural gas is the fastest growing energy source and worldwide consumption is expected to increase 92% by 2030 [5]. However, nearly all natural gas production requires some type of treatment to reduce contaminants [4]. The most abundant contaminant, carbon dioxide, has typical concentrations in subquality natural gas between 5-25%, while some reservoirs contain much higher concentrations [6, 7]. In order to meet pipeline specifications for transport and minimize pipeline corrosion, the carbon dioxide concentration must be reduced to less than 2% [7]. Other applications within the natural gas separations industry involving the removal of carbon dioxide include recovery and recycle of carbon dioxide in enhanced oil/gas recovery, recovery of methane from landfills and biogas, and recovery of carbon dioxide from flue gases [8].

The dominant process for carbon dioxide removal is amine absorption. As mentioned earlier, this thermally-driven process is expensive to install and operate and is permanent in that the equipment has a large footprint and is not scalable. The amines typically used become less efficient as carbon dioxide partial pressures increase; therefore, higher flow rates and/or larger equipment are required to maintain the separation which results in even higher costs. Also, the amines used for this process tend to be harmful to the environment and degrade in the presence of oxygen or when subjected to high temperatures, as found in the regeneration boiler, which can lead to corrosion of the equipment [9]. Membrane-based separation processes offer an attractive alternative to this traditional gas separation process at elevated pressures due to their relatively low capital and operational costs, portability, scalability, and

environmental security. In the natural gas separation industry, membrane units currently make up only 2% of all separations and are used almost entirely for carbon dioxide removal [4].

1.3 Supercritical Carbon Dioxide Separations

As the worldwide demand for natural gas continues to increase, the utilization of subquality and partially-depleted natural gas reservoirs becomes more important. Partially-depleted natural gas reservoirs are currently being investigated as potential sources for supercritical carbon dioxide ($scCO_2$) sequestration for two purposes. The first is to reduce the amount of carbon dioxide in the atmosphere which contributes to global warming. Second, repressurization of a reservoir through carbon dioxide injection enhances methane recovery. However, this process greatly increases the carbon dioxide content of the recovered natural gas [10, 11]. For each of the above scenarios, membrane separation processes again provide an attractive alternative to traditional absorption processes due to the high CO_2 content involved in the separation.

The use of $scCO_2$ as a tunable solvent also offers an environmentally safer and potentially cheaper option to typical organic solvents. Current studies using $scCO_2$ as a solvent include two and three phase catalytic reactions, polymerization reactions, and polymer processing [12]. However, in many of these processes the products (and/or byproducts) can only be removed through depressurization of the system which ultimately leads to expensive CO_2 recompression costs. In these processes, membranes provide an economical method to purify the CO_2 solvent while maintaining the high pressures required to keep it supercritical.

1.4 Research Objectives

Current industrial membrane separation units used for gas separations are comprised primarily of asymmetric hollow fiber membranes. Prior to installation and during operation, glassy polymer membranes tend to lose their productivity through a process known as physical aging. Simply stated, physical aging is a process through which polymers densify over time as a result of polymer chain relaxations. Most membrane research is conducted on thick (~25-50 μm) films; however, asymmetric hollow fibers consist of a thin (~100-200 nm) selective layer surrounding a thicker, porous support structure. Recent work has shown that aging is strongly affected by the sample dimension of the separating layer [13-15].

In natural gas separations, CO_2 is typically the highest concentration of contaminants. At high pressures, CO_2 tends to plasticize, or swell, polymer membranes which greatly diminishes the separating efficiency of the membrane. Due to their robust mechanical properties, high glass transition temperatures, and resistance to chemical breakdown, polyimides have shown promise as a membrane material for use in aggressive feed separations like this high CO_2 content application. Recent work demonstrates that crosslinking a polyimide membrane increases the pressure at which plasticization occurs, thus stabilizing the membrane at higher pressures of CO_2 [16-18]. Therefore, the first objective of this work is to determine the effects of sample dimension and crosslinking on physical aging for a state-of-the-art polyimide membrane.

Polyimides of many different dianhydride and diamine precursors have been studied extensively for gas separations in the last 15 to 20 years; however, there have been no long-term aging studies conducted to determine the effects these different precursors will have on membrane performance over time. The second objective, then,

is to determine the long-term physical aging effects on a series of fluorine containing polyimide membranes.

It is well known that subcritical carbon dioxide is a highly sorbing species and tends to plasticize glassy polymers, thus reducing the separating efficiency of the membrane [17, 19, 20]. However, few studies have been conducted to determine what effects $scCO_2$ conditioning has on polymer membrane performance. In fact, no studies exist that explore how $scCO_2$ affects high performance polymer membranes used in natural gas purification. It is clear that the use $scCO_2$ is becoming more prevalent and that polymer membranes can play an important role in the purification and re-use of CO_2 in the supercritical state. Therefore, the final objective of this study is to investigate the effects of $scCO_2$ conditioning on crosslinkable 6FDA-based polyimides.

1.5 Organization of Dissertation

Chapter 2 introduces the terminology, concepts, and models used for this work. A detailed history of previous work in these areas is also presented.

Chapter 3 presents the materials, equipment, and procedures for all of the work in this thesis. Secondary characterization techniques are also discussed.

Chapter 4 presents verification of the 6FDA-based, high performance polyimides and the effects of annealing these polyimides above the T_G. Thick and thin film gas permeation measurements to monitor physical aging are presented and discussed as well as various observations and phenomena pertaining to physical aging. Finally, refractive index measurements for the modeling of fractional free volume are presented.

Chapter 5 discusses the potential causes of the polymer insolubility and enhanced plasticization resistance when annealed above T_G for the physical aging measurements.

Chapter 6 presents the $scCO_2$ conditioning results of the 6FDA-based polyimides and discusses the impact this conditioning process exhibits on the natural gas separations.

Chapter 7 presents the long term physical aging performance of the fluorine-containing polyimides and discusses the impact different polymer backbone moieties have on the aging process.

Chapter 8 outlines the conclusions of this work and presents possible areas of future work.

1.6 References

1. Humphrey, Jimmy L. & Keller, George E., *Separation Process Technology*, New York: McGraw Hill (1997).
2. Baker, R. W., "Future directions of membrane gas separation technology", *Industrial & Engineering Chemistry Research*, **41**(6), 1393-1411 (2002).
3. Aresta, Michele, *Carbon Dioxide Recovery and Utilization*, Dordrecht: Kluwer Academic Publishers (2003).
4. Baker, Richard W., *Membrane Technology and Applications*, West Sussex: John Wiley & Sons (2004).
5. United States, Department of Energy, *International Energy Outlook 2006*, Energy Information Administration (2006).
6. Datta, Anjan K. & Sen, Pradip K., "Optimization of membrane unit for removing carbon dioxide from natural gas", *Journal of Membrane Science*, **283**(1-2), 291-300 (2006).
7. Lee, A. L., et al., "Field tests of membrane modules for separation of carbon dioxide from low-quality natural gas", *Gas Separation & Purification*, **9**(1), 35-43 (1994).
8. Nunes, S. P. & Peinemann, K. V., *Membrane Technology in the Chemical Industry*, Weinheim: Wiley-VCH (2001).
9. Korens, N., Simbeck, D. and Wilhelm, D., "Process screening analysis of alternative gas treating and sulfur removal for gasification", Revised Final Report, SFA Pacific, Inc. (2002).

10. Oldenburg, C. M., et al. “Process modeling of CO_2 injection into natural gas reservoirs for carbon sequestration and enhanced gas recovery”, *Energy & Fuels*, **15**(2), 293-298 (2001).
11. Seo, Jeong G. & Mamora, Daulat D., “Experimental and simulation studies of sequestration of supercritical carbon dioxide in depleted gas reservoirs”, *Journal of Energy Resources Technology*, **127**(1), 1-6 (2005).
12. Beckman, Eric J., “Supercritical and near-critical CO_2 in green chemical synthesis and processing”, *Journal of Supercritical Fluids*, **28**(2-3), 121-191 (2004).
13. Pfromm, P. H. and Koros, W. J., “Accelerated physical aging of thin glassy Polymer films - evidence from gas-transport measurements”, *Polymer*, **36**(12), 2379-2387 (1995).
14. McCaig, M. S. and Paul, D. R., “Effect of film thickness on the changes in gas permeability of a glassy polyarylate due to physical aging Part I. Experimental observations”, *Polymer*, **41**(2), 629-637 (2000).
15. Huang, Y. & Paul, D. R., “Physical aging of thin glassy polymer films monitored by gas permeability”, *Polymer*, **45**(25), 8377-8393 (2004).
16. Wind, J. D., Staudt-Bickel, C., et al., “The effects of crosslinking chemistry on CO_2 plasticization of polyimide gas separation membranes”, *Industrial & Engineering Chemistry Research*, **41**(24), 6139-6148 (2002).
17. Wind, J. D., Staudt-Bickel, C., et al., “Solid-state covalent cross-linking of polyimide membranes for carbon dioxide plasticization reduction”, *Macromolecules*, **36**(6), 1882-1888 (2003).
18. Wind, J. D., Paul, D. R., et al, “Natural gas permeation in polyimide membranes”, *Journal of Membrane Science*, **228**(2), 227-236 (2004).

19. Coleman, Mr. R & Koros, W. J., “Conditioning of fluorine containing polyimides – Effect of exposure to high pressure carbon dioxide on permeability”, *Macromolecules*, **30**(22), 6899-6905 (1997).
20. Raymond, P. C., et al., “Comparison of mixed and pure gas permeation characteristics for CO_2 and CH_4 in copolymers and blends containing methyl-methacrylate units”, *Journal of Membrane Science*, **77**(1), 49-57 (1993)

2.0 BACKGROUND AND THEORY

2.1 Introduction

This chapter provides the fundamental framework for interpreting gas permeation and sorption in glassy polymers. The Dual Mode sorption model is used to describe gas uptake in non-equilibrium polymers. The Free Volume model is used to rationalize changes in gas sorption and transport as a function of time within the glassy polymer in order to rationalize physical aging and the mechanisms behind this aging process. A review of previous supercritical carbon dioxide conditioning studies is also presented as a background to interpret complex phenomena observed in this study upon exposure of glassy polyimides to extremely high CO_2 pressure (>100 atm). Finally, polymer plasticization and previous efforts to inhibit this phenomenon are presented along with other non-ideal gas permeation effects such as bulk flow and nonideal gas phase fugacities.

2.2 Gas Transport in Polymers

Gas transport through a polymer medium occurs through a combined mechanism known as solution-diffusion. A penetrant from the feed stream sorbs at the surface of the upstream side of the membrane, and then diffuses through the film to the downstream surface where it desorbs into the permeate stream. The driving force for this process is the difference in chemical potential of each species across the membrane, which is related to the difference in concentration resulting from the change in partial pressure between the feed and permeate streams [1].

The uptake of a penetrant into the polymer from the feed stream is known as sorption. The sorption coefficient of a penetrant in the polymer is roughly correlated with the condensability of that penetrant; therefore, sorption comprises the thermodynamic component of the transport process. Along with penetrant condensability, fractional free volume of the polymer, penetrant-polymer interactions, and temperature affect the solubility of a penetrant in the polymer.

Diffusion is an energy activated process in which a transient gap is created between polymer chains to allow a diffusive jump of the penetrant. Therefore, the diffusion process is the kinetic component of the transport process. The diffusion coefficient (D) is mathematically described by the following relationship:

$$D = \frac{1}{6} f l^2 \tag{2.1}$$

In this equation, f is the frequency of molecular jumps and l is the average jump length [2]. The ability of a penetrant to make a jump is determined primarily by the size and frequency of the thermally generated gaps and the size of the molecule. Therefore, in general, the diffusion coefficient decreases as the thermal energy within the system decreases and the size of the penetrant increases. However, polymer chain flexibility and packing, penetrant-polymer interactions, polymer-polymer interactions, and polymer free volume and its distribution all play complex roles in determining penetrant diffusion through a polymer [2].

Gas transport through a membrane can be characterized by the permeability coefficient ($\mathrm{P_A}$) which is defined as the pressure and thickness normalized flux across the membrane:

$$P_A = \frac{N_A \cdot l}{\Delta p_A} \tag{2.2}$$

In this equation, N_A is the flux of component A through the membrane, l is the membrane thickness, and Δp is the difference in partial pressure of A acting across the membrane. The units of the permeability coefficient are generally defined as Barrers according to the following relationship:

$$1\ Barrer = 10^{-10}\ \frac{cm^3(STP) * cm}{cm^2 * s * cmHg}$$

Following Fick's first law, the flux of A through a polymer membrane may also be written as:

$$N_A = D_A \frac{(C_{A,2} - C_{A,1})}{l} \tag{2.3}$$

In this case, D_A is the diffusion coefficient averaged across the membrane, and C is the concentration of A on the upstream (2) and downstream (1) faces of the membrane. If Equation 2.3 is substituted into Equation 2.2, the following expression is obtained:

$$P_A = D_A \left(\frac{C_{A,2} - C_{A,1}}{p_{A,2} - p_{A,1}} \right) \tag{2.4}$$

When the upstream pressure is significantly greater than the downstream pressure, Equation 2.4 is reduced to:

$$P_A = D_A\left(\frac{C_{A,2}}{p_{A,2}}\right) \tag{2.5}$$

The sorption coefficient is then defined from Equation 2.5 as:

$$S_A = \frac{C_{A,2}}{p_{A,2}} \tag{2.6}$$

Therefore, permeability is also defined as the product of a kinetic parameter and thermodynamic parameter as shown in Equation 2.7 [3-5].

$$P_A = D_A \cdot S_A \tag{2.7}$$

To characterize the separation efficiency of the membrane, the ratio of permeabilities of the fast gas and slow gas provides the ideal selectivity, which is displayed as:

$$\alpha^*_{AB} = \frac{P_A}{P_B} = \frac{D_A}{D_B} \cdot \frac{S_A}{S_B} \tag{2.8}$$

This equation clearly shows the contribution of the diffusivity selectivity and solubility selectivity to the overall selectivity. For a feed gas mixture, however, the separation factor best describes the overall efficiency of the process.

$$\alpha_{AB} = \frac{y_A / y_B}{x_A / x_B} \tag{2.9}$$

In this expression, y and x refer to the mole fractions of the components in the permeate and feed, respectively. For cases in which the downstream to upstream pressure ratio approaches zero, $\alpha_{AB} \rightarrow \alpha^*_{AB}$ if values of D_i and S_i in the mixed gas case are used in Equation 2.8.

2.3 The Dual Mode Sorption and Dilation Models

Sorption in glassy polymers can be described most conveniently using the Dual Mode Sorption model. According to this model, the penetrant concentration at a given pressure is taken to be the sum of two distinct polymer regions in local equilibrium. Sorption in the "dissolved", or Henry's Law, region is characterized by a linear increase in concentration with polymer. On the other hand, sorption in the microvoids, or excess unrelaxed free volume, exhibits a pore-filling response in which the concentration asymptotically approaches a saturation level. This response assumes swelling of the polymer with increasing penetrant uptake is due primarily to dilation of the "dissolved" region associated with the Henry's Law environments. At higher swelling levels, Flory-Huggins type uptake can be used in place of the simple linear Henry's Law sorption and

swelling behavior [6]. The mathematical representation of the Dual Mode model is shown below:

$$C = k_D p + \frac{C_H' b p}{1 + b p} \tag{2.10}$$

In this expression, k_D is the Henry's Law constant, C'_H is the Langmuir Capacity constant, and b is the Langmuir affinity parameter which describes the affinity of the penetrant to be sorbed into the polymer. Both k_D and b increase with the penetrant condensability; however, all coefficients are visualized as constants at a given temperature and degree of excess unrelaxed free volume within the glassy sample [7].

Assuming polymer dilation is only a result of penetrant swelling of the Henry's Law region, the Dual Mode model can describe dilation, $\Delta V/V_o$, through the following expression,

$$\frac{\Delta V}{V_o} = k_D p \frac{v_{gas}}{22415} \tag{2.11}$$

where v_{gas} is the partial molar volume of the penetrant in the polymer at a given pressure and the constant, 22415, is a unit conversion from cc(STP) to moles. This equation, with a constant value of v_{gas}, has been used to reasonably describe a linear dilation response in polycarbonate to high CO_2 pressures [8].

2.4 The Free Volume Model

For a given penetrant, gas permeation, as described by D_i and S_i, for different polymers tends to be dominated by differences in the diffusion coefficient rather than differences in the sorption coefficient. Although many polymer characteristics affect gas diffusion, the fractional free volume of the polymer is probably the more dominant. The fractional free volume of a polymer, f, is defined as,

$$f = \frac{(V - V_o)}{V} \tag{2.12}$$

where V is the specific volume and V_o is the occupied volume of the polymer [9]. The occupied volume can be determined using a group contribution method [10,11]. The Free Volume model, presented below, correlates permeability of a specific gas to the fractional free volume present in the polymer.

$$P = A \exp\left(\frac{-B}{f}\right) \tag{2.13}$$

In this expression, A and B are empirical constants; however, B tends to scale with penetrant size. Refractive index measurements of thin polymer films can be used to determine the density, and therefore fractional free volume, through the Lorentz-Lorenz relation shown below.

$$L = \frac{n^2 - 1}{n^2 + 2} = \rho * C \tag{2.14}$$

In this equation, n is the refractive index, ρ is the density, and C is a material constant that can be determined using thick film refractive indices and densities.

2.5 Physical Aging

It is well known that amorphous glassy polymers do not exist in thermodynamic equilibrium [12]. As the polymer is cooled from a rubbery state, it passes through a glass transition temperature (T_G) in which long-range polymer chain movements become drastically hindered. At this point, the polymer "vitrifies" and forms segmental microvoids in the polymer matrix known as "excess free volume" or "unrelaxed volume". Below the glass transition temperature, the polymer densifies over time and approaches thermodynamic equilibrium due to the removal of this excess free volume in a process known as physical aging. In other words, the fractional free volume of a polymer decreases over time as the polymer ages. Figure 2.1, shown below, illustrates the relationship between the polymer specific volume and temperature.

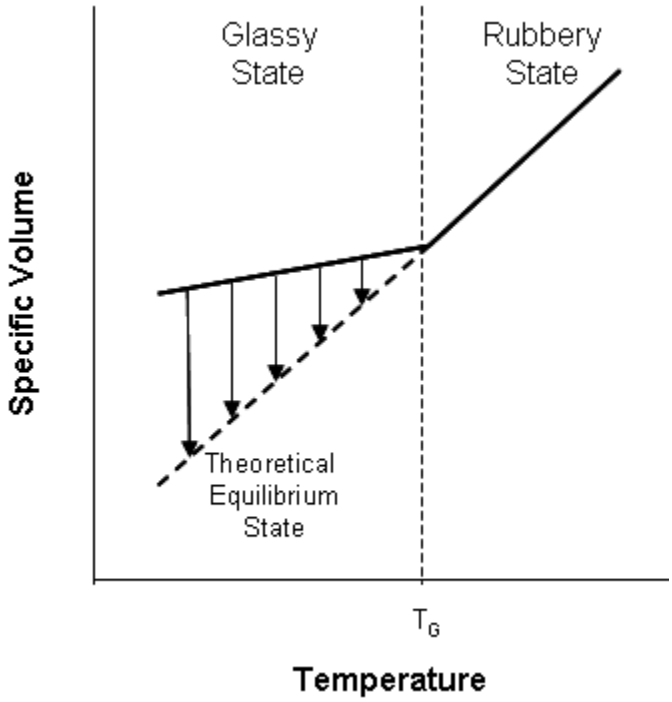

Figure 2.1: Polymer volume as a function of temperature. Arrows represent removal of excess free volume and polymer densification towards an equilibrium state.

Recent research has suggested that physical aging occurs through two independent processes, lattice contraction and diffusion of free volume [9,13,14]. Illustrations for these two processes are shown in Figure 2.2.

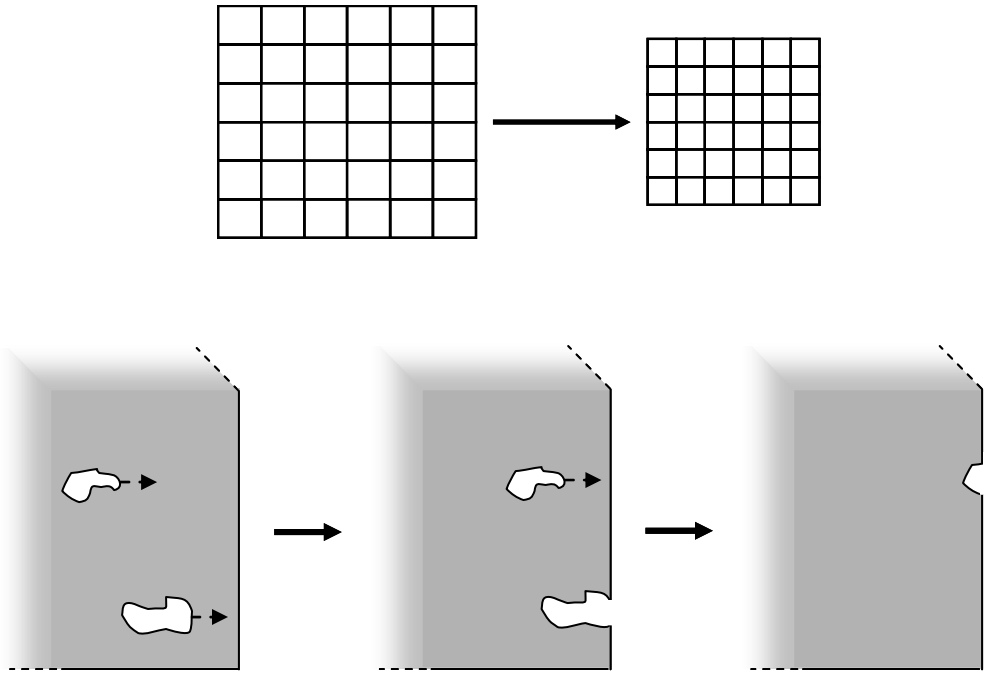

Figure 2.2: Illustrations of lattice contraction and diffusion of free volume processes for physical aging in glassy polymers

Lattice contraction is the uniform collapse of the entire unrelaxed polymer matrix [13]. This process is analogous to a sudden contraction of volume of an ideal gas when the temperature is reduced and the pressure remains constant. Since this process is identical throughout the entire sample, it is not dependent on the sample size. On the other hand, diffusion of free volume corresponds to the removal of unrelaxed free volume through diffusion of packets of volume to the surface of the sample [15]. The surface acts as a sink for these packets of excess free volume, thereby creating a gradient of free volume between the center of the sample and the surface. It is assumed that this diffusion process follows Fick's second law of diffusion; therefore, the free volume flux should be inversely proportional to the square of the sample thickness. As free volume diffuses out of the sample, the segmental mobility of the polymer decreases,

which, in turn, reduces the rate of diffusion of free volume and gives the process a self-retarding nature [12].

Prior to 1994, most physical aging research involved annealing polymer membranes and measuring transport properties at various gas pressures or exposing a polymer membrane to a gas for a prolonged period of time and tracking how the transport properties change [16-18]. Also, most work was conducted on relatively thick polymer samples and at annealing temperatures near T_G. However, Pfromm and Koros discovered that gas permeabilities of polymer membranes change significantly over extended periods of time (up to 7000 hours) at temperatures well below T_G. In particular, thin polymer films with submicron thicknesses age at a much faster rate than corresponding thick films (~2-28 microns). Figures 2.3 and 2.4 show N_2 permeabilities and He/N_2 selectivities for thin and thick films measured by Pfromm. All films were annealed above T_G and rapidly quenched to room temperature to “erase” all thermal history and create as common a starting point for all films as was possible.

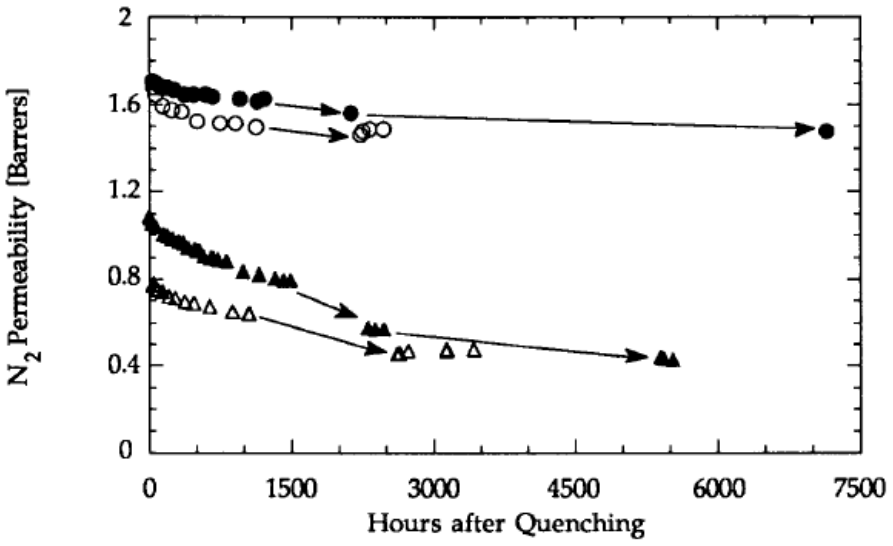

Figure 2.3: N_2 permeability of 6FDA-IPDA films at 35C and 150 psia with thicknesses of (●) 28.45 μm, (○) 2.54 μm, and (Δ) 500 nm. ▲ represents non-annealed thin films. All films are stored in dry air at 1 atm, 35 C [19].

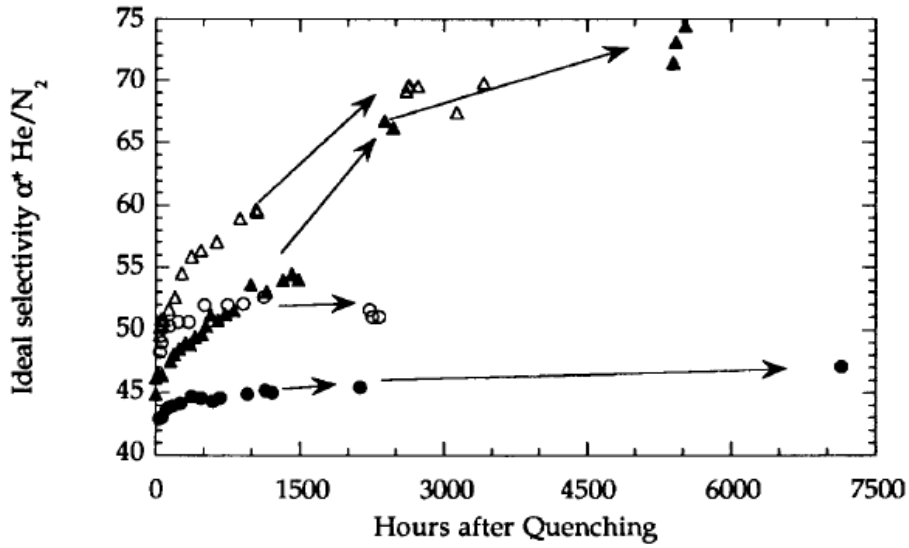

Figure 2.4: He/N_2 ideal selectivity of 6FDA-IPDA films at 35C and 150 psia with thicknesses of (●) 28.45 μm, (○) 2.54 μm, and (Δ) 500 nm. ▲ represents non-annealed thin films. All films are stored in dry air at 1 atm, 35 C [19].

Since Pfromm's work, similar results have been attained for various membrane aging experiments. Rezac and Pfromm explored aging of thin polymers on ceramic supports using O_2, N_2, and He probes [20]. Dorkenoo and Pfromm investigated film thickness effects on physical aging in polynorborene and poly(trimethylsilylpropyne) with He/N_2 separations [21,22]. Zhou et al. also tested film thickness effects and crosslinking on aging in a 6FDA-based polyimide using O_2 and N_2 [23]. Research conducted by T. S. Chung has explored aging effects with polyimide and polyimide/polyacrylonitrile composite asymmetric membranes [24,25].

In 1998, McCaig and Paul observed the possible dual mechanism of aging through gas permeability measurements using a glassy polyarylate of different thicknesses [9]. If aging were solely a function of diffusion of free volume, then gas permeabilities should fall on a single curve when plotted against the normalized aging time for films of all thicknesses. Assuming Fickian diffusion, the normalized aging time is simply time divided by the square of the thickness of the sample. However, as seen in Figure 2.5, O_2 permeabilities from different sample thicknesses initially decline at different rates before converging to a single curve. Therefore, the overall aging process seems to be a complex process involving both lattice contraction and diffusion of free volume.

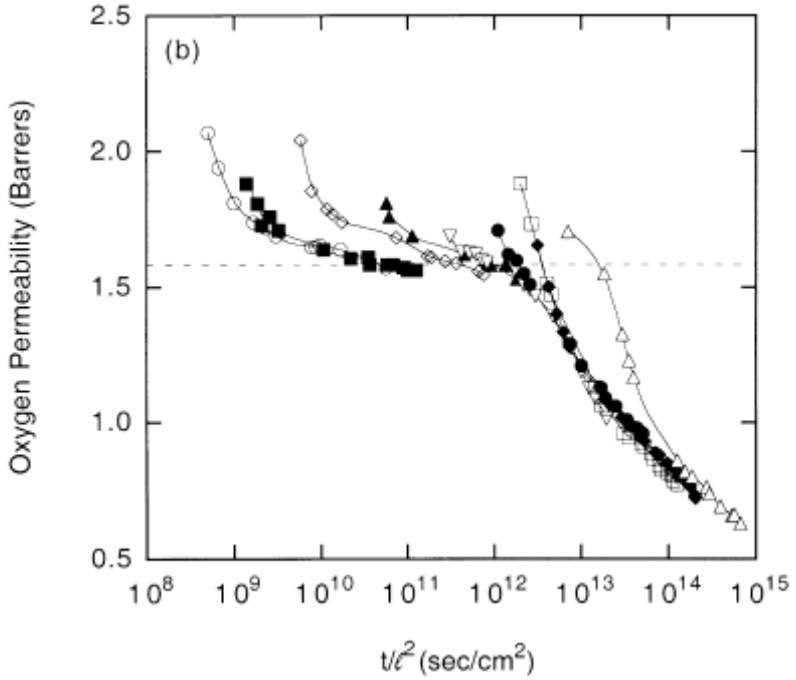

Figure 2.5: O_2 permeability of BPA-BnzDCA films as a function of normalized aging time, t/ℓ^2, at 35C and 2 atm with thicknesses of (○) 33 μm, (■) 28 μm, (◊) 9.7 μm, (▲) 4.4 μm, (▽) 1.85 μm, (●) 990 nm, (□) 740 nm, (♦) 580 nm, and (Δ) 250 nm [9]

In 2004, Huang and Paul confirmed the eventual permeability convergence to a single master curve using a polysulfone, a polyimide, and a poly(phenylene oxide) of various thicknesses [14].

Of all physical aging studies done in the last decade, very few have incorporated the study of CO_2 for the purpose of natural gas separation. CO_2 permeation measurements are typically excluded because it swells glassy polymers, which can reverse the effects of physical aging. Lin and T. S. Chung investigated aging effects with CO_2; however, the membranes examined were hollow fibers and there is little data to reveal the effects of aging in the first 20-30 days [25]. Recently, Kim et al. explored the effects of physical aging using low pressure CO_2 on a series of high-performance polyimides with the ability to be crosslinked. They found that periodic exposure to CO_2

slowed the rate of physical aging of the slower gases, thus causing CO_2/CH_4 and O_2/N_2 selectivities to decrease with aging time, which is counter to the typical aging response. Once these polymers were crosslinked, however, the slow gas physical aging isotherms of the polymer membranes with and without CO_2 exposure were nearly identical [26,27]. This result confirms that crosslinking maintains the separation efficiency of the polymer membrane while it ages in the presence of CO_2. However, addition of a crosslinking agent inherently affects the free volume of the polymer which may affect the rate at which it ages since the addition most likely affects the relaxation dynamics of the polymer. A comprehensive study on the effect of the inclusion of the crosslinking agent and the effect of the size of the crosslinking agent was not conducted.

2.6 Supercritical Carbon Dioxide Conditioning

Since the use of $scCO_2$ as a tunable solvent has attracted much interest lately, work has been conducted in the last 10 years pertaining to $scCO_2$ transport through polymer membranes as a means of CO_2 purification. Recent work has been conducted using Sepa® CF thin film, polyamide, and cellulose acetate membranes to purify $scCO_2$ after extraction of essential oils from vegetables [28-30]. In all of these studies, the working pressure for $scCO_2$ permeation is 12 MPa and the transmembrane pressure is varied from 0.5 to 4 MPa. Spricigo et al. noted a short conditioning time resulting in a decrease in the CO_2 flux through the membrane, which they attribute to membrane compaction. While these studies provide insight into oil retention and the conditioning effects of the oils on CO_2 permeation, they do not further explore the effects of $scCO_2$ on the membranes themselves. Semenova et al. studied the separating efficiency of Kapton® for $scCO_2$/ethanol mixtures and found that the CO_2 flux increased linearly with pressure from 1 to 14 MPa [31,32]. Ohya et al. and Higashijima et al. confirmed the

Kapton® response to $scCO_2$ exposure for pressures up to 12 MPa [33,34]. Chen et al. probed the effects of $scCO_2$ conditioning on polycarbonate membranes through oxygen permeation and sorption and changes in the glass transition temperature. However, after conditioning the samples at various subcritical and supercritical CO_2 densities, the chamber was depressurized in less than 5 minutes. The rapid depressurization of such a highly soluble species traps additional free volume in the polymer matrix leaving the polymer in a "puffed up" state that is very far from equilibrium. This result was evident in the large increase in the Langmuir capacity constant of oxygen and nitrogen sorption as the CO_2 density increased [35]. Finally, Patil et al. studied $scCO_2$ conditioning effects on polyvinyl alcohol and a polyamide for pressures up to 200 MPa while maintaining a transmembrane pressure drop of between 0.05 and 0.3 MPa. The CO_2 permeances are modeled using Hagen-Poisseuille's relationship for viscous flow [36]. To the author's knowledge, there has not been any research to explore the effects $scCO_2$ conditioning may have on the removal of CO_2 from natural gas.

2.7 Plasticization and Polymer Crosslinking

When Equations 2.6, 2.7, and 2.10 are combined, the following Dual Mode transport model is derived in Equation 2.15.

$$P = k_D D_D + D_H \left(\frac{C_H' b}{1 + bp} \right) \tag{2.15}$$

In this case, the diffusion coefficient has been separated into two components, diffusion in the Henry's Law (D_D) and Langmuir (D_H) regions. At low pressures, permeability decreases with increasing pressure due to the filling of Langmuir sorption sites and the

contribution of the Langmuir region term in Equation 2.15. However, as pressure continues to increase, the contribution of the Langmuir region to the overall permeability diminishes and gas permeability approaches a constant value, ie $k_D D_D$. This response is typical for non-interacting gases and is known as a typical Dual Mode permeation response. However, for more strongly sorbing and interacting penetrants like CO_2, the polymer eventually exhibits an upswing in the permeation isotherm due to swelling-induced plasticization, as evident in the schematic presented in Figure 2.6. The pressure at which this upturn occurs is often referred to as the plasticization pressure and is shown as the dashed line in Figure 2.6. On the molecular scale level, plasticization is believed to occur when the presence of the penetrant enhances segmental motion of the polymer chains. This increase in segmental motion allows for a greater frequency and size of the transient gap leading to a higher diffusion coefficient as described by Equation 2.1. Plasticization is detrimental to the purification of natural gas because it greatly reduces the selectivity of the membrane by enabling easier diffusion of the larger penetrant, CH_4, which is desired to be rejected versus CO_2.

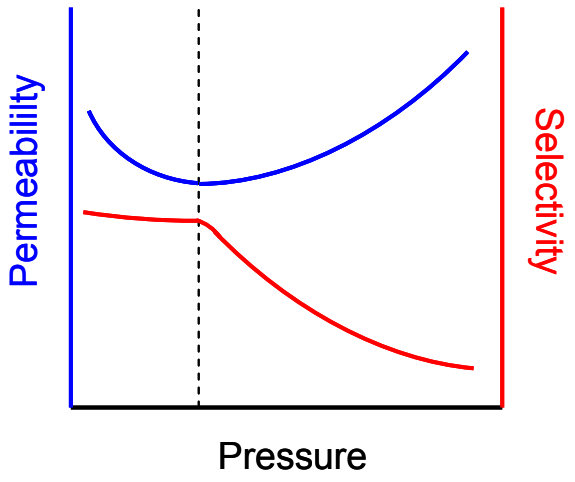

Figure 2.6: Schematic of permeation isotherm exhibiting plasticization along with corresponding decrease in selectivity

To reduce the effects of polymer plasticization with regards to natural gas purification, previous work has explored the ability to covalently crosslink high-performance gas separation polymers [37,38]. High performance polyimides containing a reactive carboxylic acid site were crosslinked using various glycol species. The hydroxyl end groups of the glycols reacted at the open carboxylic acid, or free acid, sites on the polymer backbone to form two ester linkages and a covalent crosslink. As shown in Figure 2.7, crosslinking of one of the polyimides significantly reduced the effects of plasticization [37].

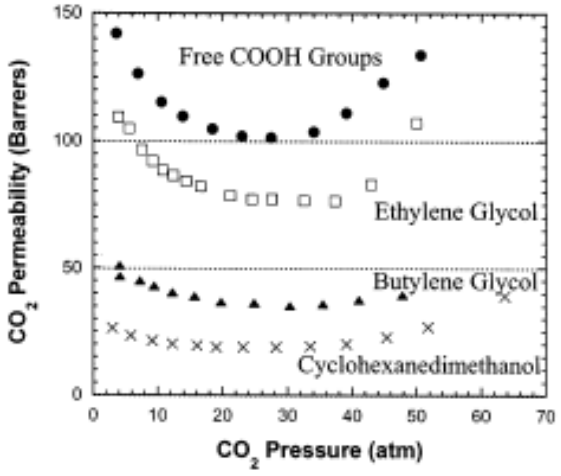

Figure 2.7: CO_2 permeation isotherm of the free acid and crosslinked versions of 6FDA-DAM:DABA (2:1) polyimide [37]

Wind et al. have extensively characterized both polymers with and without the four crosslinking agents for pure and mixed gas CO_2/CH_4 separations at different pressures; however, all work was done with thick films and polymer aging was not examined [37-40].

2.8 Non-Ideal Gas Permeation Effects

In the case of mixed gas separations of two or more feed components, competitive sorption, bulk flow, and non-ideal thermodynamic effects need to be considered. The following illustrations pertain to binary feed mixtures; however, they are relevant for all multi-component feed mixtures. "Competitive sorption" refers to the competition between the two species for a fixed number of Langmuir sorption sites. For the separation of CO_2 from CH_4, this phenomenon can result in enhanced CO_2 sorption, and therefore higher gas permeation selectivities, since CO_2 has a much higher affinity for Langmuir sorption sites [41].

The flux of a penetrant through a membrane in a binary feed mixture is composed of two components as shown in Equation 2.16.

$$N_A = -D_A \frac{\partial C_A}{\partial x} + x_A (N_A + N_B) \tag{2.16}$$

The first term corresponds to the diffusive flux, which is identical to Equation 2.3. The second term describes the convective flux of the components through the membrane. Transport through a membrane is usually associated with only the diffusive flux; however, the convective flux of the slow gas (B) in a mixture with a high flux of the fast gas (A) can be of similar magnitude to the diffusive flux of B and have an appreciable effect on the overall transport of the species. This effect results in a significant decrease in the separation efficiency of the membrane as the slow gas permeability is enhanced [38,41]. This is especially true when large concentrations of both species are present in the feed as in the case of the 50/50 CO_2/CH_4 mixed gas feed that is used in this work and presented in Chapter 6.

As presented in Equation 2.2, permeability coefficients are typically determined using the pressure difference across a membrane; however, the driving force behind gas transport is the difference in chemical potential or the fugacity of the penetrant. Because the fugacity coefficients of different penetrants deviate from unity at different rates as pressure increases, the driving force of each component changes with increasing pressure. For the CO_2/CH_4 separation, CO_2 has greater nonideality, ie the fugacity coefficient decreases more rapidly than that of CH_4, which reduces the driving force of CO_2 relative to CH_4 and hence the flux. Therefore, similar to the bulk flow effects, nonideality reduces the separation efficiency of the membrane.

An example of these effects is presented in Figure 2.8. Bulk flow and thermodynamic contributions are used to model the CO_2/CH_4 separation factor of a crosslinked polyimide probed with a 50/50 CO_2/CH_4 mixed gas feed. The Dual Mode transport model neglects bulk flow and thermodynamic nonideality contributions, while the Bulk Flow model is presented with and without thermodynamic nonideality contributions. In this case, the fugacity-based Bulk Flow model accurately describes the experimental CO_2/CH_4 separation factor.

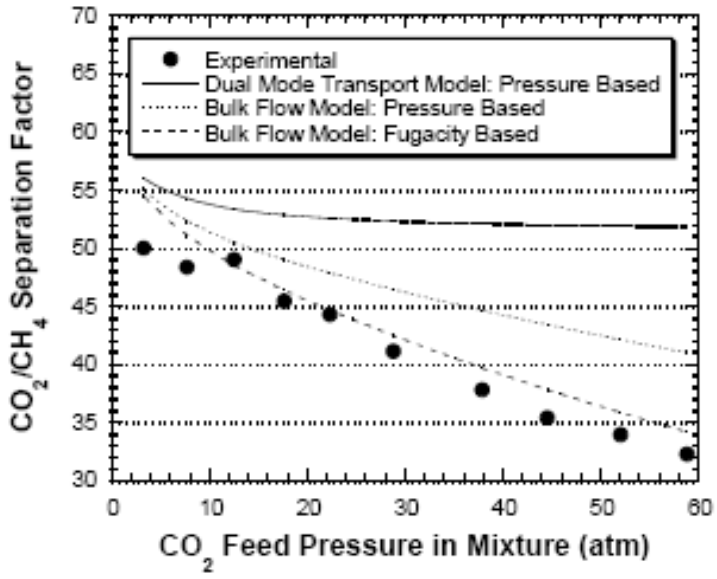

Figure 2.8: Bulk flow model predictions for separation factors of 50/50 CO_2/CH_4 mixed gas at 35 ^oC through 6FDA-6FpDA:DABA (2:1) crosslinked with ethylene glycol [42]

2.9 References

1. Koros, W. J. & Fleming, G. K., “Membrane-based gas separation”, *Journal of Membrane Science*, **83**(1), 1-80 (1993).
2. Crank, J. & Park, G. S., *Diffusion in Polymers*, London: Academic Press Inc. (1968).
3. Hines, Anthony & Maddox, Robert, *Mass Transfer – Fundamentals and Applications*, New Jersey: Prentice-Hall Inc. (1985).
4. Crank, J., *The Mathematics of Diffusion*, Oxford: Oxford University Press (1975).
5. Yampolskii, Y., Pinnau, I. & Freeman, B., *Materials Science of Membranes for Gas and Vapor Separation*, West Sussex: John Wiley & Sons (2006).
6. Petropoulos, J. H., “Mechanisms and theories for sorption and diffusion of gases in polymers”, *Polymeric Gas Separation Membranes*, Boca Rotan: CRC Press (1994).
7. Moore, T. & Koros, W. J., “Gas sorption in polymers, molecular sieves, and mixed matrix membranes”, *Journal of Applied Polymer Science*, **104**(6), 4053-4059 (2007).
8. Fleming, G. K. & Koros W. J., “Dilation of polymers by sorption of carbon-dioxide at elevated pressures – 1. Silicone-rubber and unconditioned polycarbonate”, *Macromolecules*, **19**(8), 2285-2291 (1986).
9. McCaig, M. S. and Paul, D. R., “Effect of film thickness on the changes in gas permeability of a glassy polyarylate due to physical aging Part I. Experimental observations”, *Polymer*, **41**(2), 629-637 (2000).
10. Bondi, A. *Physical Properties of Molecular Crystals, Liquids, and Glasses*. New York: Wiley (1968).

11. Park, J. Y. & Paul, D. R., "Correlation and prediction of gas permeability in glassy polymer membrane materials via a modified free volume based group contribution method", *Journal of Membrane Science*, **125**(1), 23-39 (1997).
12. Struik, L. C. E., “Physical aging in plastics and other glassy materials”, *Polymer Engineering and Science*, **17**(3), 165-173 (1977).
13. Curro, J. G., Lagasse, R. R., et al., “Diffusion-model for volume recovery in glasses”, *Macromolecules*, **15**(6), 1621-1626 (1982).
14. Huang, Y. & Paul, D. R., “Physical aging of thin glassy polymer films monitored by gas permeability”, *Polymer*, **45**(25), 8377-8393 (2004).
15. Alfrey, T., Goldfinger, G., et al., “The apparent second-order transition point of polystyrene”, *Journal of Applied Physics*, **14**(12), 700-705 (1943).
16. Chan, A. H. & Paul, D. R., “Influence of history on the gas sorption, thermal, and mechanical-properties of glassy polycarbonate”, *Journal of Applied Polymer Science*, **24**(6), 1539-1550 (1979).
17. Hachisuka, H., Kito, H., et al., “O_2 and N_2 gas permselectivity of alternating copoly(vinylidene cyanide vinyl-acetate)”, *Journal of Applied Polymer Science*, **35**(5), 1333-1340 (1988).
18. Vrentas, J. S. & Hou, A. C., “History dependence of diffusion-coefficients for glassy polymer penetrant systems”, *Journal of Applied Polymer Science*, **36**(8), 1933-1934 (1988).
19. Pfromm, P. H. and Koros, W. J., “Accelerated physical aging of thin polymer-films - evidence from gas-transport measurements”, *Polymer*, **36**(12), 2379-2387 (1995).
20. Rezac, M. E., Pfromm, P. H., et al., “Aging of thin polyimide ceramic and polycarbonate ceramic composite membranes”, *Industrial & Engineering Chemistry Research*, **32**(9), 1921-1926 (1993).

21. Dorkenoo, K. D. & Pfromm, P. H., “Experimental evidence and theoretical analysis of physical aging in thin and thick amorphous glassy polymer films”, *Journal of Polymer Science Part B - Polymer Physics*, **37**(16), 2239-2251 (1999).
22. Dorkenoo, K. D. & Pfromm, P. H., “Accelerated physical aging of thin poly[1-(trimethylsilyl)-1-propyne] films”, *Macromolecules*, **33**(10), 3747-3751 (2000).
23. Zhou, C., Chung, T. S., et al., “The accelerated CO_2 plasticization of ultra-thin polyimide films and the effect of surface chemical cross-linking on plasticization and physical aging”, *Journal of Membrane Science*, **225**(1-2), 125-134 (2003).
24. Chung, T. S. & Kafchinski, E. R., “Aging phenomenon of 6FDA-polyimide/polyacrylonitrile composite hollow fibers”, *Journal of Applied Polymer Science*, **59**(1), 77-82 (1996).
25. Lin, W. H. & Chung, T. S., “The physical aging phenomenon of 6FDA-durene polyimide hollow fiber membranes”, *Journal of Polymer Science Part B - Polymer Physics*, **38**(5), 765-775 (2000).
26. Kim, J. H., et al., “Effects of CO_2 exposure and physical aging on the gas permeability of thin 6FDA-based polyimide membranes – Part 1. Without crosslinking”, *Journal of Membrane Science*, **282**(1-2), 21-31 (2006).
27. Kim, J. H., et al., “Effects of CO_2 exposure and physical aging on the gas permeability of thin 6FDA-based polyimide membranes – Part 2. With crosslinking”, *Journal of Membrane Science*, **282**(1-2), 32-43 (2006).
28. Spricigo, C. B., et al., “Separation of nutmeg essential oil and dense CO_2 with a cellulose acetate reverse osmosis membrane”, *Journal of Membrane Science*, **188**(2), 173-179 (2001).

29. Sarmento, L. A. V., et al., “Performance of reverse osmosis membranes in the separation of supercritical CO_2 and essential oils”, *Journal of Membrane Science*, **237**(1-2), 71-76 (2004).
30. Carlson, L. H. C., et al., “Separation of D-limonene from supercritical CO_2 by means of membranes”, *Journal of Supercritical Fluids*, **34**(2), 143-147 (2005).
31. Semenova, S. I., et al., “Separation of supercritical CO_2 and ethanol mixtures with an asymmetric polyimide membrane”, *Journal of Membrane Science*, **74**(1-2), 131-139 (1992).
32. Semenova, S. I., et al., “Dependence of permeability through polyimide membranes on state of gas, vapor, liquid and supercritical fluid at high temperatures”, *Journal of Membrane Science*, **67**(1), 29-37 (1992).
33. Ohya, H., et al., “Separation of supercritical CO_2 and iso-octane mixtures with an asymmetric polyimide membrane”, *Journal of Membrane Science*, **84**(1-2), 185-189 (1993).
34. Higashijima, T., et al., “Separation of supercritical fluid mixtures of CO_2 and petroleum components with an asymmetric polyimide membrane”, *Journal of Membrane Science*, **93**(2), 165-173 (1994).
35. Chen, S. H., et al., “Effect of CO_2 treated polycarbonate membranes on gas transport and sorption properties”, *Journal of Membrane Science*, **172**(1-2), 105-112 (2000).
36. Patil. V. E., et al., “Permeation of supercritical carbon dioxide through polymeric hollow fiber membranes”, *Journal of Membrane Science*, **271**(1-2), 77-85 (2006).
37. Wind, J. D., Staudt-Bickel, C., et al., “Solid-state covalent cross-linking of polyimide membranes for carbon dioxide plasticization reduction”, *Macromolecules*, **36**(6), 1882-1888 (2003).

38. Wind, J. D., Staudt-Bickel, C., et al., “The effects of crosslinking chemistry on CO_2 plasticization of polyimide gas separation membranes”, *Industrial & Engineering Chemistry Research*, **41**(24), 6139-6148 (2002).
39. Wind, J. D., Paul, D. R., et al, “Natural gas permeation in polyimide membranes”, *Journal of Membrane Science*, **228**(2), 227-236 (2004).
40. Wind, J. D., et al., “Carbon dioxide-induced plasticization of polyimide membranes: Pseudo-equilibrium relationships of diffusion, sorption, and swelling”, *Macromolecules*, **36**(17), 6433-6441 (2003).
41. Kamaruddin, H. D. & Koros, W. J., “Some observations about the application of Fick’s first law for membrane separation of multicomponent mixtures”, *Journal of Membrane Science*, **135**(2), 147-159 (1997).
42. Wind, John, *Improving Polyimide Membrane Resistance to Carbon Dioxide Plasticization in Natural Gas Separations*, Dissertation, University of Texas-Austin (2002).

3.0 MATERIALS AND CHARACTERIZATION TECHNIQUES

3.1 Introduction

This chapter describes all the materials, procedures, and characterization techniques used in this work. The polymers for each study are introduced as well as the synthesis and crosslinking procedures where applicable. This chapter introduces the permeation system, high-pressure permeation system, low-pressure quartz spring sorption, and high-pressure quartz spring sorption as the equipment used to conduct experiments. All membrane preparation and test procedures are described which include solution casting, spin casting, membrane masking, permeation testing, and sorption testing. Finally, the secondary techniques used to characterize the polymer are presented which include GPC, DSC, H-NMR, C-NMR, Spectroscopic Ellipsometry, Fluorescence Spectroscopy, Density Gradient Column, WAXD, TGA, and FTIR.

3.2 Polymer

It is well known that polyimides have exceptional gas separation properties. Selected members in this family that have both "stiff" backbones and packing-inhibited groups within the backbone create an attractive distribution of free volume for performing subtle size and shape discrimination between similarly sized penetrants [1]. Polyimides are also easily solution processable and can withstand extreme operating temperatures (prolonged use up to 200C is typical) [1]. A 6FDA-based copolymer polyimide was chosen to examine the effects of membrane aging and $scCO_2$ conditioning for natural gas separation. This polymer, shown below in Figure 3.1, was synthesized using (4,4'-hexafluoroisopropylidene) diphthalic anhydride (6FDA) and the diaminomesitylene

(DAM) and 3,5-diaminobenzoic acid (DABA) diamines. Packing inhibitions due to the DAM moiety provide considerable free volume, which enhances the productivity of the membrane for natural gas separations. Due to the relatively high fractional free volume compared to other polyimides, this polymer is also ideal for a physical aging study since changes in the free volume will be relatively larger than in lower free volume polymers. On the other hand, the DABA moeity provides a carboxylic acid group which can be used to crosslink the polymer through a subsequent condensation reaction involving diol crosslinking agents.

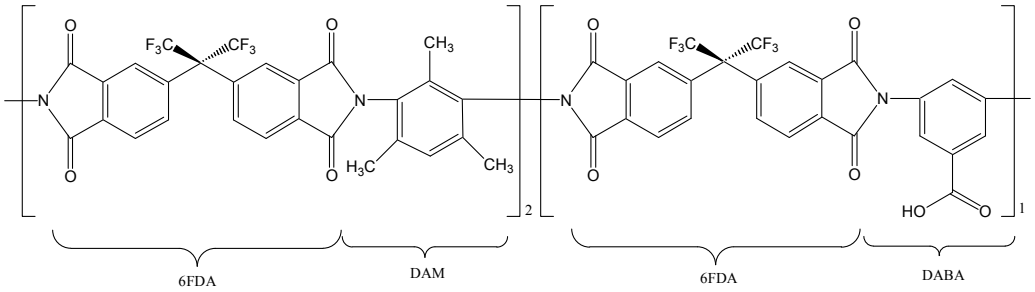

Figure 3.1: The 6FDA-DAM:DABA (2:1) structure

This polyimide is synthesized through a two-step polycondensation reaction. In the first step, stoichiometric amounts of the three monomers were added to NMP at room temperature to make a 20 wt% solution. This solution was stirred at room temperature for 18 hours to produce the polyamic acid. The second step involves heating the highly viscous solution to 200 ^{o}C for 24 hours to close the imide ring and complete the imidization of the polymer. At the beginning of this step, orthodichlorobenzene was added to the solution and allowed to reflux into a Dean Stark trap to facilitate the removal of water which can cleave the amide bond and reduce molecular weight. Great care was taken to remove water from all aspects of the

synthesis to further the reactions and prevent chain scissioning. This was done through drying all chemicals over dried molecular sieves, drying the monomer before addition, flaming and purging all glassware, and maintaining a pure N_2 purge during all steps of the reactions. Once imidization was complete, the solution was precipitated into a 50/50 water/methanol mixture to phase separate the polymer. The polymer was then blended and washed multiple times with the water/methanol solution at room temperature to remove as much NMP as possible. Further details of this reaction are described elsewhere; however, thermal imidization was used in the present work to achieve a higher degree of imidization [2]. A single, large batch of this 6FDA-DAM:DABA (2:1) polymer (~120 g) was synthesized and used to conduct all of the work presented in this thesis in order to eliminate variation from different batches complicating the studies.

Ethylene glycol and 1,4-benzenedimethanol, shown in Figure 3.2, were chosen as the two crosslinking agents for the physical aging and $scCO_2$ conditioning studies. These crosslinking agents represent the smallest possible crosslink and a large, rigid crosslink in order to better understand the effects of crosslinking for the two studies.

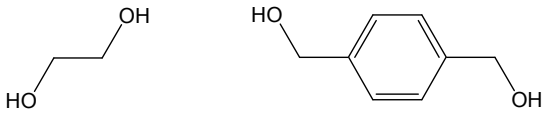

Figure 3.2: Ethylene glycol and 1,4-benzenedimethanol crosslinking agents

To create a crosslinkable polymer, approximately 5-10 g of the free acid (the base 6FDA-DAM:DABA (2:1) polymer with an open carboxylic acid site) was added to NMP to make a 6 wt% solution. An acid catalyst, p-toluene sulfonic acid, was then added in the amount of 1.7 mg catalyst/g polymer, and a large excess of glycol was added in the amount of approximately 70 times the stoichiometric requirement. This solution was

then heated to 140 ^{o}C for 18-24 hours to react one end of the glycol to the carboxylic acid and form the monoesterified polymer. During this heated step, water was distilled from the solution to drive the reaction toward esterification [3]. The monoesterified polymer solution was then precipitated in the same way as the polymer synthesis. To complete the crosslinking reaction, polymer films are solution cast and annealed to high temperatures which will be discussed in later sections. Again, further details of this crosslinking procedure are described elsewhere; however, about 1/3 of the amount of catalyst was used in the present work [2].

Approximately 18 years ago, research was conducted to study the effects of various 6FDA-based polyimide isomers to better understand how each moiety affected gas permeation and sorption properties. Many of these film samples were saved and stored at room conditions in a dry environment until recently where a few have been selected to be re-examined to study the effects of these different moieties on long-term physical aging. The following polymers were selected, and shown below in Figure 3.3, to study these effects: 6FDA-6FpDA, 6FDA-6FmDA, and BPDA-6FpDA. The original polymer was supplied by the Hoechst Celanese Corporation, and the details of the membrane film preparation of these polymers are presented elsewhere [4]. Polymer films from both originally cast films and masked films were selected to be retested.

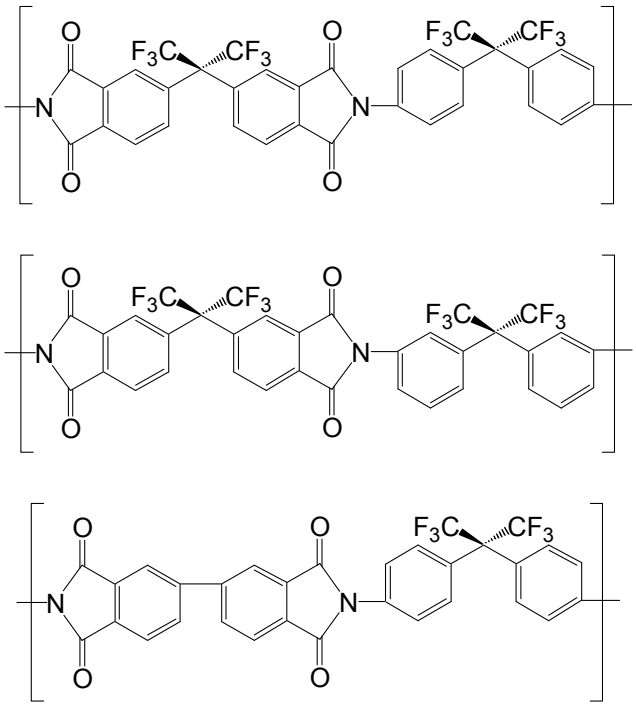

Figure 3.3: Chemical structures of 6FDA-6FpDA, 6FDA-6FmDA, and BPDA-6FpDA respectively

3.3 Gases

Since the nature of this work is to study the effects of physical aging on the 6FDA-DAM:DABA (2:1) polymer and crosslinkable derivatives for the purposes of natural gas purification, pure CO_2 and pure CH_4 were chosen to probe the polymers for gas permeation and sorption. These films were probed with He as well, which provides a test with a non-interacting gas of similar permeability to CO_2. Finally, to investigate the effects that physical aging may have on the separation of a gas mixture, gas permeation measurements were conducted using a 90/10 CH_4/CO_2 gas mixture. For the $scCO_2$ conditioning study of the 6FDA-DAM:DABA (2:1) polymer, a special CO_2 cylinder that contains a dip tube was used to fill the Isco syringe pump with liquid CO_2 thus enabling the pump to run longer with fewer refills. As before, a gas mixture of 50/50 CH_4/CO_2

was used to probe the conditioned samples to determine the effects conditioning may have on the separation of a mixed gas feed. For the long-term physical aging study of the 6FDA-based polyimide isomers, CH_4, N_2, O_2, and CO_2 were used for permeation and sorption measurements to mirror the work performed at the onset of physical aging. The gases, grade, and purity for all of this work are presented below in Table 3.1. All gases for the present work were supplied by Airgas. The gas information for the initial measurements of the long-term aged polyimides is presented elsewhere [4].

Table 3.1: Gas information for polymer preparation, permeation, and sorption

Gas	Grade	Purity
CO_2	Research	99.998%
CO_2 w/ Dip Tube	Specialty	99.9995%
CH_4	Research	99.99%
90/10 CH_4/ CO_2	Certified Gas Standard (±2%)	10.00% CO_2
50/50 CH_4/ CO_2	Certified Gas Standard (±2%)	50.0% CO_2
He	Research	99.9999%
O_2	Research	99.999%
N_2	Ultra High Purity	99.999%

3.4 Experimental Equipment

3.4.1 Gas Permeation

The gas permeation measurements in this work were acquired using constant-volume, variable-pressure systems. However, certain modifications to typical gas permeation systems described in have been performed to tailor the systems to each of the studies in this work [5,6]. The permeation systems used for the physical aging study of the 6FDA-DAM:DABA (2:1) polymers were outfitted with two different downstream volumes (10 mL and 500 mL) to allow for the low gas flux of thick, dense films (~50 μm) and high gas flux of the thin films (~600 nm). The large downstream volume was isolated from the rest of the downstream with a valve. In order to maintain constant upstream pressure during high-flux gas permeation measurements, a 1000 mL volume was also added to the upstream with a valve to isolate it during low-flux measurements. This dual-volume configuration is displayed below in Figure 3.4. All physical aging experiments were conducted at 35 ^{o}C.

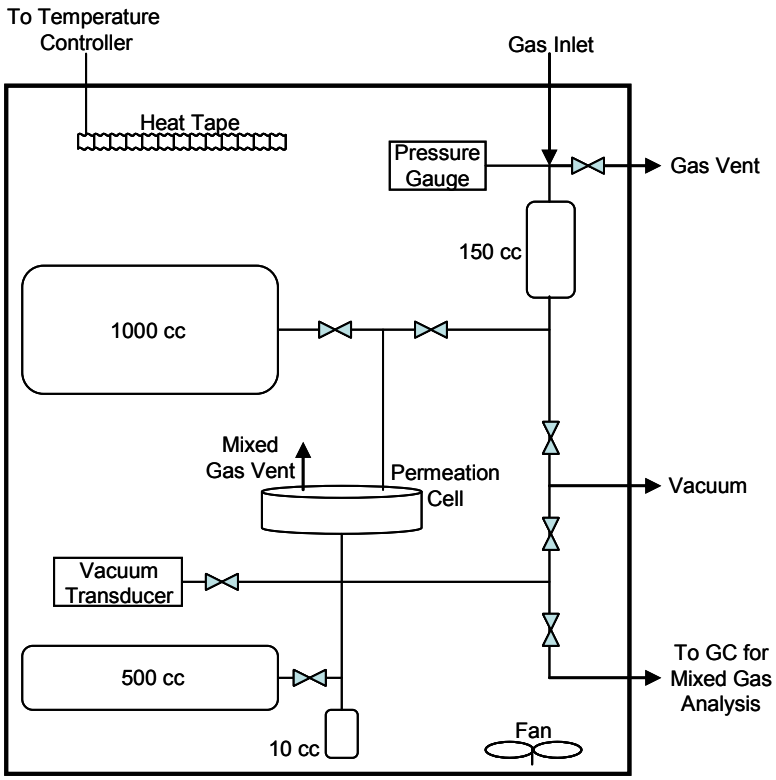

Figure 3.4: Constant-volume, variable-pressure permeation system with dual upstream and downstream volumes

For the $scCO_2$ conditioning study with the 6FDA-DAM:DABA (2:1) polymers, a 500 cc Isco syringe pump (500D Model) was connected between the gas cylinder and upstream side of the membrane cell in order to generate the high pressures required for the supercritical state of CO_2. A schematic of this high-pressure permeation system is shown below in Figure 3.5, and further details of the system are described elsewhere [7]. All $scCO_2$ permeation experiments were conducted at 35 ^oC.

Permeation measurements for the long-term aging of the 6FDA-based polyimide isomers were conducted on the same permeation systems as the 6FDA-DAM:DABA (2:1) physical aging experiments.

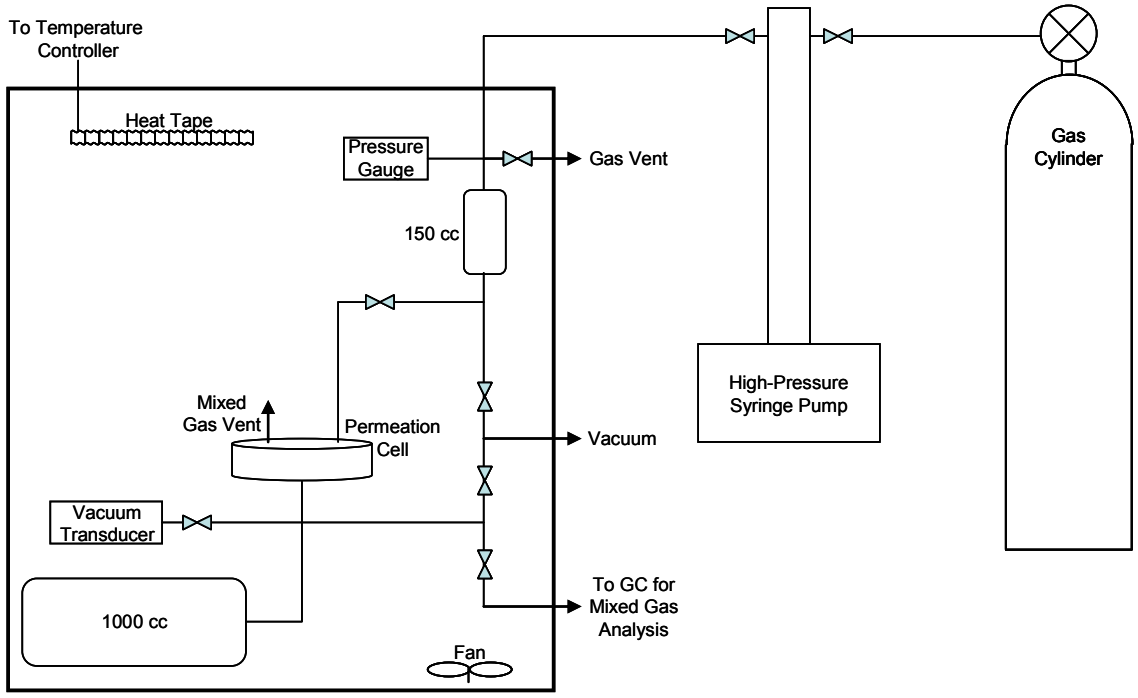

Figure 3.5: High-pressure permeation system with Isco syringe pump

The permeate from the 90/10 and 50/50 CH_4/CO_2 mixed gas permeations was analyzed using a Hewlett Packard 5890 Series II GC equipped with an 8' HayesepQ 80/100 mesh column. The details of the GC conditions and sample injection can be found elsewhere [8].

3.4.2 Gas Sorption

Sorption measurements were performed using the gravimetric sorption technique; however, each study was conducted with a different experimental setup and chamber depending on the needs of the experiment. The sorption chamber for the $scCO_2$ conditioning measurements was a high-pressure Jerguson transparent gauge (model 19-TCH-32) that has been outfitted with a bolted flange on one end to allow access to the inner chamber. The stock gaskets between the chamber and borosilicate

glass were replaced with Grafoil gaskets to provide a better seal in the $scCO_2$ environment. A Grafoil gasket was also used in the flange. The maximum pressure for this gauge is 3000 psia. Dilation and sorption measurements were taken simultaneously using the apparatus shown in Figure 3.6.

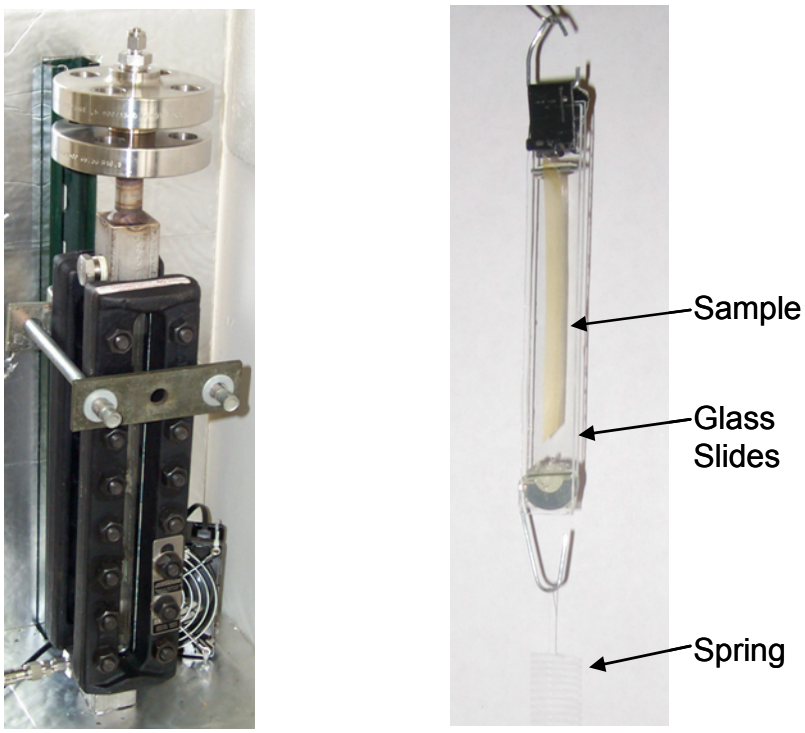

Figure 3.6: Picture of high pressure chamber for quartz spring sorption and dilation sample holder

The dilation sample was sandwiched between two glass slides and fixed at the upper end to allow measurements of the free-standing lower end as the polymer dilates. Two metal wires were epoxied into place at the top and bottom of one of the glass slides to maintain a gap of about 1/16" between the slides. The quartz spring was attached to a paper clip hook at the bottom of the glass slides to allow the sorption sample to be suspended beneath the dilation sample. Two cathetometers were then set to measure

the movements of both samples during experiments. An Isco syringe pump was again used to pressurize the CO_2 into the supercritical state for conditioning measurements. A schematic of this sorption system is shown below in Figure 3.7.

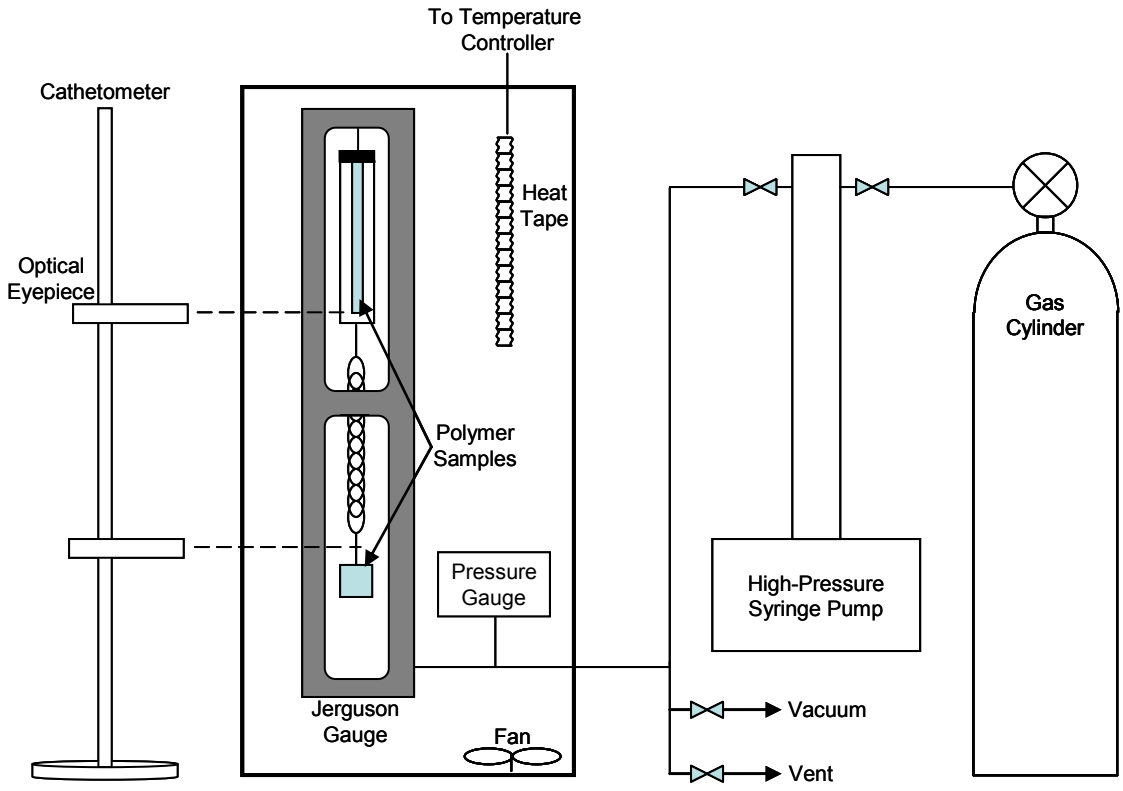

Figure 3.7: Schematic of high-pressure gravimetric sorption apparatus

Sorption measurements for the long-term aging of the 6FDA-based polyimide isomers were taken using a similar system as described above with a few differences. A medium-pressure Jerguson transparent gauge (model 23-TL-10) was used since the 2" chamber diameter allows for greater ease in loading and unloading samples than the 5/8" chamber diameter of the 19-TCH-32 model. A Bausch and Lomb optical reader was used in lieu of a cathetometer to provide more accurate measurements since these

polyimides have much lower sorption capacity for CH_4 and N_2 as compared to O_2 and CO_2.

The quartz springs were calibrated with known weights and a cathetometer, and the spring constants ranged from 0.34-0.59 cm/mg. In all cases, the buoyancy of the sample, copper wire used to hold the sample, and the spring itself were determined and also included in the sorption calculations [9]. All sorption experiments were conducted at 35 ^{o}C.

3.5 Membrane Preparation

3.5.1 Casting

All thick membrane films were solution cast into a Teflon® mold in a controlled environment glove bag. The glove bag was purged with pure nitrogen for 15 minutes to remove water and then saturated with THF from an open jar within the bag for 15 minutes. A 5 wt% polymer solution in THF was then filtered with a syringe through a 0.20 μm PTFE filter into the mold. The mold was covered with a glass dish to reduce the rate of THF evaporation. Approximately 24 hours later, the film was vitrified and could be removed from the glove bag. Thick film thicknesses range from 50 μm for the physical aging study to between 50 and 75 μm for the scCO_2 conditioning study. As mentioned earlier, all films for the long-term aging of the 6FDA-based polyimide isomers were cast between 1988 and 1991, and the details of that procedure can be found elsewhere [4].

To cast uniform, defect-free thin films, 9 wt% polymer solutions in cyclohexanone were spin coated onto bare silicon wafers in a cleanroom environment. The silicon wafers are n-type wafers with a crystal orientation of [1,0,0] and were provided by Waferworld, Inc. Only new wafers were used in the spin coating process. The polymer

solutions were filtered with a syringe through a 0.20 μm filter as before and then sonicated for 15 minutes to remove any bubbles. Once inside the cleanroom, the silicon wafer was rinsed thoroughly with filtered acetone and wiped dry with a chemwipe. The wafer was then centered on the spin chuck and rinsed again with acetone during a trial spin. A small quantity (~2 mL) of polymer solution was then poured onto the center of the wafer, and the spin coating process was started. The spin coating process consisted of a rapid ramp to 2300 rpm in 1 second followed by constant velocity at 2300 rpm for 70 seconds. Thin film thicknesses range from 550 nm to 700 nm.

Free-standing thin films were then formed by lifting the polymer film from the wafer onto a rectangular copper wire frame (0.005" diameter) [10]. Approximately 1" x 1" squares were cut into the film on the surface of the wafer with a razor blade, and de-ionized water was poured onto one of the seams. The water causes polymer delamination from the wafer surface allowing the wire frame to be placed underneath the film to collect the sample. The wire frame was shaped such that the polymer film only overlapped two sides of the frame to allow stress relaxation. Approximately, 7-9 free-standing samples were produced from one wafer.

3.5.2 Annealing Procedures

Glassy polymer properties are dependant on the thermal history of the polymer. Therefore, to conduct a comprehensive physical aging study, all samples must be prepared in the same manner to ensure repeatability and to accurately compare samples. When an asymmetric hollow fiber is initially spun, the polymer solution is quenched almost instantaneously in a non-solvent. In order to mirror this immediate quench and remove all thermal history of the samples, each sample was annealed above the glass transition temperature and rapidly quenched by removing it from the

oven directly to ambient conditions. Because the glass transition temperature for the 6FDA-DAM:DABA (2:1) free acid and crosslinkable derivatives is so high (374 ^{o}C), a Thermcraft split-tube furnace was outfitted with an internal thermocouple for temperature control and a helium purge to create an inert annealing environment. The furnace tube was purged with at least 10 times its volume prior to thermal annealing, and the helium purge was maintained at approximately 50 sccm during the annealing process. All samples, both thick and thin, were annealed in a free-standing state. The thermal annealing procedures for both the free acid and crossliked films are shown below in Figure 3.8.

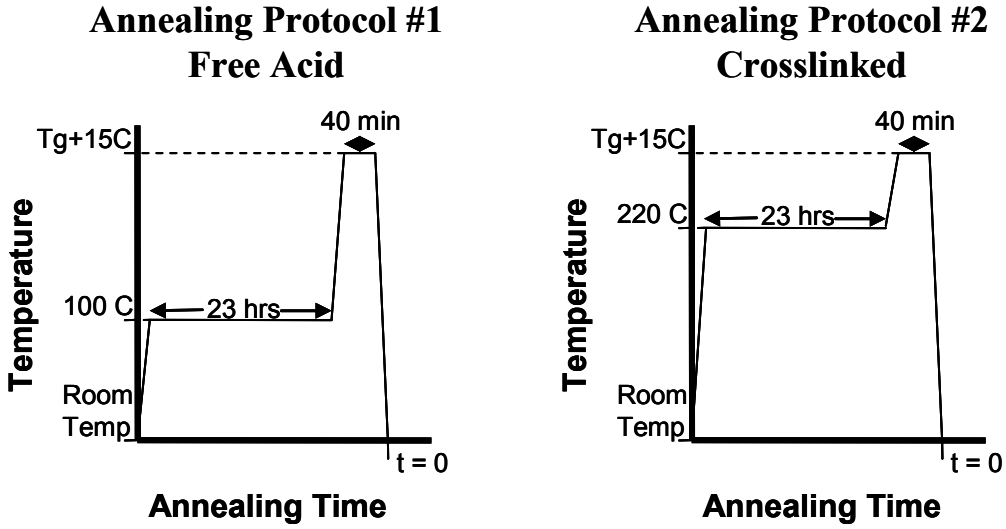

Figure 3.8: Thermal annealing profiles for the 6FDA-DAM:DABA (2:1) free acid and crosslinked films

The free acid polymer was dried at low temperatures for 23 hours to remove any residual casting solvent and annealed to 15 degrees above T_G for 40 minutes; whereas, the crosslinked polymer is dried at 220 ^{o}C for 23 hours to complete the crosslinking reaction before annealing above T_G for 40 minutes. At the 40 minute mark, the films

were rapidly quenched to room temperature through immediate removal from the pyrolysis oven, which took approximately 2 to 4 seconds. This point of removal is considered time zero for the aging study. For the rest of this work, the 100 ^{o}C procedure in Figure 3.8 will be referred to as 'Annealing Protocol #1', and the 220 ^{o}C procedure will be referred to as 'Annealing Protocol #2'.

The 6FDA-DAM:DABA (2:1) free acid and crosslinked thick films for the $scCO_2$ conditioning study were annealed at 220 ^{o}C for 48 hours in a vacuum oven. Liquid N_2 was maintained in the vacuum traps during annealing.

3.5.3 Membrane Masking

Two different masking procedures were employed for permeation testing. For the physical aging study of the 6FDA-DAM:DABA (2:1) polymer, films were sandwiched between two pieces of aluminum tape with center holes cut out. A schematic of this membrane mask is shown in Figure 3.9. Unlike the typical masking procedure, no epoxy was applied to the perimeter of the sample to seal the interface of the membrane and tape. This allowed free range of motion without restrictions to the sample as it aged. Since these samples were only probed with 2 atm of gas, there was no leakage of the gas around the sample through the tape adhesive, even with CO_2. For the thin film samples, a Whatman® Anopore membrane support with 0.02 μm pores was placed on the downstream side of the film to prevent tearing when pressure is applied. The resistance to gas permeation associated with this support is negligible. The thick films did not require this support. For polymer characterization samples that were probed with high pressures, Duralco 4525 high-temperature epoxy was applied to the membrane tape interface to prevent bypass through the adhesive. This type of mask, which is not taped to the permeation cell, allowed for samples to be placed into and removed from

the cell without damaging the mask. Therefore, permeation systems could be kept in constant use while samples not in use were stored in a vacuum oven.

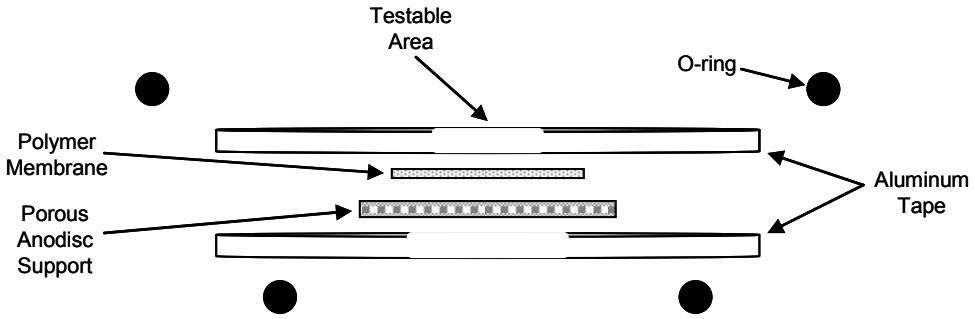

Figure 3.9: Cross-section of a membrane mask for physical aging of the 6FDA-DAM:DABA (2:1) polymers

To be consistent with previous work, masking of the $scCO_2$ conditioning samples was between a thick aluminum sheet and aluminum tape [5]. Duralco 4525 epoxy was applied to seal the interface of the aluminum sheet and the sample. The mask was then placed inside a permeation cell, and vacuum was pulled on the downstream for 24 hours to allow the epoxy to cure over a flattened sample. After approximately 1 hour, the epoxy was checked for air bubbles to ensure no weak points existed in the mask. This epoxy was specifically chosen for these high pressure CO_2 tests because the polymer film did not delaminate from the epoxy during conditioning.

To mask the 6FDA-based polyimide isomers, the same procedure as the aging of the 6FDA-DAM:DABA (2:1) polymers was used; however, Devcon 5-minute epoxy (#14250) was applied to seal the tape edge to prevent bypass since some of the samples had time lags of many hours. Once the epoxy was applied, the sample was quickly loaded into a permeation cell, and vacuum was pulled on the downstream until the epoxy set.

3.6 Permeation and Sorption Procedures

3.6.1 Physical Aging of the 6FDA-DAM:DABA (2:1) Polymers

The masking procedure for permeation testing of a polymer film takes approximately 15 minutes; therefore, the time between the rapid quench and when the films are loaded into a permeation cell and system is about 25 minutes. Vacuum was then pulled on both the upstream and downstream for one hour to degas the film and system. Therefore, the first gas was tested at approximately 1.5 hours into the physical aging process. For the permeation measurements, gases were allowed to permeate for at least 10 time lags before data collection was started. Since the time lag for the thin films is negligible, the gas was allowed to permeate for 5 minutes to allow the gas to reach thermal equilibrium in the system. Thick film permeation was conducted with the large upstream and downstream volumes isolated from the system; whereas, thin film permeation utilized these volumes due to the high fluxes of the gases. The sequence of gas testing for all physical aging films was He, CH_4, CO_2, and the 90/10 CH_4/CO_2 gas mixture; and, as stated earlier, all gases were tested at 2 atm to probe the effects of physical aging without affecting the polymer. Polymer films were generally kept in the permeation system for the first 4-6 days of physical aging. Beyond that time, the sample was removed from the cell after the series of gas testing and stored under vacuum in a vacuum oven at 35 ^{o}C.

To obtain enough mass for gravimetric sorption, four polymer coated silicon wafers were prepared, and the polymer films were removed with a copper wire frame measuring 4.5” in diameter. These films were then annealed 15 degrees above T_G in an inert environment for 40 minutes inside a Hewlett Packard 5880 GC oven. Once thermally quenched, the samples were tied together with the 0.005” copper wire and

placed inside the gravimetric sorption chamber. The timing of the sorption measurements was nearly identical to that of the permeation measurements. However, only CH_4 and CO_2 were used to probe the physical aging effects on polymer sorption.

3.6.2 Supercritical Carbon Dioxide Conditioning of the 6FDA-DAM:DABA (2:1) Polymers

The $scCO_2$ conditioning permeation isotherms consist of a pressurization cycle up to 1500 psia at 150 psi intervals, approximately 10 days at constant pressure, and a depressurization cycle at 150 psi intervals. At high pressures, CO_2 plasticizes and can induce glassy state relaxations in the polymer; therefore, permeabilities may no longer be constant after ten time lags of permeation, and they vary with conditioning time and pressure interval. As a result, true steady-state CO_2 permeabilities can not be determined upon pressurization and depressurization of the system. Therefore, a defined conditioning time of 12 ± 1 hours was chosen for each pressure interval following which the permeability measurement was taken. After the measurement, the pressure was immediately increased to the next interval setpoint. Following the 10 day isobaric conditioning, the depressurization cycle was started. This cycle consisted of a 5 hour pressure reduction at a rate of 0.5 psi/min and a 7 hour conditioning time at that pressure interval, following which the permeability measurement was taken.

The $scCO_2$ sorption experiments were conducted in exactly the same manner as the $scCO_2$ permeation experiments.

3.6.3 Long-term Physical Aging of the 6FDA-based Polyimide Isomers

All permeation and sorption measurements were taken after 10 time lags of permeation or gas exposure.

3.7 Secondary Polymer Characterization Techniques

3.7.1 Gel Permeation Chromatography

The molecular weight of the 6FDA-DAM:DABA (2:1) free acid polymer used for the physical aging and $scCO_2$ conditioning work was determined using a GPC. The sample was prepared as a 4 wt% solution in THF and analyzed by James Russum in the School of Chemical & Biomolecular Engineering at the Georgia Institute of Technology. The GPC used a polystyrene standard to quantatively determine the number and weight average molecular weights.

3.7.2 Differential Scanning Calorimetry

The glass transition temperature of the 6FDA-DAM:DABA (2:1) free acid polymer was determined using a DSC in the Tennenbaum Research Group of the School of Materials Science and Engineering at the Georgia Institute of Technology. The second heat cycle with a midpoint determinant was used to determine the glass transition temperature.

3.7.3 Fourier Transform Infrared Spectroscopy

FTIR was used to qualitatively determine the extent of imidization of the 6FDA-DAM:DABA (2:1) polymers and to examine the polymer for any chemical changes

following the high-temperature annealing process associated with resetting the thermal history of the polymer. A Bruker Tensor 27 instrument with a resolution of 4 cm^{-1} and at least 64 scans was used to measure the absorbance of polymers films. In the case of this tool used in conjuction with TGA, the external detector was purged with N_2 overnight and was filled with liquid N_2 at least 30 minutes before measurement began.

3.7.4 H-Nuclear Magnetic Resonance

Proton NMR was used to determine the extent of reaction for the monoesterification procedure. When the diol was chemically attached to the open acid site of the 6FDA-DAM:DABA (2:1) free acid polymer, the diol hydrogen peaks were measured relative to other hydrogen peaks from the polymer backbone to quantitatively determine how many open acid sites were esterified. 2.5 wt% solutions in deuterated-DMSO were measured on a Varian Mercury Vx 300 in the School of Chemistry at the Georgia Institute of Technology.

3.7.5 C-Nuclear Magnetic Resonance

Carbon NMR was used to determine changes in the polymer structure following thermal treatment above T_G. Cleavage of any carbon-containing species from the polymer backbone will result in reduced peak intensity in C-NMR. Approximately 50 mg of fine polymer powder was prepared and run on a Bruker DSX 300 in the School of Chemistry at the Georgia Institute of Technology.

3.7.6 Density Gradient Column

A Techne DC-1 density gradient column was used to measure the density of the polymer films. Calcium nitrate tetrahydrate in de-ionized water solutions were used to assemble the column which was calibrated with glass floats with an accuracy of 0.0001 g/cm^3.

3.7.7 Spectroscopic Ellipsometry

Spectroscopic ellipsometery was used to measure the thickness and refractive index of the thin 6FDA-DAM:DABA (2:1) polymer films [10]. The EASE program was used on a J.A. Woollam M-2000 to allow for model fitting with the controlled environment attachment. The model used a single Cauchy layer was used on top of a 1nm, fixed SiO_2 layer. Thickness, A, B, C, and the Delta offsets for the glass windows were fit using the model.

3.7.8 Fluorescence Spectroscopy

Fluorescence spectroscopy was used to measure trends in charge transfer complexing of the polyimides in this work. Polymer films were measured using a 50x objective at 365 nm on a CRAIC 1000 spectrometer in the Srinivasarao Research Group of the School of Polymer, Textile & Fiber Engineering at the Georgia Institute of Technology.

3.7.9 Thermogravimetric Analysis

TGA was used to measure mass loss of a sample under various thermal treatments. This technique was often employed in conjuction with FTIR to measure the

spectra of the evolved gases. A Netzsch STA 409PC in instrument with an N_2 flow rate of 30 mL/min was used for all samples.

3.7.10 Prism Wave-Guide Coupler

A Metricon PC-2010 prism coupler was used to measure the refractive indices of thick polymer films [11].

3.7.11 Wide-Angle X-ray Diffraction

WAXD measurements were performed by the Kumar Research Group of the School of Polymer, Textile & Fiber Engineering at the Georgia Institute of Technology. The d-spacing values were determined using the AreaMax software.

3.8 References

1. Ohya, H., Kudryavtsev, V. V. & Semenova, S. I., *Polyimide Membranes: Applications, Fabrications, and Properties*, Tokyo: Kodansha Ltd. (1996).
2. Wind, John, *Improving Polyimide Membrane Resistance to Carbon Dioxide Plasticization in Natural Gas Separations*, Dissertation, University of Texas-Austin (2002).
3. Wind, J. D., Staudt-Bickel, C., et al., "Solid-state covalent cross-linking of polyimide membranes for carbon dioxide plasticization reduction", *Macromolecules*, **36**(6), 1882-1888 (2003).
4. Coleman, Maria, *Isomers of Fluorine-Containing Polyimides For Gas Separation Membranes*, Dissertation, University of Texas-Austin (1992).
5. Moore, Theodore T., et al., "Characterization of low permeability gas separation membranes and barrier materials; design and operation considerations", *Journal of Membrane Science*, **245**(1-2), 227-231 (2004).
6. Perry, John, *Formation and Characterization of Hybrid Membranes Utilizing High-Performance Polyimides and Carbon Molecular Sieves*, Dissertation, Georgia Institute of Technology (2007).
7. Damle, Shilpa & Koros, William J., "Permeation equipment for high-pressure gas separation membranes", *Industrial & Engineering Chemistry Research*, **42**(25), 6389-6395 (2003).
8. Moore, Theodore, *Effects of Materials, Processing, and Operating Conditions on the Morphology and Gas Transport Properties of Mixed Matrix Membranes*, Dissertation, University of Texas-Austin (2004).

9. Punsalan, David, *A Sorption and Dilation Investigation of Amorphous Glassy Polymers and Physical Aging*, Disseration, University of Texas-Austin (2001).
10. Huang, Y. & Paul, D. R., “Experimental methods for tracking physical aging of thin glassy polymer films by gas permeation”, *Journal of Membrane Science*, **244**(1-2), 167-178 (2004).
11. Hardaker, S. S., et al., “Quantitative characterization of optical anisotropy in high refractive index films”, *Journal of Polymer Science Part B – Polymer Physics*, **31**(13), 1951-1963 (1993).

4.0 THICKNESS DEPENDENT PHYSICAL AGING OF A CROSSLINKABLE POLYIMIDE

4.1 Introduction

This chapter presents the research focused on the physical aging of the 6FDA-DAM:DABA (2:1) polyimide and the crosslinked derivatives. A polymer characterization analysis is first presented to confirm the efficacy of the polymer used in this work. Thick and thin film physical aging results for the polyimide are then presented and discussed for the free acid and crosslinked derivatives to understand the effects that physical aging has on the gas separation properties of the polymer. Various observations and phenomena pertaining to the physical aging of the free acid and crosslinked films are discussed. Finally, the effects of physical aging as monitored through secondary characterization techniques such as gas sorption, refractive index, and wide-angle x-ray diffraction are discussed.

4.2 Polyimide Verification

Once the large batch of 6FDA-DAM:DABA (2:1) was synthesized, it was examined with GPC, DSC, IR, NMR, gas permeation, and gas sorption to ensure that the polymer and crosslinkable derivatives matched that of previous work. The GPC results exhibited a normal distribution with a small hump at the tail end which corresponds to 1-2 repeat unit oligomers. When these small oligomers are excluded from the molecular weight determination, the number average molecular weight of the 6FDA-DAM:DABA (2:1) polymer is 59,600 g/mol with a PDI of 2.11. This molecular

weight was deemed sufficient for subsequent monoesterification reactions to produce the crosslinkable derivatives. GPC was not run on the crosslinkable polymers to determine the extent of chain scissioning from the reaction; however, the batches of crosslinkable polymer used for all subsequent work yielded films that were creasable which suggests the molecular weight is sufficiently high.

DSC tests using the midpoint transition of the second heat cycle revealed a glass transition temperature of 374 ^{o}C which is within the range (358-376 ^{o}C) reported elsewhere for this polymer [1,2]. IR measurements of 6FDA-DAM:DABA (2:1) free acid film samples confirmed as complete imidization as is detectable with this technique. A free acid film dried at 60 ^{o}C is compared to a free acid film annealed using Annealing Protocol #1 in Figure 4.1.

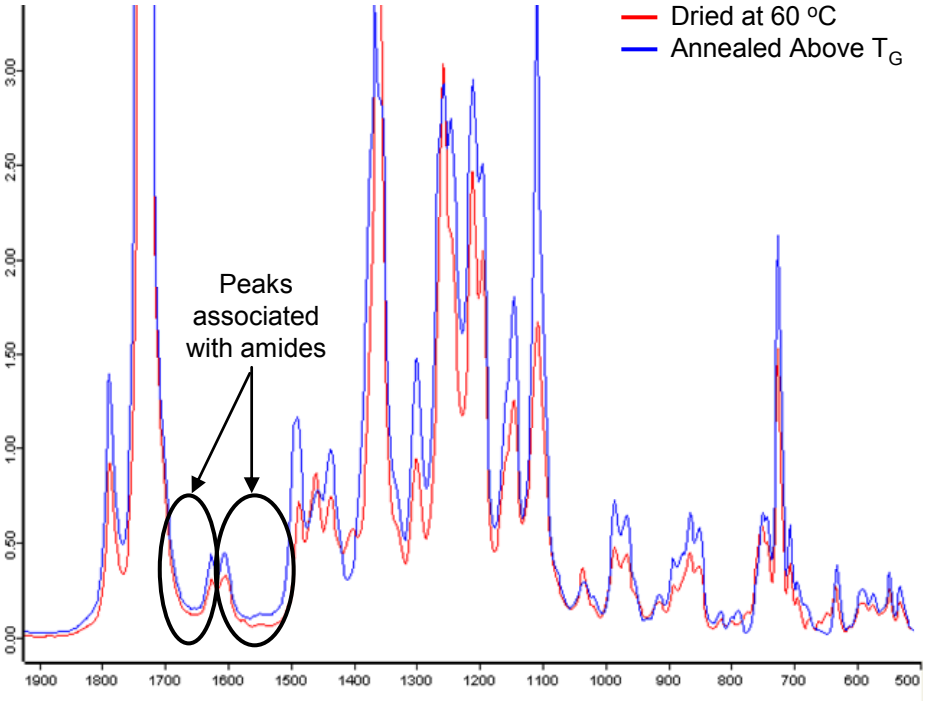

Figure 4.1: IR spectra of a dried free acid film and a free acid film rapidly quenched from above T_G

Amides show strong absorption at 1695-1630 cm^{-1} resulting from C=O stretching and an absorption at 1550 cm^{-1} associated with the bend-stretch of the H-N-C bond of a monosubstituted amide; whereas, cyclic imides exhibit a strong band from 1740-1670 cm^{-1} [3]. Since there are no peaks in the initial spectrum at 1650 cm^{-1} and 1550 cm^{-1} and these troughs do not change as the polymer is heated above T_G, this measurement confirms that the thermal imidization process described in Chapter 3.2 completed the imidization reaction.

Solution H-NMR was utilized to determine the extent of the monoesterification reaction which attaches the crosslinking agent to the acid group on the polymer backbone. This quantitative analysis is conducted by determining the ratio of the proton peaks associated with the crosslinking agent to proton peaks associated with parts of the polymer backbone. Because there are multiple proton peaks from the backbone and the 1,4-benzenedimethanol crosslinking agent to use for the analysis, all possible combinations were calculated and the minimum extent of reaction for each crosslinking agent is presented in Table 4.1.

Table 4.1: Monoesterification yield for the crosslinkable 6FDA-DAM:DABA (2:1) polymers

Crosslinking Agent	Monoesterification Yield
Ethylene Glycol	56%
1,4-Benzenedimethanol	63%

Since it is possible for the alcohol end of the crosslinking agent to react with either an open acid site or an acid site with another crosslinking agent attached, quantitative analysis to determine the extent of crosslinking is not possible. However, if all crosslinking agents only reacted with open acid sites, only 50% yield is required for complete crosslinking. Therefore, the yields reported in Table 4.1 were deemed sufficient for this work.

Gas permeation tests were conducted to ensure the synthesized 6FDA-DAM:DABA (2:1) and the crosslinkable derivatives yielded similar results to what is reported in literature [1,4]. CO_2 permeation isotherms for the free acid, ethylene glycol crosslinked, and 1,4-benzenedimethanol crosslinked films are presented in Figures 4.2 - 4.4. The free acid and ethylene glycol crosslinked films were annealed at 220 ^{o}C for 24 hours and the 1,4-benzenedimethanol crosslinked film was annealed at 295 ^{o}C for 24 hours to match the previous work with these polymers.

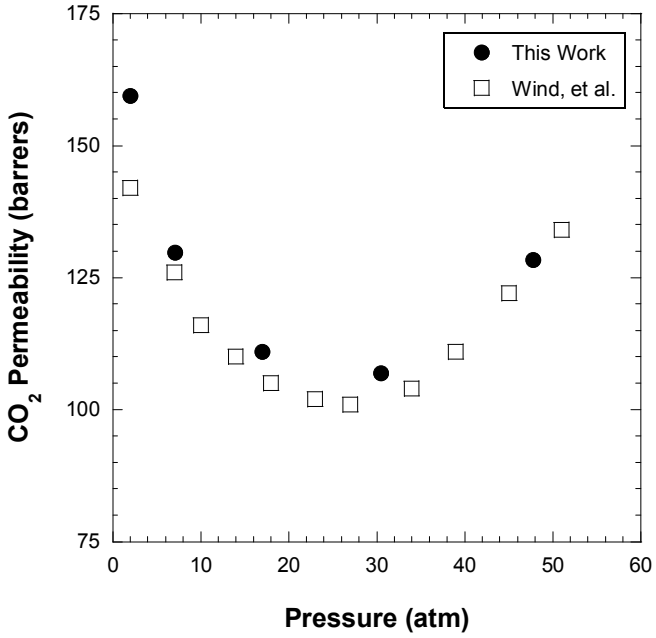

Figure 4.2: CO_2 permeation isotherms for the free acid polymer annealed at 220 ^oC for 24 hours. Permeation tests conducted at 35 ^oC (M-271). [4]

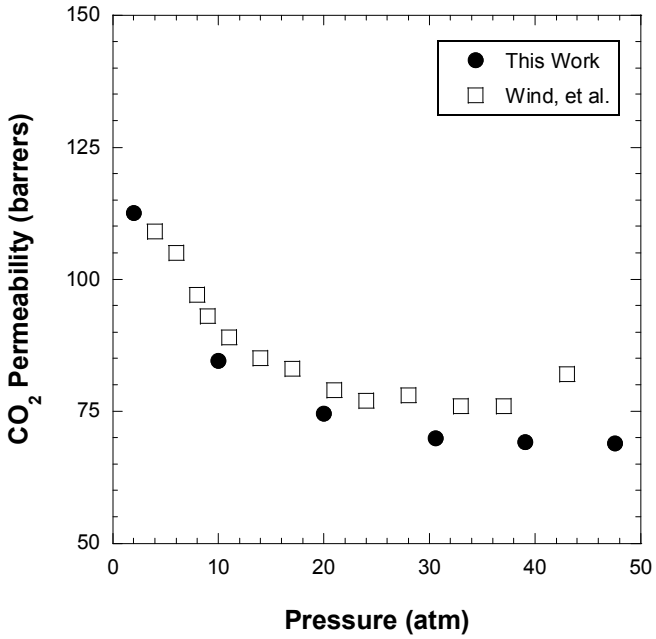

Figure 4.3: CO_2 permeation isotherms for the ethylene glycol crosslinked polymer annealed at 220 ^oC for 24 hours. Permeation tests conducted at 35 ^oC (M-222). [4]

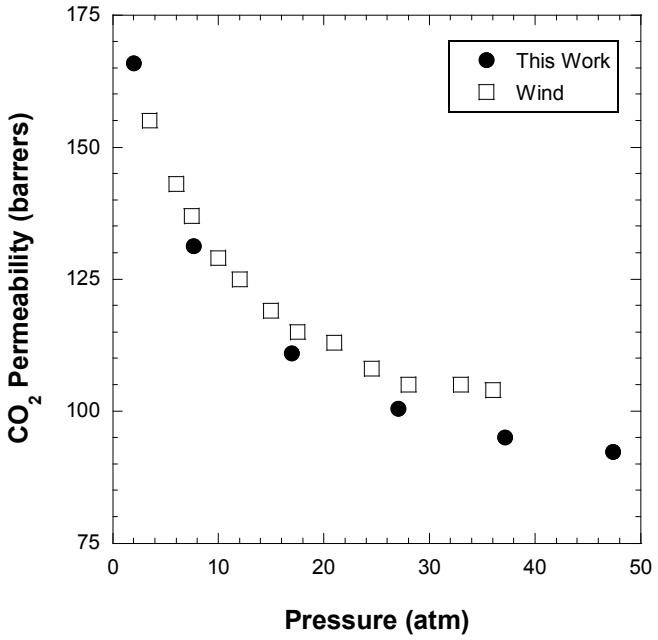

Figure 4.4: CO_2 permeation isotherms for the 1,4-benzenedimethanol crosslinked polymer annealed at 295 ^oC for 24 hours. Permeation tests conducted at 35 ^oC (M-282). [1]

As can be seen in the above figures, the free acid polymer for this work plasticizes at a similar pressure at 35 ^oC as that reported in literature, and the crosslinked films exhibit as good or better plasticization resistance compared to the crosslinked polymers from previous work.

Finally, CO_2 sorption was measured for the 6FDA-DAM:DABA (2:1) free acid polymer annealed at 220 ^oC for 24 hours and compared to that in literature with identical annealing history [5]. Figure 4.5 displays the sorption isotherm along with the Dual Mode model using the parameters from Wind, et al. Again, the CO_2 uptake is nearly identical to the previous work with this polymer. The Dual Mode sorption parameters are shown in Table 4.2 for comparison. The uncertainty associated with these parameters was determined from a model fit using Microcal Origin® software.

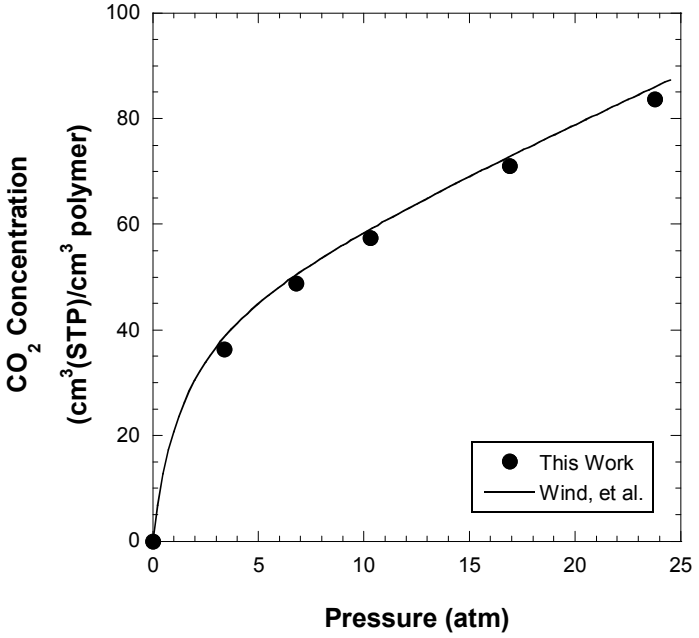

Figure 4.5: CO_2 sorption isotherm for the free acid polymer annealed at 220 °C for 24 hours. Sorption tests conducted at 35 °C (S-30). [5]

Table 4.2: Dual Mode model parameters for free acid films annealed at 220 °C

6FDA-DAM:DABA (2:1) Free Acid	k_D (cm^3 STP/(cm^3-atm))	C_H' (cm^3 STP/cm^3)	b (1/atm)
This Work	1.64 ± 0.01	48.1 ± 0.4	0.52 ± 0.01
Wind, et al.	1.77	46.60	0.689

Based on the analyses presented above, the 6FDA-DAM:DABA (2:1) free acid and ethylene glycol and 1,4-benzenedimethanol crosslinkable derivatives were determined to be sufficient for all work presented in this thesis.

4.3 The Effects of Annealing the 6FDA-DAM:DABA (2:1) Polymers Above T_G

When rapidly quenching the 6FDA-DAM:DABA (2:1) films from above T_G, large amounts of excess fee volume become trapped in the polymer matrix. In order to confirm this, CO_2 permeation and sorption isotherms were measured for the free acid polymer and compared to that of a film rapidly quenched from above T_G. Figure 4.6 displays the permeation isotherm for a film dried at 220 ^oC for 24 hours and a film annealed using the Annealing Protocol #2 discussed in Chapter 3.5.2. Protocol #2 was chosen for the free acid (ie noncrosslinkable) polymer in order to make a direct comparison to the film dried at 220 ^oC. However, since annealing above T_G erases any prior thermal history of the polymer, whether Protocol #1 or Protocol #2 is used should not affect the results of the free acid polymer. As expected with the entrapment of greater excess free volume, the free acid film rapidly quenched from above T_G exhibits more than double the CO_2 permeability of the film annealed to 220 ^oC. Surprisingly, the quenched film also exhibited greater plasticization resistance than the annealed film. This response is counter to what is expected of a higher free volume sample of the same polymer and will be discussed in greater detail in Chapter 5.

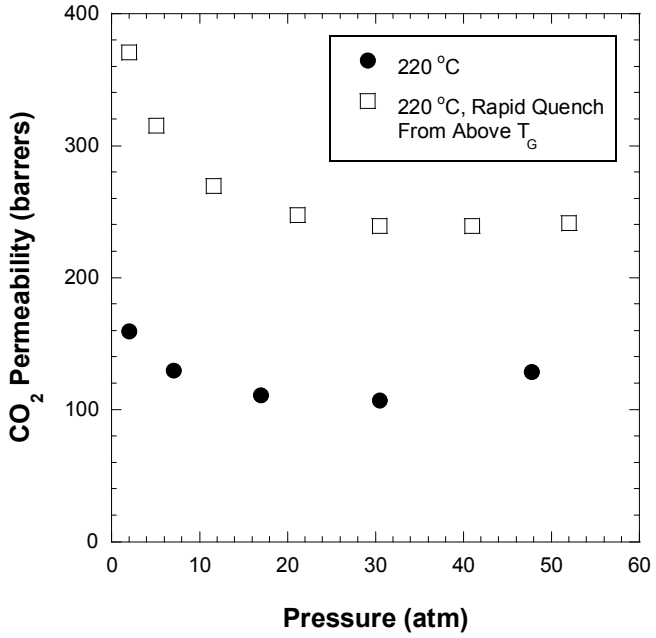

Figure 4.6: CO_2 permeation isotherms for free acid films annealed at 220 °C for 23 hours and annealed at 220 °C for 23 hours followed by rapid quenching from above T_G (M-271, M-305)

As with the permeation data above, CO_2 sorption isotherms were conducted on an annealed free acid film and a quenched free acid film. Figure 4.7 displays these results and provides the Dual Mode model fit for each data set, and Table 4.3 provides the Dual Mode model parameters.

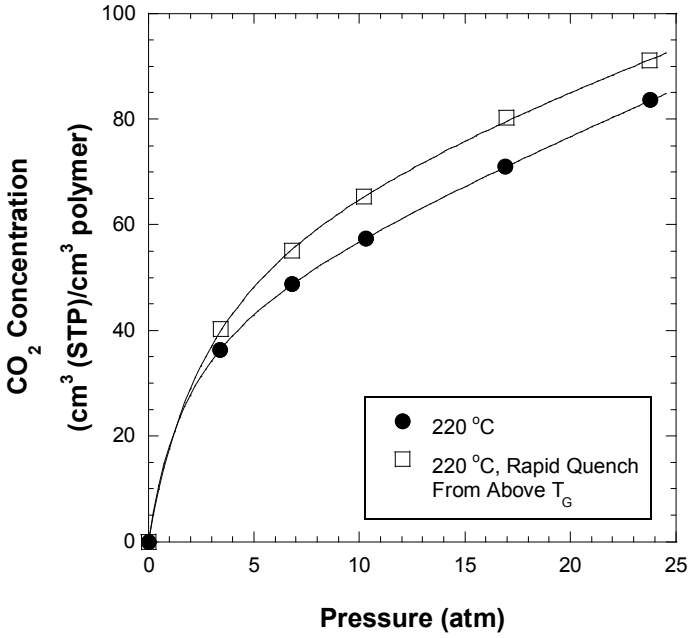

Figure 4.7: CO_2 sorption isotherms for free acid films annealed at 220 °C for 23 hours and annealed at 220 °C for 23 hours followed by rapid quenching from above T_G. Lines are the Dual Mode model fit for each data set (S-27, S-30).

Table 4.3: Dual Mode model parameters for free acid films annealed at 220 °C and annealed at 220 °C followed by rapid quenching from above T_G

6FDA-DAM:DABA (2:1) Free Acid Film	k_D (cm^3 STP/(cm^3-atm))	C_H' (cm^3 STP/cm^3)	b (1/atm)
220 °C	1.64	48.1	0.52
220 °C, Rapid Quench From Above T_G	1.33	67.5	0.32

Consistent with the permeation data, the quenched free acid film has a higher CO_2 sorption capacity than the annealed film which is highlighted by the significant increase in C_H' from 48.1 to 67.5 cm^3(STP)/cm^3. The decrease in k_D and b was not expected and

suggests that the rapid quench from above T_G altered the polymer in some way than just entrapping additional excess free volume. This possibility will be discussed in later sections and in Chapter 5. Nonetheless, these permeation and sorption data confirm large amounts of excess free volume are trapped within the polymer upon rapid quenching from above T_G.

4.4 Investigation of the Physical Aging of the 6FDA-DAM:DABA (2:1) Polymers Through Gas Permeation

4.4.1 Physical Aging Study Parameters

One of the goals of this study was to decouple the effects of crosslinking and the crosslinking agent on physical aging of the polyimide. Because the crosslinked derivatives contain the extra crosslinking moiety which occupies space, direct comparison of the free acid polymer to the crosslinked polymer is not possible. Therefore, physical aging of the free acid should be compared to that of the monoesterified, but uncrosslinked, polymer to determine the effect of the crosslinking moiety on the aging process. Moreover, physical aging of the monoesterified polymer should then be compared to that of the crosslinked polymer to determine the effect that crosslinking has on the aging process. To achieve these comparisons, monoesterified polymer was “thermally reset” using Annealing Protocol #1 to obtain physical aging results for an uncrosslinked polymer with the attached crosslinking agent. However, wide angle x-ray diffraction and gas permeation measurements comparing the monoesterified polymer annealed with Protocol #1 and Protocol #2 indicate the short, 40 minute anneal above T_G in Protocol #1 provided enough thermal energy for crosslinking to occur. Figure 4.8 displays the WAXD pattern of the ethylene glycol monoesterified polymer annealed using the two protocols, and the average d-spacing values are

essentially identical at 5.9 Å as determined by the AreaMax software. Figure 4.9, which displays the CO_2 permeability isotherm vs aging time of the same polymer, confirms little difference in gas permeation between the monoesterified polymer that is either dried or crosslinked before annealing above T_G.

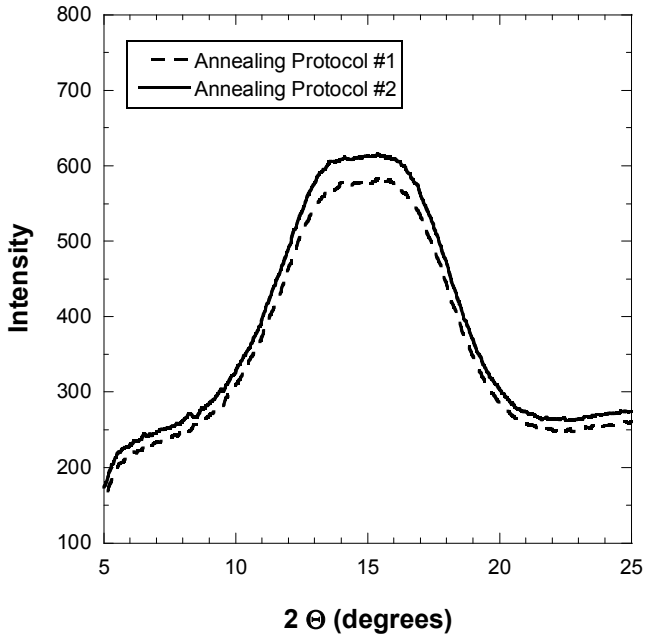

Figure 4.8: WAXD pattern for the ethylene glycol monoesterified polymer

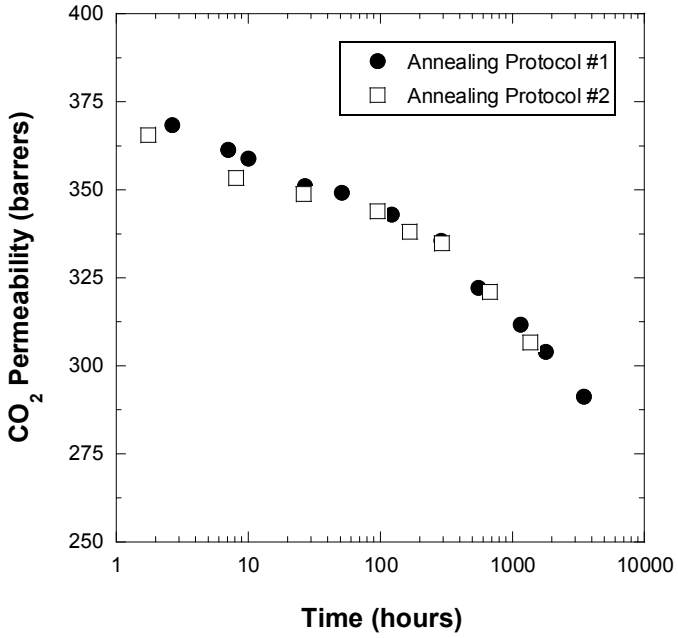

Figure 4.9: CO_2 permeability isotherm vs aging time for the ethylene glycol monoesterified polymer

Therefore, upon rapid quenching from above T_G, the monoesterified film annealed with Protocol #1 was nearly identical to the monoesterified film annealed with Protocol #2. For this reason, Chapter 4.4.2 and 4.4.3 discuss physical aging of the free acid and crosslinked films only and exclude physical aging of the monoesterified, uncrosslinked films.

Furthermore, the data analysis and discussion in this chapter regarding the physical aging of the free acid and the two crosslinked polymers do not, in fact, illuminate the differences in the physical aging of an uncrosslinked and crosslinked samples. As will be shown in Chapter 5, the free acid polymer, when thermally treated to temperatures above T_G, undergoes a decomposition of the carboxylic acid side group which results in a crosslinked sample. Therefore, the data presented in this chapter ultimately compares and discusses the physical aging of three different crosslinked 6FDA-DAM:DABA (2:1) polyimide derivatives, one through a side group degradation

crosslinking mechanism and two through a glycol esterification reaction at the carboxylic acid site.

4.4.2 Thick Film Physical Aging

4.4.2.1 Pure Gas Permeation

To understand the effects of physical aging, gas permeabilities are compared to "bulk" gas permeability values for each polymer. These bulk values are considered the standard permeabilities for the polymer and are useful as a point of reference. These bulk permeability values are obtained by drying the films at 220 ^{o}C for 24 hours, and the values for the free acid and crosslinked 6FDA-DAM:DABA (2:1) polymers are presented in Table 4.4. The CO_2 permeability value for the 1,4-benzenedimethanol crosslinked film is significantly less than what is presented in Figure 4.4 because this film is annealed to only 220 ^{o}C as opposed to 295 ^{o}C. This effect has been observed for the same polymer crosslinked with 1,4-cyclohexanedimethanol at 220 ^{o}C and 295 ^{o}C. In this case, there was a 3-fold increase in CO_2 permeability when annealed at 295 ^{o}C [5]. Wind et al. do not conclusively determine the cause of this permeability enhancement; however, they attribute this increase in permeability to an increase in free volume caused by either greater disruptions in chain packing through further crosslinking or elimination of the crosslinking agent that occurs during the crosslinking reaction.

Table 4.4: Bulk permeabilities for the free acid, monoesterified, and crosslinked 6FDA-DAM:DABA (2:1) polymers at 2 atm, 35 ^{o}C

Polymer	CO_2 Permeability (Barrers)	CH_4 Permeability (Barrers)	He Permeability (Barrers)	CO_2/ CH_4 Selectivity	He/ CH_4 Selectivity
Free Acid	159	4.64	196	34.3	42.2
Ethylene Glycol Crosslinked	126	3.60	165	35.0	45.8
1,4-Benzene-dimethanol Crosslinked	77	1.94	118	39.7	60.8

Physical aging of the free acid, ethylene glycol crosslinked, and 1,4-benzenedimethanol crosslinked thick films was examined by measuring gas permeation as a function of aging time. As mentioned earlier, these films are approximately 50 microns thick. The CO_2, CH_4, and He permeabilities along with the CO_2/CH_4 and He/CH_4 pure gas selectivities are presented in Figure 4.10.

As mentioned in Chapter 4.3, the initial gas permeabilities following the rapid quench from above T_G are significantly greater than the bulk values for these polymers. Therefore, even when crosslinked prior to annealing above T_G, the polymer has enough mobility in the rubbery state to allow excess amounts of free volume to become trapped in the polymer matrix. Surprisingly, there is not a significant difference in the initial gas permeabilities for the free acid and crosslinked films which implies that the size of the crosslink does not have a large effect on the amount of additional free volume acquired in the rubbery state.

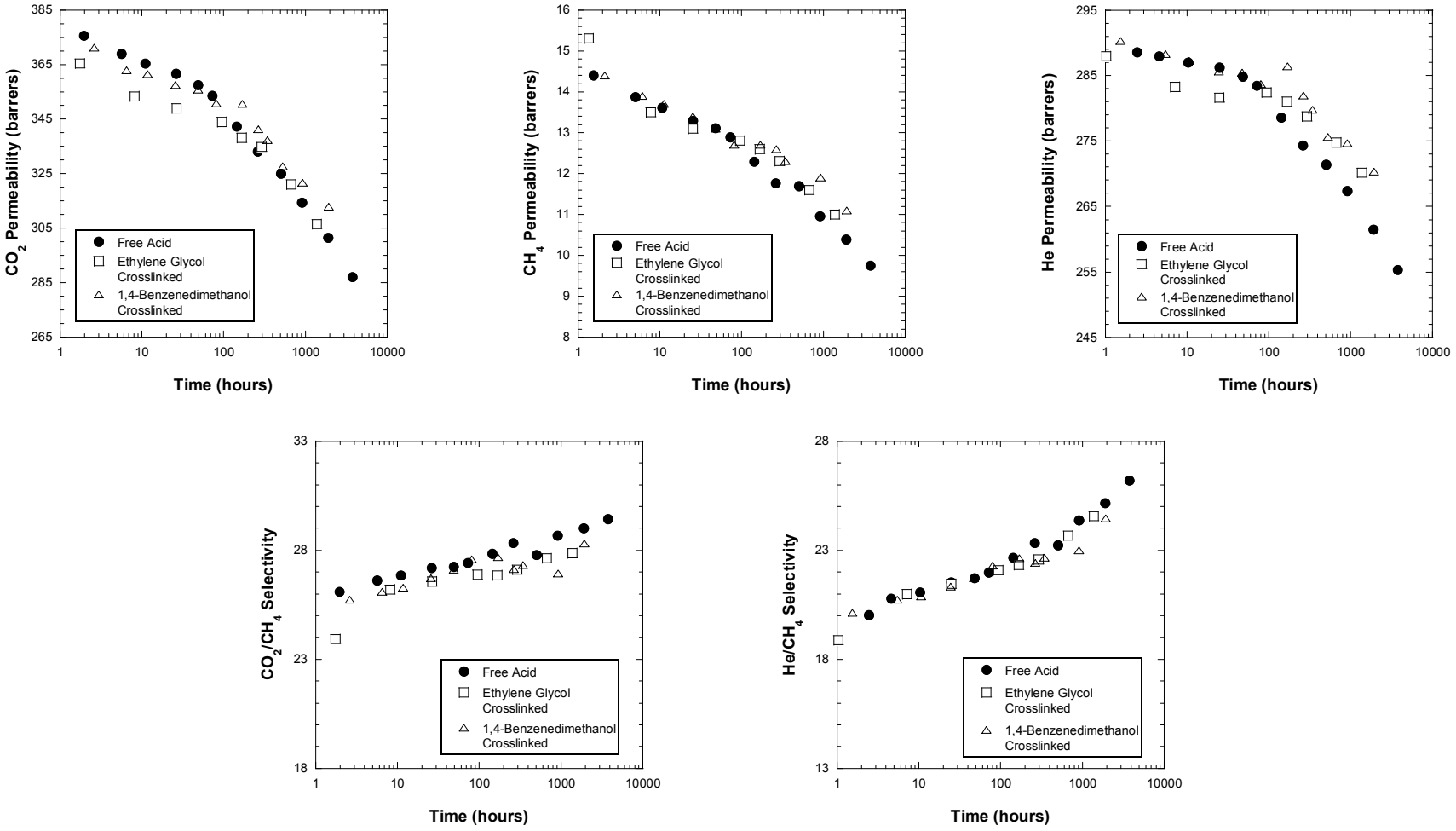

Figure 4.10: CO_2, CH_4, and He permeability isotherms and CO_2/CH_4 and He/CH_4 selectivity isotherms for the 6FDA-DAM:DABA (2:1) free acid, ethylene glycol crosslinked, and 1,4-benzenedimethanol crosslinked thick films. Gas permeation at 2 atm, 35 ^{o}C. (M-158, M-196, M-279)

After more than 1000 hours of aging, the gas permeabilities remain well above the bulk values for each of the polymers. One interesting thing to note, the bulk CO_2 permeabilities for all films are lower than the bulk He permeabilities. However, when rapidly quenched from above T_G, the CO_2 permeabilities of all films are higher than the He permeabilities. This is most likely a result of the significant increase in the Langmuir sorption capacity of the polymer following the rapid quench from above T_G. This increase greatly favors CO_2 transport over He transport since CO_2 is much more condensable than He.

In a corresponding manner, the CO_2/CH_4 and He/CH_4 selectivities begin below the bulk values for the free acid and crosslinked films and gradually increase with aging time. As in the case with the gas permeabilities, the selectivities never reach the bulk selectivity values after more than 1000 hours of physical aging. The increase in CO_2 permeabilities compared to the He permeabilities mentioned above is highlighted by the greater decrease in the initial He/CH_4 selectivities as compared to the CO_2/CH_4 selectivities as well. For the free acid polymer, this is illustrated by a 53% decrease in the He/CH_4 selectivity as compared to only a 24% decrease in the CO_2/CH_4 selectivity.

Ultimately, there is little difference in the physical aging rates of the thick films as observed through gas permeation. This result is somewhat expected considering that one of the two mechanisms of physical aging, diffusion of free volume, is greatly diminished at these sample thicknesses causing a much slower rate of physical aging. For these 50 μm thick samples, there is approximately only a 6%, 16%, and 24% decrease in the He, CO_2, and CH_4 permeabilities, respectively, with a 10% and 20% increase in the CO_2/CH_4 and He/CH_4 selectivities after 1000 hours of physical aging. As will be shown in a later section, penetrant solubility changes very little with aging time; therefore, the size of the penetrant is the dominant factor in determining changes in gas transport with respect to physical aging. This phenomenon is apparent with the

increasing percent change in permeability as penetrant size increases. This also illustrates the significant impact that removal of the excess free volume has on the penetrant size discriminating ability of the polymer.

4.4.2.2 90/10 CH_4/CO_2 Mixed Gas Permeation

The 90/10 CH_4/CO_2 mixed gas permeation yielded similar results for the free acid, ethylene glycol crosslinked, and 1,4-benzenedimethanol crosslinked films. However, the CO_2 permeabilities and CO_2/CH_4 separation factor for each film were quite different than the pure gas measurements. Only the free acid mixed gas permeation results are presented in Figures 4.11 and 4.12 for brevity.

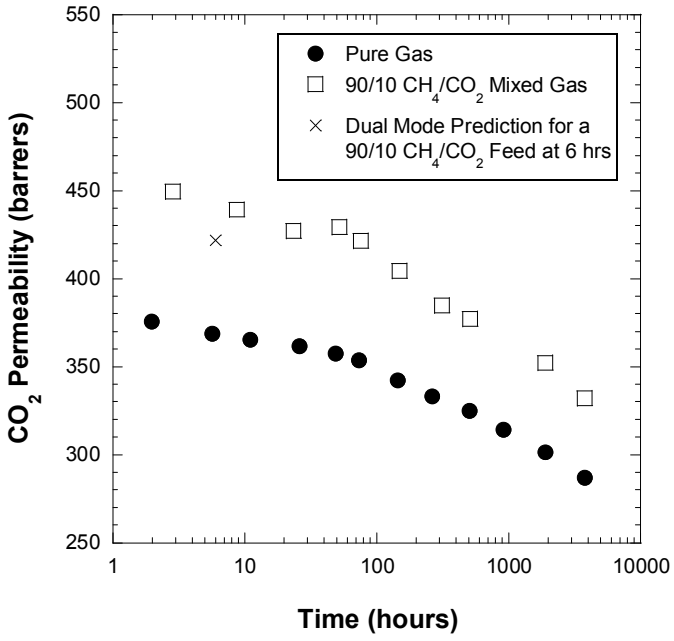

Figure 4.11: CO_2 permeation isotherms for pure gas (2 atm feed) and 90/10 CH_4/CO_2 mixed gas (2 atm feed) measurements in the free acid (M-158)

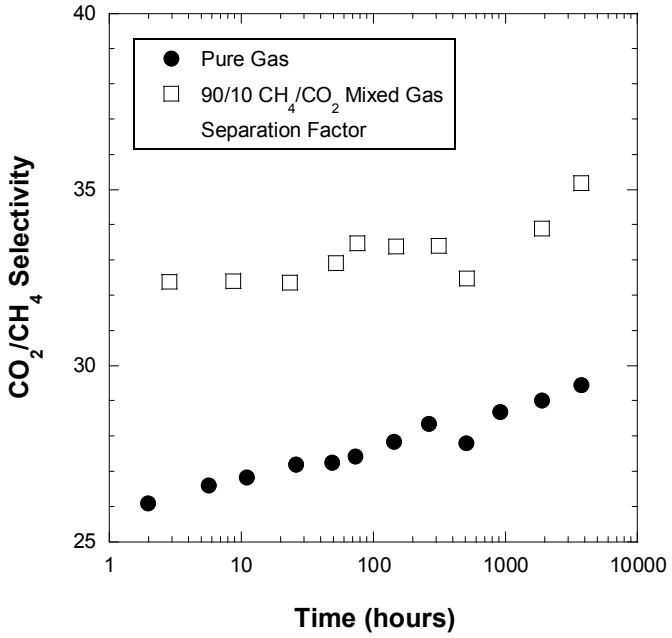

Figure 4.12: CO_2/CH_4 selectivity isotherms for pure gas (2 atm feed) and 90/10 CH_4/CO_2 mixed gas (2 atm feed) measurements in the free acid

Using Equation 2.15 expanded for a two component feed, the Dual Mode model can be used to predict the CO_2 permeability in the mixed gas feed to ensure the validity of the enhanced CO_2 permeability observed in Figure 4.11. Utilizing the CO_2 permeability data in Figure 4.6 and the Dual Mode parameters in Table 4.5, a mixed gas CO_2 permeability of 422 Barrers is predicted at 6 hours of physical aging and shown in Figure 4.11. This time value is modeled because the data in Figure 4.6 was collected at this aging time.

Table 4.5: Dual Mode parameters for the free acid rapidly quenched from above T_G

Parameter	CO_2	CH_4
k_D (cm^3 STP/(cm^3-atm))	1.33	0.19
C_H' (cm^3 STP/cm^3)	67.5	43.5
b (1/atm)	0.32	0.10
D_D (cm^2/s)	1.27×10^{-6}	-
D_H (cm^2/s)	8.89×10^{-8}	-

This increase in the CO_2 permeability is the result of a CO_2 partial pressure of only 0.2 atm in the mixed gas feed; whereas, the pure gas CO_2 pressure is 2.0 atm. Therefore, as the Dual Mode model indicates, this lower CO_2 feed pressure yields a higher CO_2 permeability over all time periods as shown in Figure 4.11. The CH_4 permeabilities for both the pure gas and mixed gas feed are nearly identical since the CH_4 partial pressure in the mixed gas feed is 1.8 atm as compared to 2.0 atm in the pure gas feed. As a result of these non-equivalent CO_2 and CH_4 feed partial pressures, the CO_2/CH_4 separation factor is enhanced compared to the pure gas selectivity as shown in Figure 4.12. Despite these absolute differences in permeability and selectivity, the rate of physical aging as probed with the 90/10 CO_2/CH_4 mixed gas is identical to that of the pure gas permeation measurements.

4.4.3 Thin Film Physical Aging

4.4.3.1 Pure Gas Permeation

On the opposite end of the thickness spectrum, submicron thin films similar to the thick films reported above were examined in a similar manner. The thin films used in this work range from 590-720 nm. All gas permeation data for the free acid, ethylene glycol crosslinked, and 1,4-benzenedimethanol crosslinked thin films are presented in Figure 4.13. As with the thick films, the initial gas permeabilities for all gases in the thin films are greatly enhanced compared to the bulk permeability values. However, as shown by the inclusion of the free acid bulk permeability values on the permeation plots, the thin film samples age much more rapidly than the thick film samples and even fall below the bulk permeability values after ~100 hours of physical aging. Therefore, after rapid quenching from above T_G which entraps a large excess of free volume, only 4 days of physical aging is required for the thin films to reach the bulk state of the polymer. This result has huge implications for industrial production of asymmetric hollow fiber membranes which tend to have selective skin thicknesses on the order of 100 nm, and initially contain additional entrapped free volume caused by the rapid polymer phase separation in a nonsolvent. By the time a membrane module reaches the point of use, however, the productivity of the membrane will be significantly less than what is expected from the bulk polymer properties.

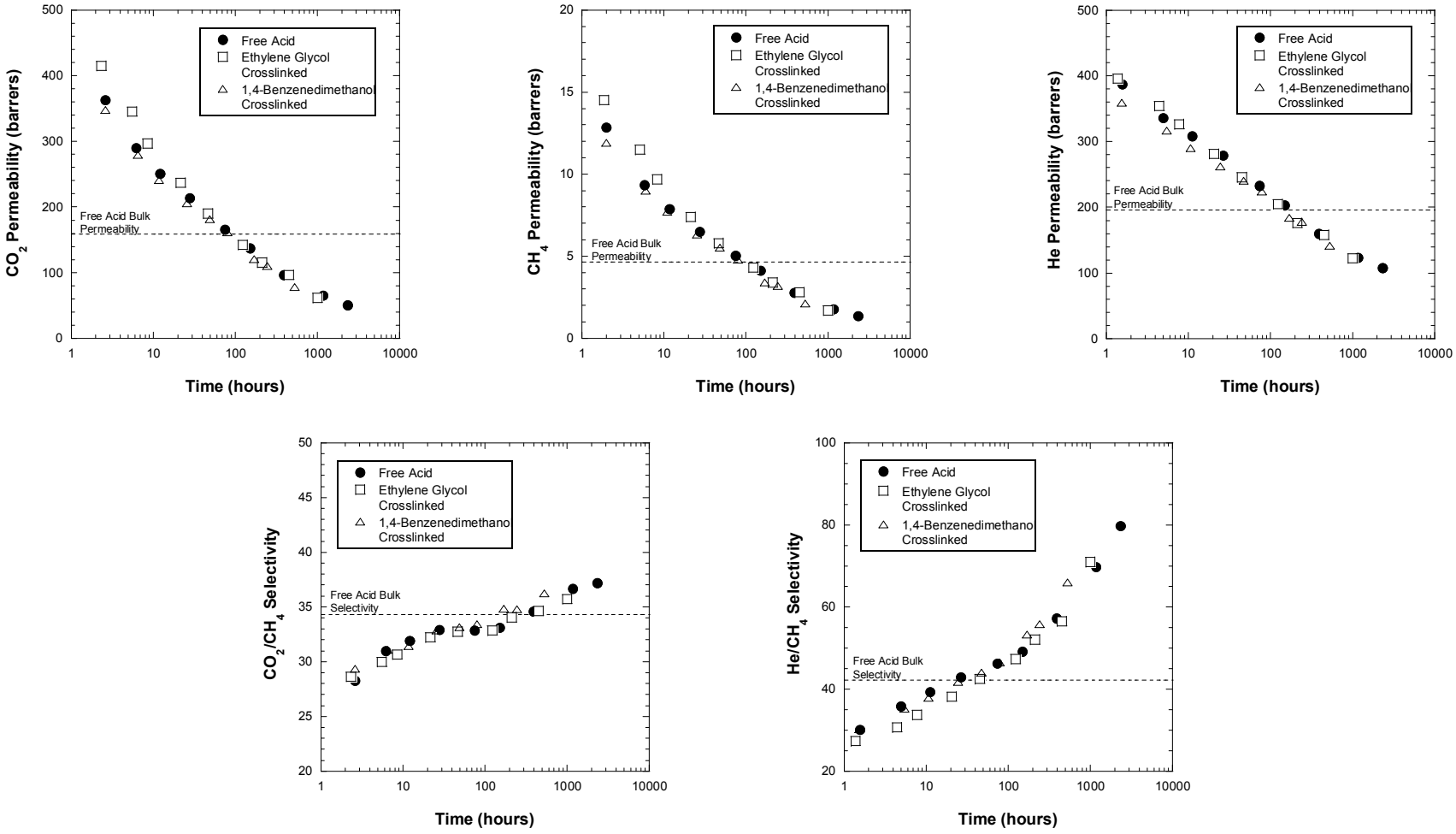

Figure 4.13: CO_2, CH_4, and He permeability isotherms and CO_2/CH_4 and He/CH_4 selectivity isotherms for the 6FDA-DAM:DABA (2:1) free acid (720 nm), ethylene glycol crosslinked (640 nm), and 1,4-benzenedimethanol crosslinked (670 nm) thin films. Gas permeation at 2 atm, 35 ^{o}C. (M-223, M-255, M-197)

Surprisingly, even in the thin films in which the diffusion of free volume contribution greatly enhances the aging process, there is little difference in the physical aging of the free acid and crosslinked films as probed through gas permeation. This response is further highlighted by Figure 4.14 which displays near identical normalized CH_4 permeabilities in all three films. Similar to the thick films, reduction in gas permeabilities scales with penetrant size. There is approximately a 70%, 83%, and 87% decrease in the He, CO_2, and CH_4 permeabilities with a 25-30% and 130-160% increase in the CO_2/CH_4 and He/CH_4 selectivities after 1000 hours of physical aging.

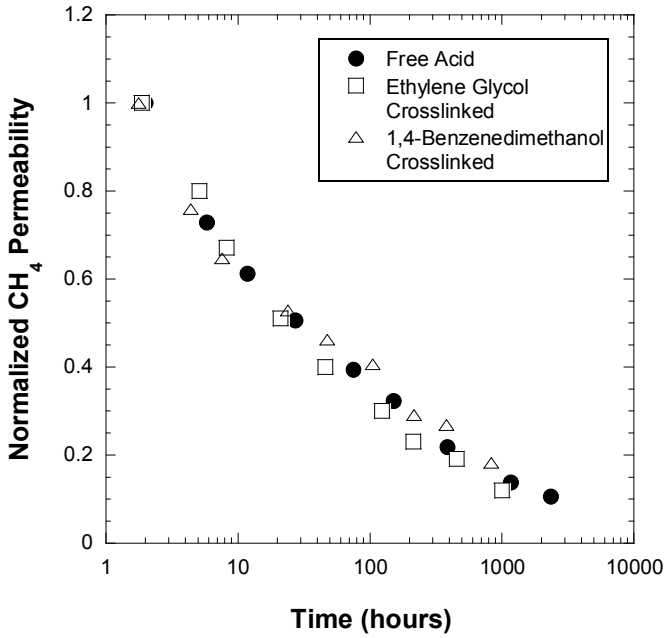

Figure 4.14: Normalized CH_4 permeabilities of the free acid (720 nm), ethylene glycol crosslinked (640 nm), and 1,4-benzenedimethanol crosslinked (670 nm) films

The similar physical aging results of the free acid and ethylene glycol and 1,4-benzenedimethanol crosslinked films is most likely due to the resulting crosslinking of the free acid polymer when annealed above T_G. Therefore, these physical aging results

are actually comparing three different crosslinked polymers as opposed to one noncrosslinkable polymer and two crosslinked polymers. As mentioned earlier, the crosslinking of the free acid will be discusses in more detail in Chapter 5. Ultimately, the size of the crosslinking agent does not greatly affect the rate of physical aging as monitored through gas permeation.

The corresponding selectivities display increasing trends that also surpass the bulk film selectivities; however, there are is an unexpected response that requires further study and clarification. For all three polymers, the He/CH_4 selectivities display a discontinuity at 200 hours, after which time, the rate of selectivity enhancement increases. This response will be discussed in Chapter 4.4.6.

4.4.3.2 90/10 CH_4/CO_2 Mixed Gas Permeation

As with the pure gas permeation results for the thin films, the 90/10 CH_4/CO_2 mixed gas permeation, in Figures 4.15 and 4.16, yielded similar results for the free acid, ethylene glycol crosslinked, and 1,4-benzenedimethanol crosslinked films. Similar to the pure gas thin film measurement, there is an 82% and 87% reduction in the CO_2 and CH_4 permeabilities, respectively, after 1000 hours of physical aging. The corresponding separation factors also exhibited a 25-30% increase similar to the pure gas selectivities.

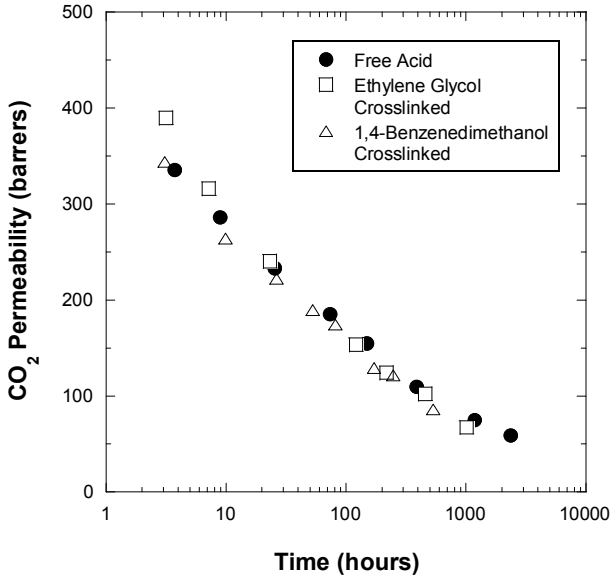

Figure 4.15: CO_2 permeation isotherms for the 90/10 CH_4/CO_2 mixed gas (2 atm feed) measurements of the free acid (720 nm), ethylene glycol crosslinked (640 nm), and 1,4-benzenedimethanol crosslinked (670 nm) films

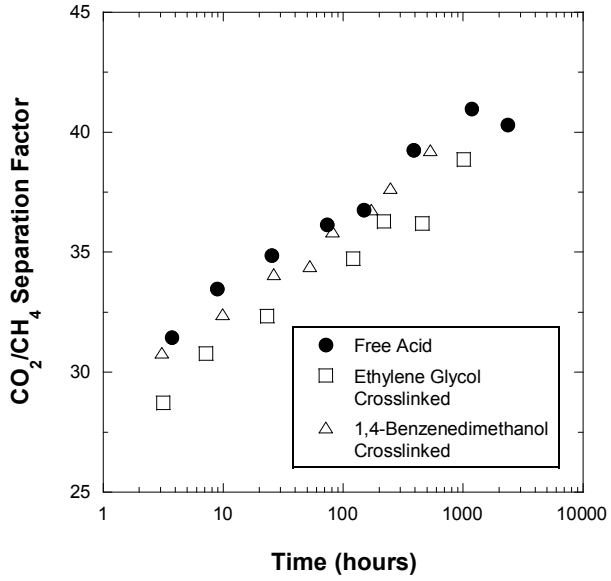

Figure 4.16: CO_2/CH_4 separation factor isotherms for the 90/10 CH_4/CO_2 mixed gas (2 atm feed) measurements of the free acid (720 nm), ethylene glycol crosslinked (640 nm), and 1,4-benzenedimethanol crosslinked (670 nm) films

4.4.4 Comparison of Thick vs Thin Film Physical Aging

As described in Chapter 2.5, physical aging is thought to occur through two different mechanisms, lattice contraction and diffusion of free volume. The thick and thin film permeability data presented in Figures 4.10 and 4.13 further confirms the belief that there are two different mechanisms at play in physical aging. Consider the comparison of the physical aging of a thin (720 nm) and thick (48.5 μm) free acid film shown in Figure 4.17. Assuming that the diffusion of free volume is a Fickian process, the rate of free volume removal should scale with the square of the thickness of the sample. Therefore, the thick film should age 4500X slower than the thin film if diffusion of free volume is the only process involved in physical aging, ie $(48.5/0.72)^2 = 4500$.

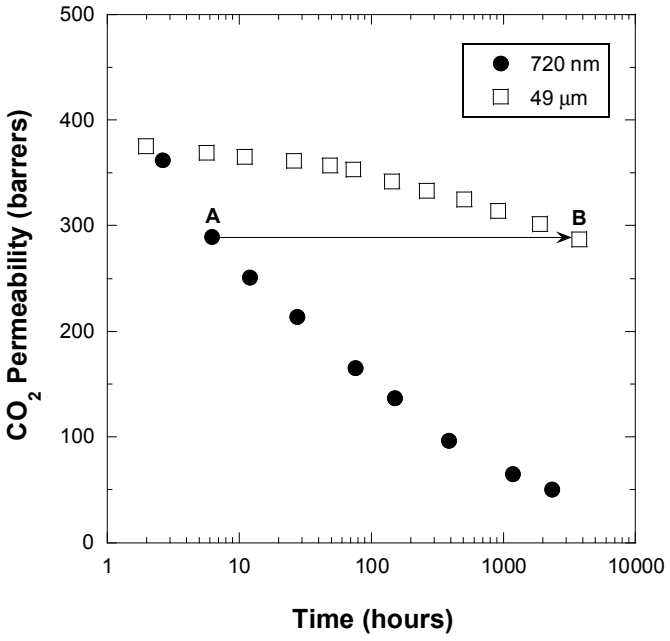

Figure 4.17: Physical aging comparison of thick vs thin free acid permeabilities

However, for the thick film (point B) to reach an equivalent permeability of the thin film (point A) is only about 600X the time scale. Based on the diffusion of free volume mechanism, the thick film should not reach this equivalent permeability until 28,000 hours. The fact that the thick film ages much more rapidly than it should if diffusion of free volume is the only mechanism of physical aging confirms the existence of another mechanism, namely lattice contraction. This point is also highlighted by the same permeation data as a function of normalized aging time (t/ℓ^2) presented in Figure 4.18. Again, if diffusion of free volume is the only mechanism of physical aging, these two permeation data sets should fall on a single normalized curve. Even though it appears that these two films would eventually converge onto a single slope, more data with intermediate film thicknesses is required to confirm this possible convergence.

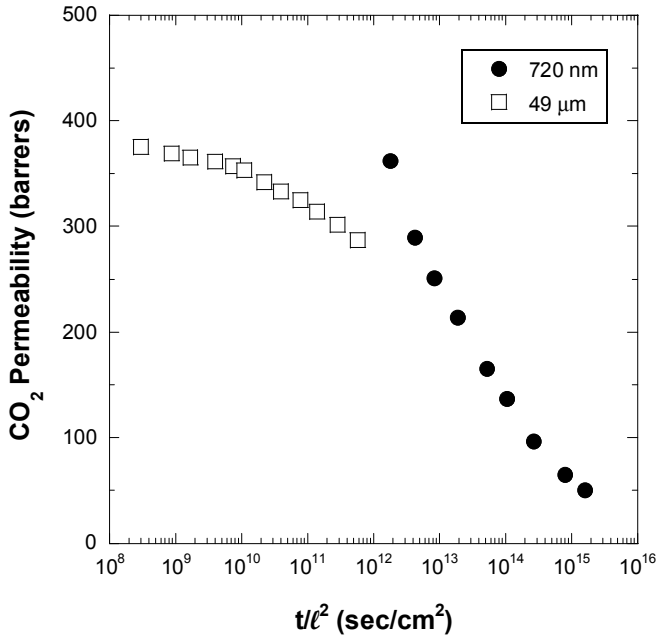

Figure 4.18: Physical aging comparison of thick vs thin free acid permeabilities as a function of normalized aging time (t/ℓ^2)

The combination of these two mechanisms makes physical aging a highly complex process that needs to be considered in all long term scientific studies on glassy polymers, whether with thin or thick film samples.

4.4.5 Thick Film Regeneration

In order to ensure that the reduction in gas permeabilities over time is actually a consequence of the removal of excess free volume and not a chemical change within the polymer, the polymer IR signature was measured in a free acid thick film aged to ~4000 hours and compared to a free acid film immediately following the rapid quench from above T_G. Also, the thick free acid film displayed in Figure 4.10 was removed from the mask and annealed again using Protocol #1 to ensure that the high free volume state of the polymer could be thermally regenerated when annealed above T_G.

Figure 4.19 displays the IR spectra for the initially quenched and aged free acid films. Aside from the truncated strong absorption peaks in the thick "Aged" film (ie carbonyl peak at 1700 cm^{-1}, etc), the spectra are essentially identical. Figure 4.20 presents the CO_2 permeabilities for the thick film presented in Figure 4.10 following one and two thermal annealing cycles. Even though the CO_2 permeability reached 285 Barrers after nearly 4000 hours of physical aging, upon thermal regeneration above T_G, the CO_2 permeability of the same film increased back to 385 Barrers. This response confirms that the reduction in gas permeability over time is in fact attributable to the removal of excess free volume since annealing above T_G reintroduces free volume into the film. Also, the IR data confirms that no chemical changes are occurring in the polymer during the physical aging process.

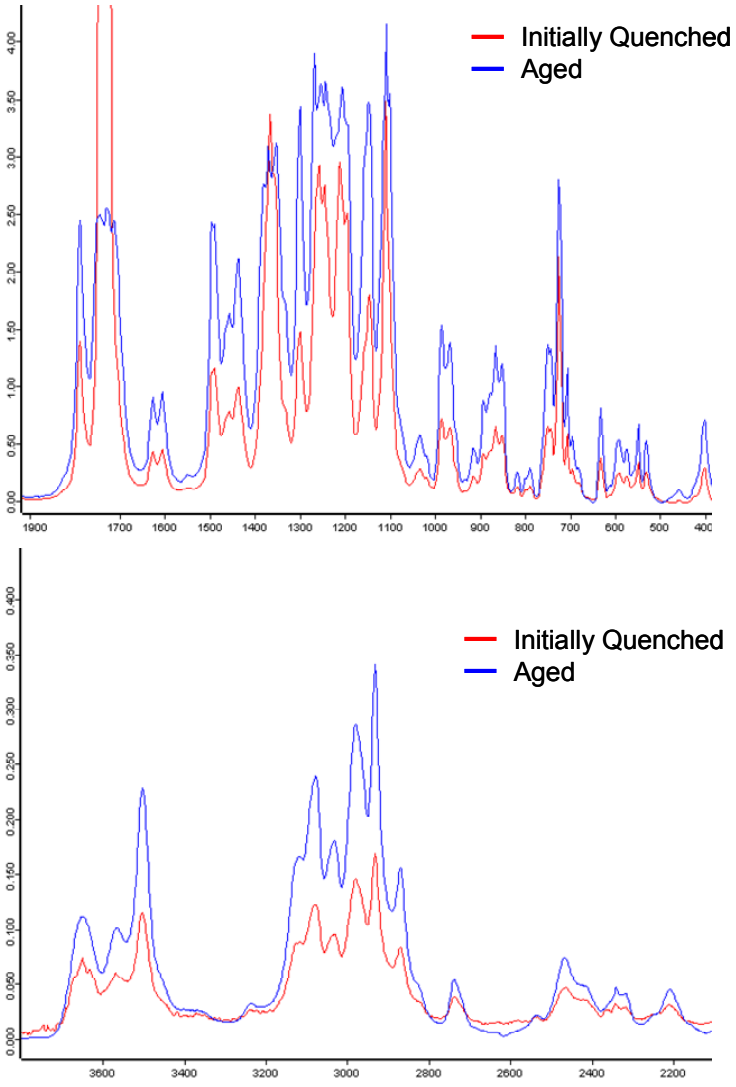

Figure 4.19: IR spectra for an initially quenched and an aged (~4000 hours) free acid film

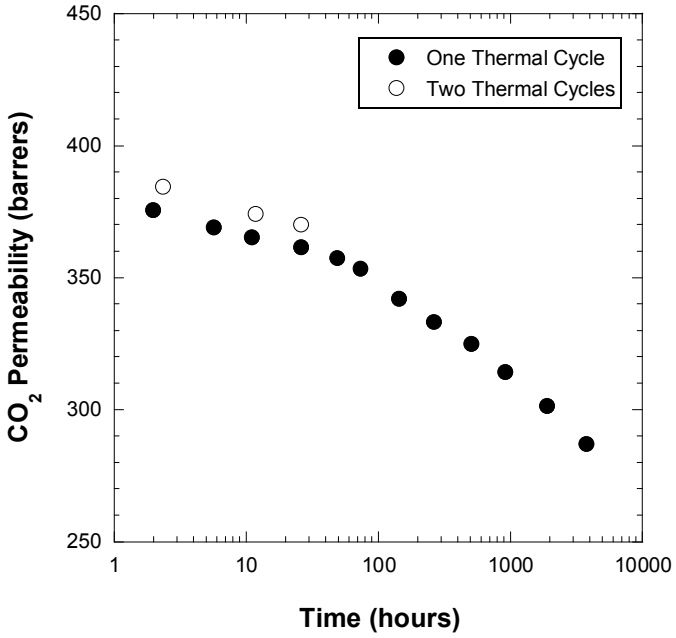

Figure 4.20: CO_2 permeation isotherm confirming thermal regeneration of the free acid film

4.4.6 Thin Film He/CH_4 Selectivity Response

As shown in Figure 4.13, the He/CH_4 selectivities of the thin films appear to display a discontinuity at 200 hours with an increase in the rate of selectivity enhancement beyond 200 hours. Previous physical aging studies on similar polyimide films which were periodically exposed to low pressure CO_2 resulted in constant or decreasing CO_2/CH_4 and O_2/N_2 selectivities over time [6]. Because CO_2 is such a highly sorbing penetrant, periodic exposure to CO_2, even at 2 atm, appears to hinder polymer chain relaxations and slow the physical aging process. This phenomenon appeared to have a greater effect on the larger penetrant molecules, which resulted in decreasing selectivities. Therefore, the short periodic CO_2 exposure involved in the CO_2 permeation tests throughout the aging time was believed to be hindering the physical aging process. At longer aging times, ie greater than 200 hours, the time between the short CO_2

exposures is significantly increased which would allow more time for recovery of the aging process and an enhancement in the rate of selectivity increase.

In order to probe the effect that periodic CO_2 exposure may have on the physical aging, a thin free acid film was prepared in the same manner as that in Figure 4.13 and probed only with He and CH_4 throughout the aging process. Figures 4.21 and 4.22 display the CH_4 permeability and He/CH_4 selectivity responses for the thin free acid film probed with and without CO_2.

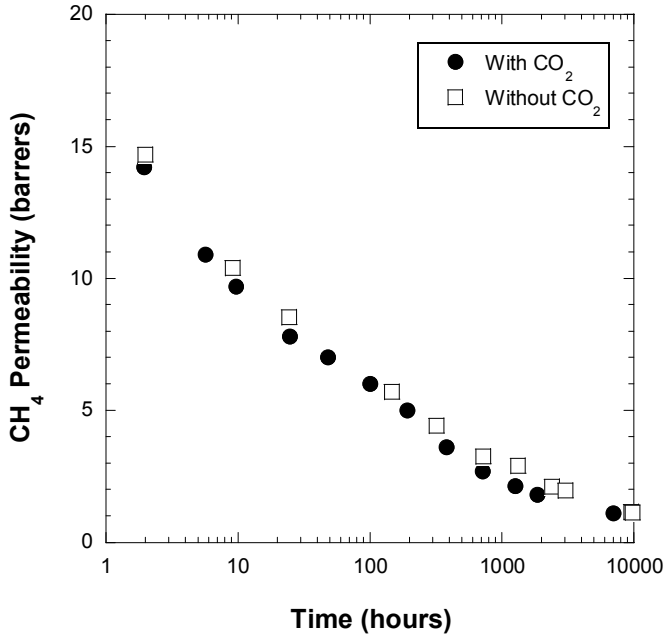

Figure 4.21: CH_4 permeability of thin free acid films probed with (770 nm) and without (720 nm) CO_2

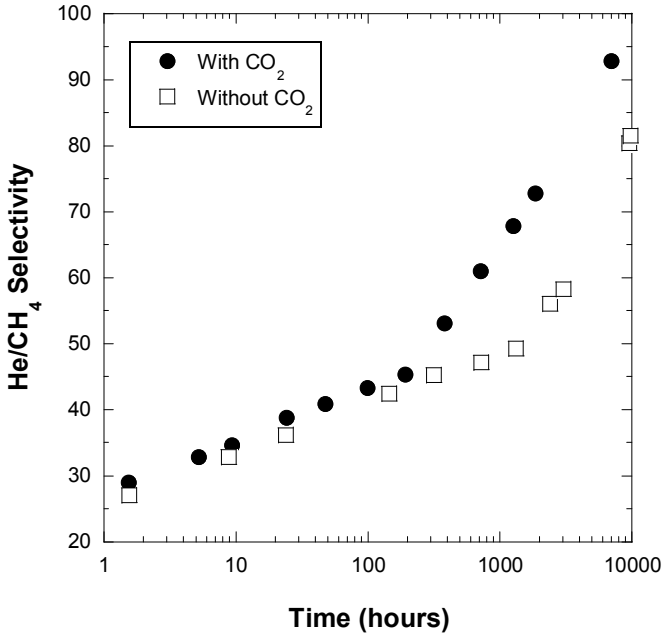

Figure 4.22: He/CH_4 selectivity of thin free acid films probed with (770 nm) and without (720 nm) CO_2

The thin film probed with only He and CH_4 displays a similar discontinuity in the He/CH_4 selectivity as the film probed with CO_2; however, this break occurs at a much longer aging time, ~1500 hours. It appears that the periodic CO_2 exposure actually enhances the aging process and causes the rate increase of the He/CH_4 selectivity to occur at shorter aging times. In this case, the highly sorbing CO_2 may act as a molecular "lubricant" for the polymers chains which can enhance mobility and accelerate the formation of charge transfer complexes in the polymer.

Charge transfer complexes are coplanar overlaps between π-bonding orbitals in the aromatic groups of the polymer. They are known to form in polyimides through the alignment of electron-donating and electron-accepting portions of the backbone, and fluorescence spectroscopy has been used to characterize the extent of these charge transfer complexes [7-9]. Free acid thick films were annealed to different temperatures

under vacuum and measured with fluorescence spectroscopy to probe the formation of these charge transfer complexes in this particular polyimide. Aromatic species with CF_3 groups are known to have electron-accepting properties; whereas, aromatic species with methyl groups are known to have electron-donating properties [10]. Therefore, the 6FDA-DAM:DABA (2:1) free acid polymer should be an ideal candidate to observe the formation of these complexes. As shown in Figure 4.23, as the annealing temperature of the free acid polymer increases, the fluorescence intensity increases indicating a higher degree of complex formation in the polymer. It should be noted that this data was collected using different settings for the spectrometer than the rest of the fluorescence data in this thesis; therefore, the intensities in this data set are not comparable to other data sets. However, the observed trend is unaffected by these different settings.

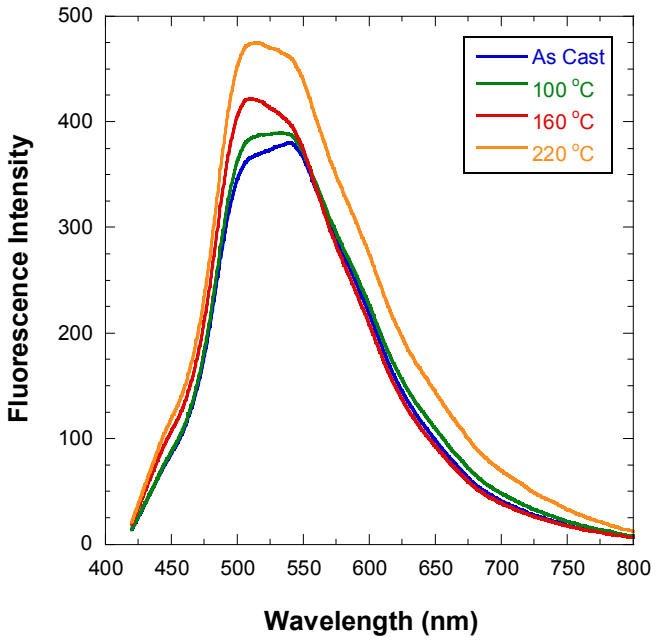

Figure 4.23: Fluorescence spectra of the free acid polymer at different annealing temperatures

The emission wavelength observed in the free acid is similar to that observed in other polyimides [7-9]. It is unclear whether intermolecular or intramolecular chain complexes are being formed; however, some research concludes that intermolecular complexes make up at least part of the complex formations [7,8].

To further probe the formation of charge transfer complexes in the physical aging process, a thin free acid film sample was prepared for fluorescence spectroscopy monitoring during the aging process. This sample was annealed in the same free-standing manner as the gas permeation samples using Protocol #1 and, following rapid quenching from above T_G, the film was laid back down onto a clean silicon wafer. A small (~3mm x 3mm) area on the film was marked off in order to measure the same spot throughout the course of physical aging. Because the instrument calibration can change over time, a standard was measured with every sample measurement and the subsequent fluorescence intensity data is presented relative to that standard. A thick free acid film annealed at 220 ^{o}C for 24 hours was used as the standard since it should exhibit very little change relative to the thin free acid film. Repeated fluorescence measurements on the same spot of a free acid film resulted in decreasing fluorescence intensity, which indicates the polymer undergoes a photo-bleaching process during exposure. Therefore, the fluorescence shutter was only opened during the few seconds a measurement was taken on the sample. Also, the exposure area was rastered within the 3mm x 3mm to prevent photo-bleaching from affecting the measurements. Three measurements were taken for each aging time of the sample. Figure 4.24 displays the average normalized fluorescence intensity at each time for the free acid film.

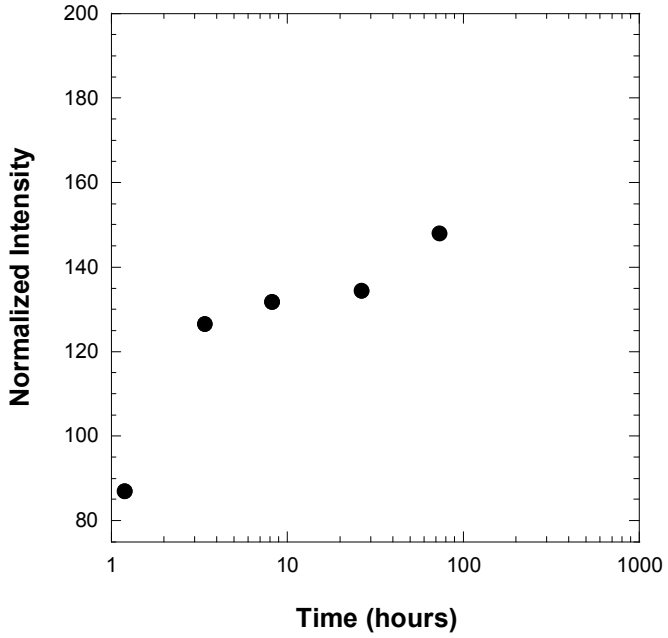

Figure 4.24: Normalized fluorescence intensity of the free acid thin film

This data indicates that charge transfer complexes continue to form throughout the aging process of the polymer. On a molecular scale, as excess free volume leaves the system, an increase in the polymer chain packing density allows alignment of the electron-donating and electron-accepting portions of the backbone and the formation of the charge transfer complexes. These complexes can act as physical crosslinks in that they further restrict chain mobility; thus enhancing the penetrant size discriminating capability of the polymer. Therefore, for aromatic polymers, such as this polyimide, the removal of excess free volume through physical aging may not be the only mechanism governing the reduction in gas permeability and enhancement in gas pair selectivity.

Another possible cause for the selectivity enhancement observed in Figure 4.22 is the changing distribution of free volume. Previous work with positron annihilation lifetime spectroscopy confirms that the amount and distribution of free volume within a glassy polymer changes with sub-T_G temperatures [11,12]. Therefore, it is not

unreasonable to expect the distribution of free volume within this polyimide to change throughout the physical aging process. While the following illustration is only speculative, it does provide a reasonable explanation for the aging effects observed in the gas permeation experiments. The lines represent the nominal gas molecules sizes with respect to the free volume distribution.

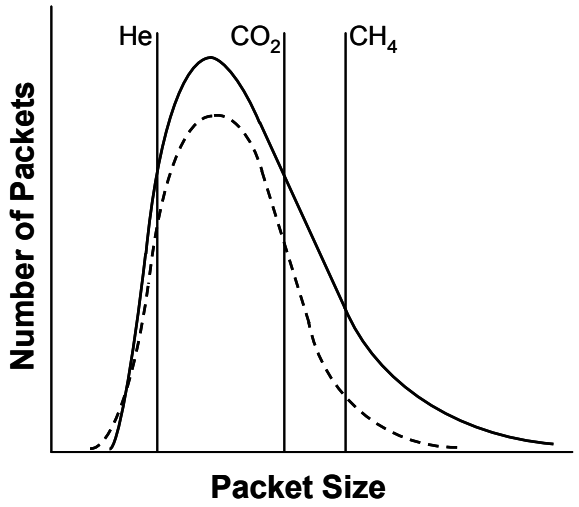

Figure 4.25: Illustration of possible changes in free volume distribution: initially quenched from above T_G (—), aged (---)

During physical aging, packets of free volume may combine or split which alters the free volume distribution in the polymer. As the free volume distribution becomes narrower, the relative access of a larger gas molecule to this free volume decreases with respect to a smaller gas molecule. Therefore, the size-discriminating selectivity of this gas pair increases. The change in the rate of the He/CH_4 selectivity enhancement may therefore also come as a result of a narrower distribution of free volume as the physical aging process progresses.

4.4.7 Thin Film Permeability Measurement Reproducibility

One of the difficulties in this work was collecting "non-defective" permeability measurements of the thin films. In these "defective" cases, typical aging responses, ie decreases in permeability with time, were observed; however, the gas pair selectivities displayed different trends. Also, the absolute permeabilities of all gases were higher and the selectivities lower than those of "non-defective" films. An example of this is presented in Figure 4.26 which displays the CO_2 permeabilities and CO_2/CH_4 selectivities of two different 1,4-benzenedimethanol crosslinked thin films.

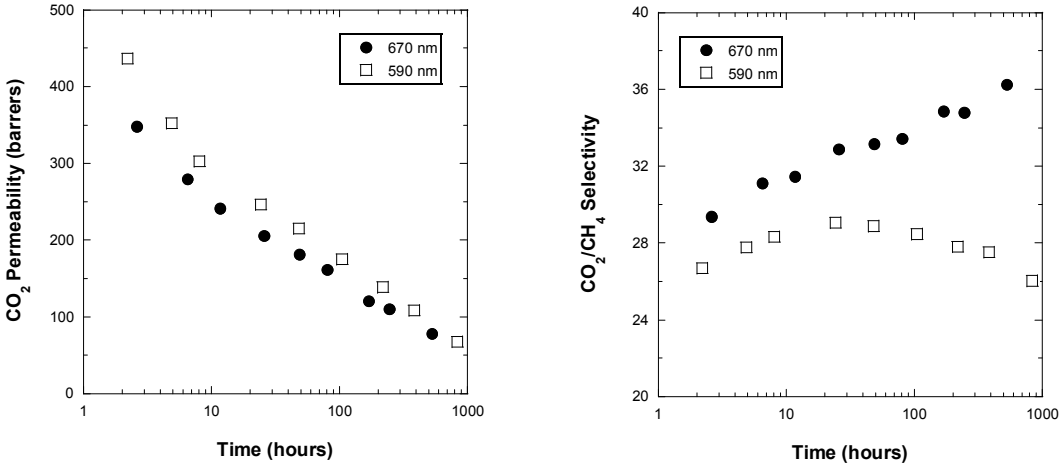

Figure 4.26: CO_2 permeability and corresponding CO_2/CH_4 selectivities of 1,4-benzenedimethanol crosslinked thin films (M-197, M-247)

As can be seen, even though the CO_2 permeabilities appear to age at the same rate (they are identical when normalized to the first data point), the CO_2/CH_4 selectivities have drastically different responses. This effect is highlighted even more by the CO_2/CH_4 mixed gas separation factors shown in Figure 4.27 which shows an even larger reduction in the separation factor of the "defective" film.

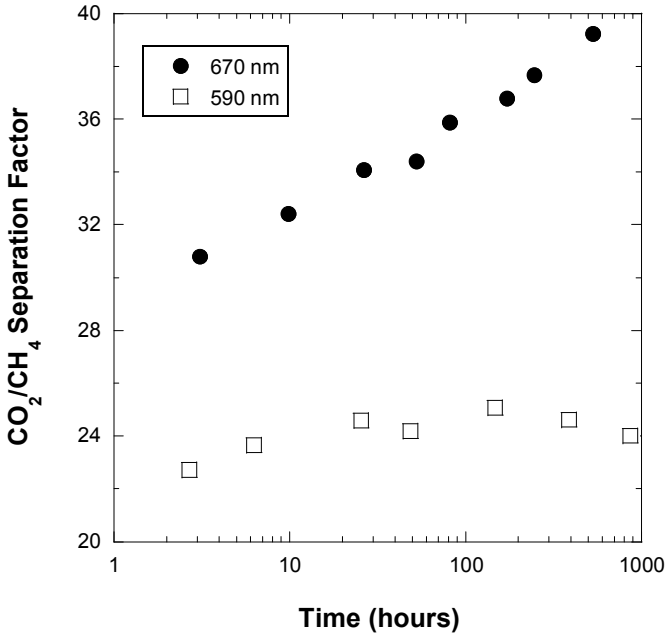

Figure 4.27: CO_2/CH_4 separation factor for 1,4-benzenedimethanol crosslinked thin films using 90/10 CH_4/CO_2 mixed gas feed (M-197, M-247)

At this point in time, it is unclear what the "defect" in these films actually is; however, a likely possibility is one or more particles that span through the polymer film yet have some interaction with the polymer to prevent viscous flow of gases. This effect was more prevalent in thinner films (~300-400 nm) than the films reported in this work (~600-700 nm).

Because of the observed responses in the above data, only films with reproducible selectivity data were presented in this work. As an example of the reproducibility of the thin film permeation data presented in Figure 4.13, Figure 4.28 displays the CO_2 permeability physical aging responses of four different ethylene glycol crosslinked thin films.

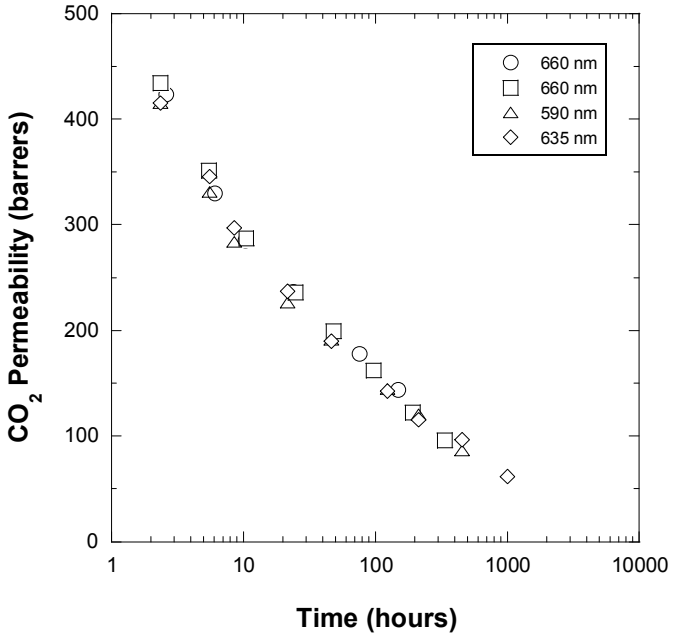

Figure 4.28: CO_2 permeabilities for physical aging response of four different ethylene glycol crosslinked thin films (M-207, M-209, M-254, M-255)

4.5 Secondary Measurements of Physical Aging in the 6FDA-DAM:DABA (2:1) Polymers

4.5.1 Gas Sorption of the Thin Free Acid Polymer

Gas sorption measurements with CO_2 and CH_4 to monitor the physical aging of the thick 6FDA-DAM:DABA (2:1) films were conducted; however, the penetrant uptake at 2 atm did not statistically change up to 2000 hours of aging in the thick films. The rate of physical aging in these thick films is too slow to be monitored through corresponding sorption measurements. Therefore, only sorption measurements of a thin film are presented here.

In order to create a sample with enough mass for gravimetric sorption measurements using a 50mg/300mm quartz spring, four thin free acid films were spin

cast onto silicon wafers. These films were removed intact onto a thin copper wire ring measuring 4.5 inches in diameter, and subsequently annealed above T_G using Protocol #1. Upon rapid quenching from above T_G, these films ranged in thickness from 600-700 nm. All four films were then tied together using thin copper wire to make the sample for sorption measurements.

As with the thick films, CH_4 sorption measurements of the thin free acid film are not presented because the uptake is too small at 2 atm to display any statistical changes. Therefore, only the CO_2 sorption isotherm as a function of aging time is presented in Figure 4.29. As expected, the sorption of CO_2 in the free acid decreases as the polymer ages. Since these sorption measurements were only conducted at 2 atm and not over a pressure range, changes in the Henry's Law or Langmuir regions of the polymer through physical aging can not be determined. However, using Equation 2.7, this data can be used to determine changes in the diffusion coefficient of the thin free acid film as physical aging occurs.

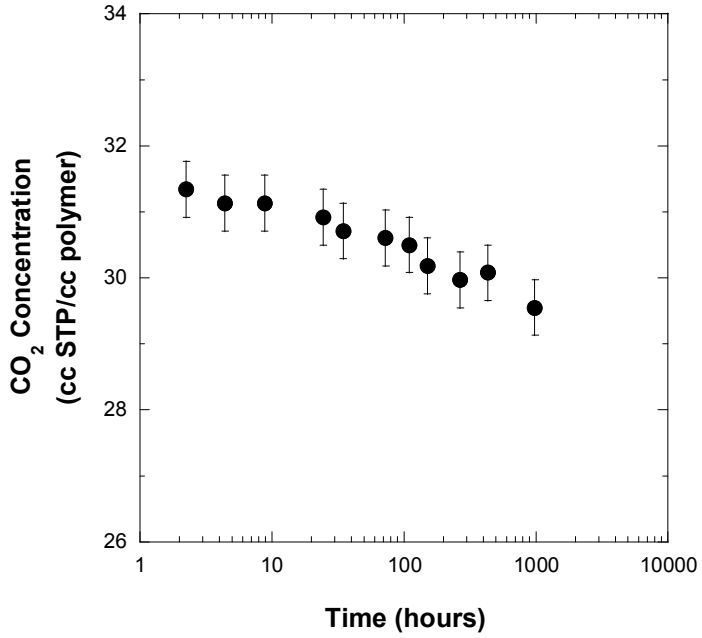

Figure 4.29: CO_2 sorption isotherm for the thin 6FDA-DAM:DABA (2:1) free acid

Figure 4.30 presents the diffusion coefficient as a function of physical aging time in the thin free acid polymer. The uncertainty associated with the sorption coefficients was carried over in the determination of the diffusion coefficient; however, the uncertainty in the diffusion coefficients is smaller than the actual data points and is therefore not visible. As would be expected with a large decrease in CO_2 permeability coupled with such a relatively small decrease in the CO_2 sorption of the free acid polymer over time, there is a significant decrease in the CO_2 diffusion coefficient over time. After 1000 hours of physical aging, there is nearly an order of magnitude decline in the diffusion coefficient from $2x10^{-7}$ to $3x10^{-8}$ cm^2/s. These values fall in the range of reported diffusion coefficients of structurally similar polyimides [13-17].

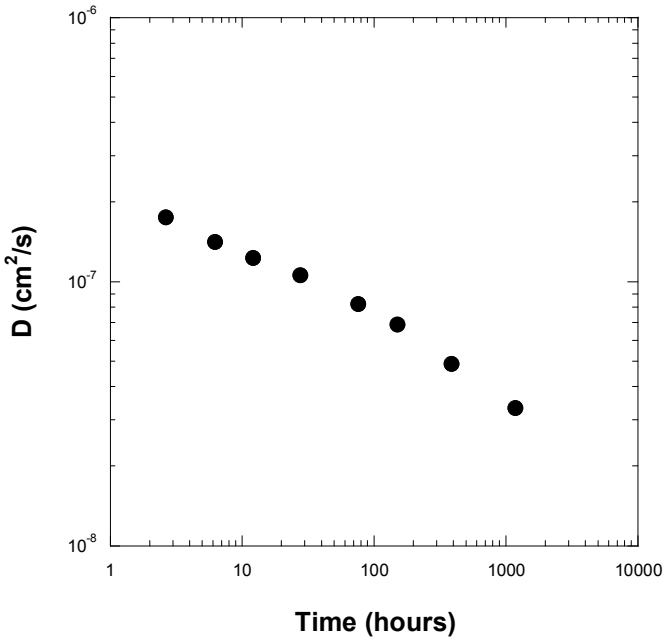

Figure 4.30: CO_2 diffusion coefficient isotherm for the thin 6FDA-DAM:DABA (2:1) free acid

This data confirms that the physical aging process has a greater effect on the diffusion, or kinetic, aspect of gas transport. Crosslinking the polymer, which should stabilize the diffusion of gases, is expected to hinder this decline in the gas diffusion coefficient and restrict the largest contribution to physical aging. However, while the original intention of this work was to compare an uncrosslinked (free acid) to crosslinked polymers, as will be shown in Chapter 5, the free acid polymer undergoes a crosslinking reaction at temperatures near T_G. Therefore, comparison of the diffusion coefficients of an uncrosslinked vs crosslinked polymer was not possible.

4.5.2 Refractive Index Measurements in Thin Films

As a means of confirming the removal of free volume and subsequent densification of the thin films as a result of physical aging, refractive index

measurements were taken over time on prepared samples. These measurements, when coupled with standard densities and refractive indices of thick films, can be used to determine the changes in fractional free volume of the polymer over time. The changes in fractional free volume can then be correlated to the changes in gas permeability over time using the Free Volume model. Unfortunately, even after accounting for various experimental conditions, such as using a controlled-atmosphere to control humidity and calibrating the window parameters in the software, consistent changes in refractive indices could not be measured over the aging time of the thin films. This procedure is discussed in more detail in Appendix A.

4.5.3 Wide Angle X-Ray Diffraction Measurements in Thick Films

WAXD measurements were conducted on free acid and ethylene glycol crosslinked thick films a few days following the rapid quench from above T_G and on a different set free acid and ethylene glycol crosslinked films that had been aged to 15,000 hours. The results are shown below in Table 4.6.

Table 4.6: Average d-spacing values for initially quenched and aged films

Polymer	Initially Quenched d-spacing (Å)	Aged d-spacing (Å)
Free Acid	6.0	6.3
Ethylene Glycol Crosslinked	5.9	6.2

Surprisingly, the d-spacing value as measured by the AreaMax software increase in both aged films as compared to the initially quenched films. This result is contrary to what is

expected in the physical aging process, and is most likely a result of either the inaccuracy of the technique or the differences in measuring two different films between the initially quenched and aged samples. Regardless of the cause of this result, WAXD does not appear to be a useful technique in monitoring the physical aging of glassy polymers.

4.6 Summary

All of the polymer characterization techniques confirm that the 6FDA-DAM:DABA (2:1) free acid, ethylene glycol crosslinked, and 1,4-benzenedimethanol crosslinked polymers match that of previous studies and are sufficient for the work presented in this study. Also, gas permeation and sorption measurements of the free acid film rapidly quenched from above T_G confirm the entrapment of large amounts of excess free volume in the polymer matrix prior to the physical aging studies.

Wide angle x-ray diffraction and gas permeation measurements indicate no difference between the monoesterified, yet uncrosslinked, films and crosslinked films following thermal treatment above T_G. Therefore, decoupling the effects of added volume of the crosslinking agent and the actual crosslinking was not possible. As a result, only the free acid, ethylene glycol crosslinked, and 1,4-benzenedimethanol crosslinked films were compared for the physical aging studies. Gas permeation results exhibited significant reductions in gas transport through the thin films (70-87%) as compared to the thick films (6-24%); while CO_2/CH_4 and He/CH_4 selectivity enhancements in the thin films (25% & 130%) was also significantly higher than the thick films (10% & 20%). Comparison of the aging rates of the free acid thin and thick films confirms that physical aging is a complex combination of the two physical aging processes, diffusion of free volume and lattice contraction.

Thermal regeneration of an aged free acid film indicates the gas transport properties are recoverable following treatment above T_G. This response and identical IR spectra from the start and end of the aging process further confirm that physical aging is process involving the removal of excess free volume and not a result of a chemical change within the polymer. Fluorescence spectroscopy measurements throughout the aging time indicate continued formation of charge transfer complexes. These complexes further hinder chain mobility and add to the complex nature of physical aging.

Thin film sorption measurements show the minimal effect that physical aging has on the sorption capacity of the film. Therefore, there is almost an order of magnitude reduction in the diffusion coefficient of the thin film (from $2x10^{-7}$ to $3x10^{-8}$ cm^2/s) for an aging period of 1000 hours. Refractive index measurements on the thin films were conducted to characterize the effect that removal of excess free volume has on gas permeability; however, consistent results could not be achieved. Finally, wide angle x-ray diffraction measurements on thick films resulted in data contrary to what is expected for physical aging.

4.7 References

1. Wind, John, *Improving Polyimide Membrane Resistance to Carbon Dioxide Plasticization in Natural Gas Separations*, Dissertation, University of Texas-Austin (2002).
2. Kim, J. H., et al., "Physical aging of thin 6FDA-based polyimide membranes containing carboxyl acid groups - Part 1. Transport properties", *Polymer*, 47(9), 3094-3103 (2006).
3. Colthup, N. B., Daly, L. H., Wiberley, S. E., *Introduction to Infrared and Raman Spectroscopy*, San Diego: Academic Press Inc. (1990).
4. Wind, J. D., Staudt-Bickel, C., et al., "Solid-state covalent cross-linking of polyimide membranes for carbon dioxide plasticization reduction", *Macromolecules*, **36**(6), 1882-1888 (2003).
5. Wind, J. D., et al., "Carbon dioxide-induced plasticization of polyimide membranes: Pseudo-equilibrium relationships of diffusion, sorption, and swelling", *Macromolecules*, **36**(17), 6433-6441 (2003).
6. Kim, J. H., et al., "Effects of CO_2 exposure and physical aging on the gas permeability of thin 6FDA-based polyimide membranes – Part 1. Without crosslinking", *Journal of Membrane Science*, **282**(1-2), 21-31 (2006).
7. Wachsman, E. D. & Frank, C. W., "Effect of cure history on the morphology of polyimide – fluorescence spectroscopy as a method for determining the degree of cure", *Polymer*, **29**(7), 1191-1197 (1988).
8. Kawakami, H., et al., "Gas transport properties in thermally cured aromatic polyimide membranes", *Journal of Membrane Science*, **118**(2), 223-330 (1996).

9. Zhou, F. B. & Koros, W. J., “Study of thermal annealing on Matrimid® fiber performance in pervaporation of acetic acid and water mixtures”, *Polymer*, **47**(1), 280-288 (2006).
10. Lakowicz, J. R., *Principles of Fluorescence Spectroscopy*, Singapore: Springer (2006).
11. Sandreczki, T. C., et al., “Sub-glass-transition-temperature annealing of polycarbonate studied by positron annihilation spectroscopy”, *Macromolecules*, **29**(11), 4015-4018 (1996).
12. Wang, B, et al., “Effect of temperature on the free volume in glassy poly(ethylene terephthalate)”, *Macromolecules*, **35**(10), 3993-3996 (2002).
13. Chung, T. S., et al., “Gas transport properties of 6FDA-durene/1,3-phenyldiamine (mPDA) copolyimides”, *Journal of Applied Polymer Science*, **81**(14), 3552-3564 (2001).
14. Chung, T. S., et al., “Pressure and temperature dependence of the gas-transport properties of dense poly[2,6-toluene-2,2-bis(3,4-dicarboxylphenyl)hexafluoropropane diimide] membranes”, *Journal of Polymer Science Part B - Polymer Physics*, **42**(2), 354-364 (2004).
15. Chung, T. S., et al., “PAMAM dendrimer-induced cross-linking modification of polyimide membranes”, *Langmuir*, **20**(7), 2966-2969 (2004).
16. Wang, L. N., et al., “The gas permeation properties of 6FDA-2,4,6-trimethyl-1,3-phenyldiamine (TMPDA)/1,3-phenylenediamine (mPDA) copolyimides”, *Polymer Bulletin*, **60**(1), 137-147 (2008).
17. Wind, J. D., et al. “Relaxation dynamics of CO_2 diffusion, sorption, and polymer swelling for plasticized polyimide membranes”, *Macromolecules*, **36**(17), 6442-6448 (2003).

5.0 THERMALLY INDUCED CROSSLINKING OF THE 6FDA-DAM:DABA (2:1) FREE ACID POLYIMIDE

5.1 Introduction

This chapter examines the 6FDA-DAM:DABA (2:1) free acid polymer following the rapid quench from above T_G. Different phenomena that can occur during thermal treatment of this polyimide, such as charge transfer complexing, decomposition, and chemical crosslinking, are analyzed through various characterization techniques. Finally, a possible mechanism of thermally induced crosslinking without a crosslinking agent, ie a glycol, is introduced and substantiated to explain the insolubility and enhanced plasticization resistance observed in a free acid film annealed above T_G.

5.2 Free Acid Response to Annealing Above T_G

Chapter 4.2 illustrated the effects of annealing the 6FDA-DAM:DABA (2:1) free acid film above T_G as it pertains to the physical aging work conducted throughout the rest of the chapter; however, other phenomena were observed resulting from annealing above T_G that were not consistent with a polymer simply traversing the glass transition temperature. First, following the rapid quench from above T_G, the free acid polymer is no longer soluble in any of the typical solvents used for casting these polymers into films, such as cyclohexanone, THF, and NMP. In fact, a free acid film annealed above T_G remained insoluble after boiling in NMP for 18 hours. Second, CO_2 permeation results indicate enhanced plasticization resistance in a free acid film rapidly quenched from above T_G. Figure 5.1 displays the same data as Figure 4.6; however, the CO_2

permeabilities have been normalized with respect to the first data point at 2 atm to better illustrate the enhancement in plasticization resistance of the free acid film quenched from above T_G.

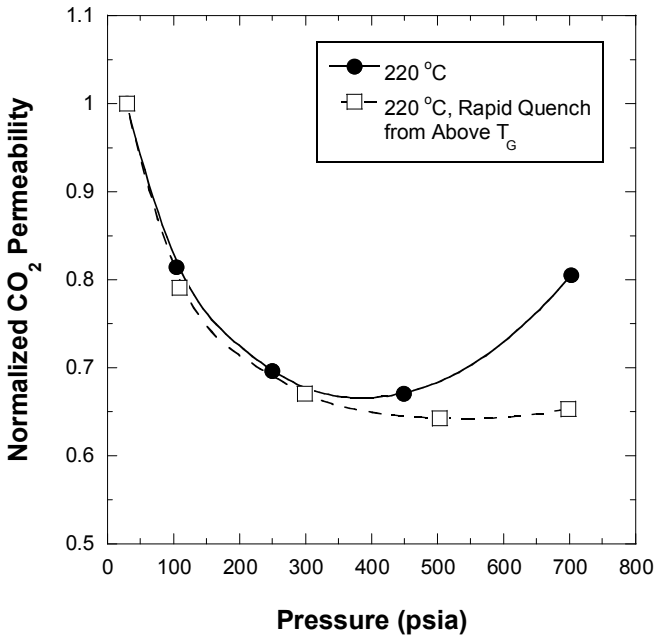

Figure 5.1: Normalized CO_2 permeation isotherms for 6FDA-DAM:DABA (2:1) free acid films annealed at 220 °C for 23 hours and annealed at 220 °C for 23 hours followed by rapid quenching from above T_G. The curves are to guide the eye. (M-271, M-273)

There are a few possible explanations for these responses of the free acid quenched from above T_G which will be explored in this chapter. First, as discussed in Chapter 4.4.6, this polymer is capable of forming charge transfer complexes which has been shown to stabilize another polyimide against plasticization [1-3]. This stabilization may also lead to greater insolubility in typical solvents. From a thermodynamic standpoint, when the polymer is in the rubbery region during the annealing process, enhanced chain mobility will allow alignment of the necessary components to form these complexes which results in an energetically more favorable state. Second, thermal

degradation of similar polyimides has been shown to create a carbon structure with enhanced gas separation properties [4-6]. This new material should be resistant to penetrant swelling since it consists of a rigid, ultramicroporous carbon structure. The T_G of the free acid is sufficiently high (374 ^oC) that the beginning stages of polymer degradation may be occurring which could lead to these stabilization effects. Finally, even though this free acid polymer is considered to be 'noncrosslinkable', ie it does not have the glycol crosslinking agent chemically attached to the DABA acid site, the high annealing temperature may cause some form of chemical reaction or reorganization to occur which could then stabilize the polymer. The remaining sections in this chapter address each scenario, and a possible mechanism for the polymer stabilization is proposed.

5.3 Fluorescence Spectroscopy of Thermally Quenched Polymers

Figure 5.2 presents fluorescence spectra of a free acid film dried at 70 ^oC for 24 hours and a film annealed using Protocol #1. Each curve is a representation of three different measurements per sample. The samples used for these measurements are adjacent samples from the same cast film, and both samples per polymer were measured on the spectrometer at the same time to eliminate the issue of changes in instrument calibration over time.

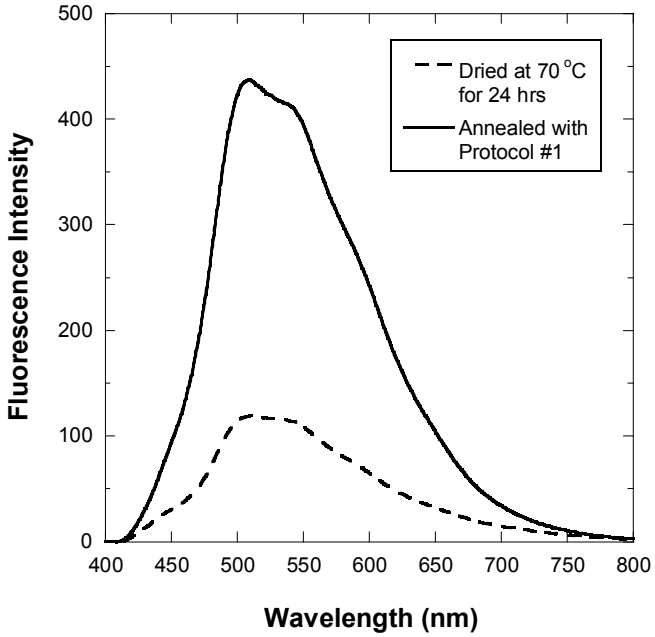

Figure 5.2: Fluorescence spectra of a dried and thermally quenched free acid sample

As a complementary measurement, a structurally similar polymer, 6FDA-DAM, was examined with fluorescence spectroscopy in the same manner as described above, and solubility tests were performed in THF and NMP. Figure 5.3 displays the fluorescence spectra for 6FDA-DAM.

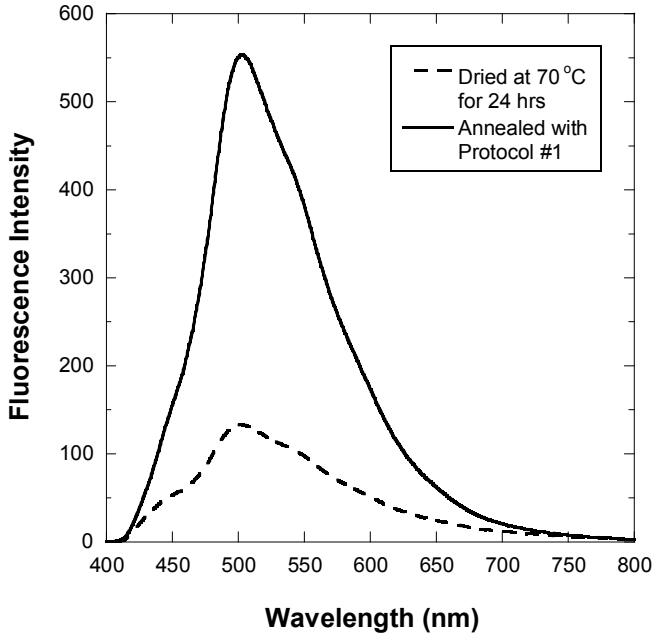

Figure 5.3: Fluorescence spectra of a dried and thermally quenched 6FDA-DAM sample

Even though this polymer is structurally different than the free acid, rapid quench from 389 °C increased the film thickness from 33 μm to 74 μm confirming this film surpassed the glassy transition. Surprisingly, solubility tests revealed the 6FDA-DAM polymer to be soluble in both THF and NMP at room temperature following the high-temperature treatment.

These data reveal many insights in annealing the free acid above T_G. As mentioned in the previous section, when in the rubbery state, these polymers are expected to form charge transfer complexes which leads to a more favorable energy state. The fluorescence spectra for both the 6FDA-DAM:DABA (2:1) free acid and 6FDA-DAM confirm this hypothesis as shown by the four-fold increase in fluorescence intensity when quenched from above T_G. Also, the 6FDA-DAM solubility in THF and NMP following thermal treatment demonstrates that charge transfer complexes are not

sufficiently strong enough to stabilize these polymers against dissolving in typical solvents. Ultimately, these data show that charge transfer complexes are not the cause of the insolubility and enhanced plasticization resistance of the free acid, and the DABA moiety of the free acid is most likely responsible for these effects following the rapid quench from above T_G.

5.4 Investigation of Oligomer Crosslinking in the Free Acid

Previous work has explored the ability to crosslink polyimides with both small and large molecule diamines [7-10]. While the polymer film is immersed in a methanol/diamine solution at room temperature, the diamines cleave the imide ring and form an amide linkage on the polymer backbone. The opposite end of the diamine then reacts with another imide ring in a similar manner. The result is a crosslinked polymer through the newly formed amides. The purpose of the methanol is to swell the polymer to enhance the chain mobility which allows alignment for the crosslinks to form. When the large batch of 6FDA-DAM:DABA (2:1) free acid was synthesized and analyzed with GPC, a small secondary distribution existed in the low molecular weight region. Based on the polystyrene calibration, this low molecular weight material is equivalent to 1-3 repeat unit oligomers. If these small chain oligmers contain either DAM or DABA end groups, it is reasonable to conclude that the high temperature annealing above T_G provides enough polymer mobility to form the amide crosslinks mentioned above. To test this possibility, the low molecular weight polymer was removed from a small batch of the free acid, and the remaining high molecular weight polymer was heat treated using Protocol #2 and examined with solubility tests and gas permeation.

A small batch of the free acid was placed in a near-theta solvent (50/50 THF/Methanol) and mixed for 18 hours to greatly swell the polymer and dissolve the low

molecular weight species. The remaining polymer was then placed in a fresh 50/50 THF/Methanol solution and mixed again for 18 hours. Once removed and dried, approximately 75% of the polymer remained. Both the washed and extracted polymer were examined with GPC to determine the efficiency of the extraction. The washed polymer contains only high molecular weight material; whereas, the extracted polymer contains a mix of high and low molecular weight material. The molecular weight values and PDI for each are presented below.

Table 5.1: Molecular weight information for the washed and exracted free acid polymer

Polymer	Mn	PDI
Washed Free Acid	78,337	1.904
Extracted Free Acid	912	4.449

Upon thermal treatment with Protocol #2, the high molecular weight polymer remains insoluble in both THF and NMP. Furthermore, as shown in Figure 5.4, after rapid quenching from above T_G, the CO_2 plasticization resistance of the washed free acid is nearly identical to the original free acid. Therefore, the small chain oligomers that are present in the original free acid polymer are not responsible for the crosslinking effects that are observed following rapid quench from above T_G.

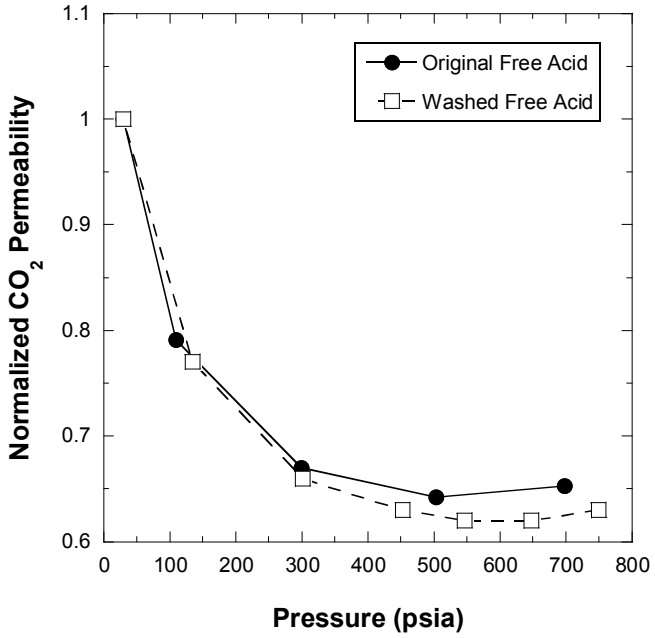

Figure 5.4: Normalized CO_2 permeability for the washed and original free acid polymer following rapid quenching from above T_G

5.5 TGA-IR of the 6FDA-DAM:DABA (2:1) Free Acid

TGA measurements coupled with IR of the evolved gases were conducted on the free acid polymer to characterize the decomposition of the polymer. The temperature was ramped up to 800 ^oC at a rate of 5 ^oC/min in a nitrogen purge. Figure 5.5 displays the mass loss of the polymer and temperature profile of the measurement.

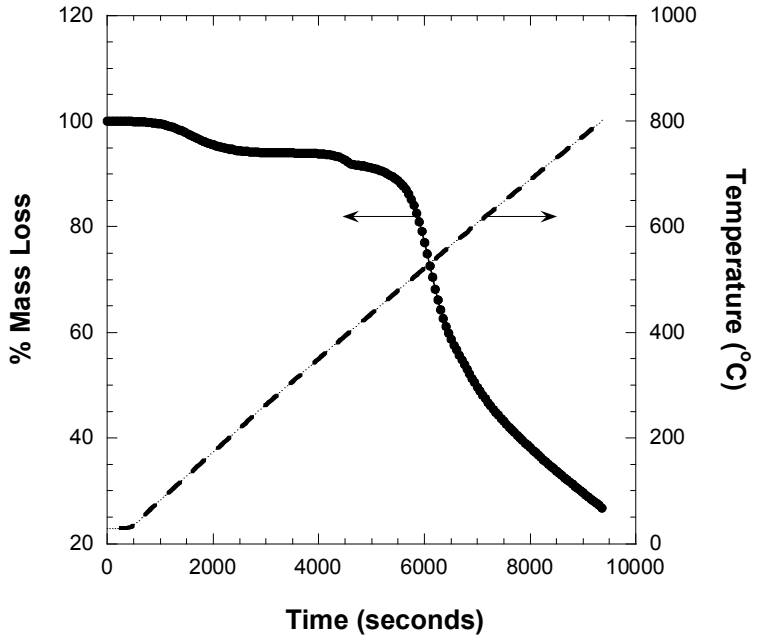

Figure 5.5: % Mass loss and temperature profile of TGA measurement of the 6FDA-DAM:DABA (2:1) free acid polymer for decomposition characterization

The first mass loss begins at 80 ^{o}C and can be attributed to water evolution and possibly trace amounts of residual solvent since mass loss continues until approximately 220 ^{o}C. There is also a second mass loss between 350 ^{o}C and 415 ^{o}C which will be addressed in later sections. The significant mass loss associated with polymer decomposition begins at 470 ^{o}C. Figure 5.6 displays the 3-D IR spectra of gas evolution, and Figure 5.7 displays the IR trace at 1150 cm^{-1} which corresponds to HCF_3 evolution which has been determined to be one of the first byproducts of decomposition in similar polyimides [11]. The large, growing peak at 3200 cm^{-1} is a water peak associated with ice formation on the external IR detector.

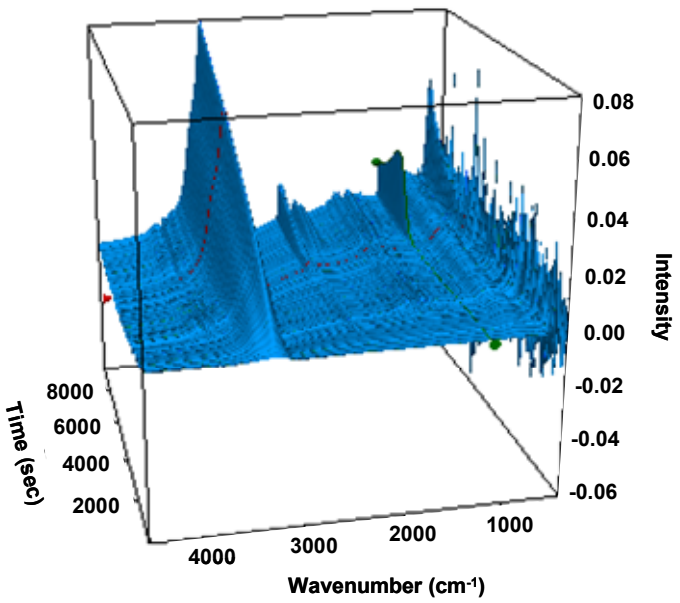

Figure 5.6: 3-D IR spectrum of evolved gases for the 800 °C TGA of the free acid

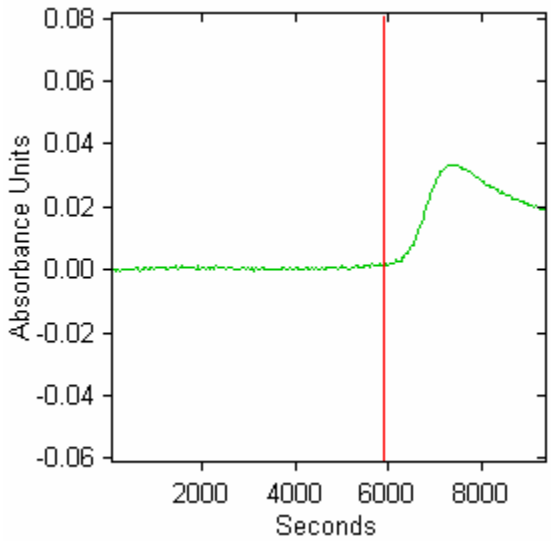

Figure 5.7: IR Trace of 1150 cm^{-1} from the above 3-D IR spectrum. This wavelength is associated with HCF_3 evolution during decomposition.

These spectra confirm that decomposition of the 6FDA-DAM:DABA (2:1) free acid polymer does not begin until 470 ^{o}C. Since the annealing protocols discussed in Chapter 3.5 only go up to 389 ^{o}C, carbon formation from polymer decomposition is not responsible for the observed insolubility and plasticization resistance of the rapidly quenched free acid.

5.6 Investigation of Dianhydride Formation

Previous work with polymethacrylates and poly(mono-n-akyl itaconates) have discovered the presence of dianhydride formation at carboxylic acid sites as one of the first steps of thermal degradation [12-17]. These formations occur as increased chain mobility at higher temperatures allows alignment of the acid site and subsequent anhydride formation with the loss of water. Velada et al. concluded that linear, intermolecular dianhydride formation was responsible for polymer crosslinking and resulting insolubility in typical solvents [16]; and, many other studies have shown that intermolecular dianhydride formation can occur in these polymers [12,13,15]. Also, upon further heating these dianhydrides have been shown to release CO_2 and for a ketone crosslink [14,15]. The presence of the carboxylic acid site on the DABA moiety lends the possibility of these same dianhydride formations to create intramolecular or intermolecular crosslinks.

Unfortunately, IR wavelengths typically associated with dianhydride formation, 3600-2500, 1795, 1750, and 1022 cm^{-1}, are coupled with other structures in the free acid and are not independently discernible following the rapid quench from above T_G. Therefore, IR can not be used to detect these formations. However, the doubly conjugated benzophenone, which would result from the decomposition of the dinahydride between two DABA groups, has an IR absorbance near 1680-1640 cm^{-1}

[18]. As shown in Figure 4.1 though, there is no shoulder or additional peak in this range resulting from annealing the free acid above T_G.

To determine if these formations are occurring in the free acid, an experiment was performed to hydrolyze the possible dianhydride and return the polymer to the previous uncrosslinked state. To do this, a previous free acid film that was rapidly quenched from above T_G was placed in 95 ^oC water for 8 hours in an attempt to hydrolyze any crosslinks that may have formed. Following the high temperature water conditioning, a CO_2 permeation isotherm was performed to determine if the enhanced plasticization resistance deteriorated to the typical uncrosslinked response. Figure 5.8 presents the CO_2 permeation results of the rapidly quenched film and the same film after the water conditioning.

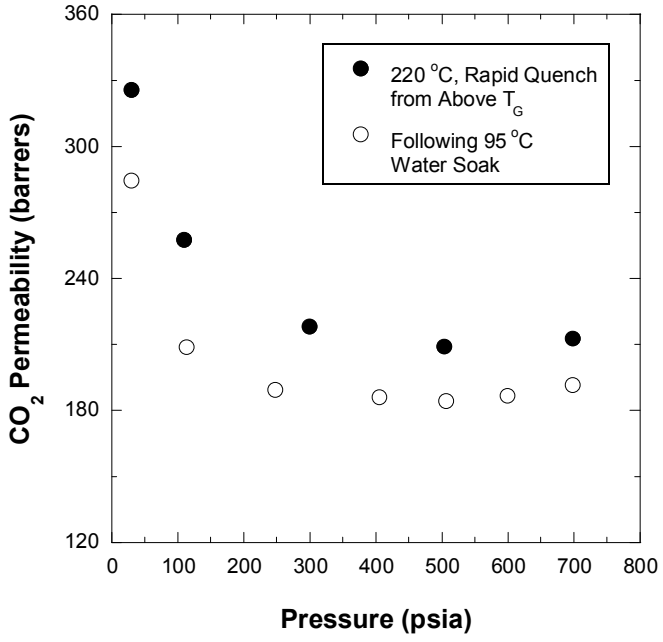

Figure 5.8: CO_2 permeation isotherm of a free acid film rapidly quenched from above T_G and then conditioned overnight in 95 ^oC water

The decrease in all permeabilities following water conditioning is a result of physical aging of the film. Approximately two months elapsed between the rapid quench and water treatment. This rigorous water treatment should be sufficient to hydrolyze any anhydride formation; however, the plasticization resistance following the treatment is nearly identical to that following rapid quench from above T_G. Figure 4.2 presented the CO_2 permeation isotherm of an uncrosslinked free acid film, and there is a clear upswing in the CO_2 permeability at approximately 350 psia which is not apparent in the water treated permeation isotherm. If dianhydride formation does occur without any subsequent reactions when the free acid is annealed above T_G, it is most likely eliminated following the rapid quench and does not play a role in the observed insolubility effects and plasticization resistance.

5.7 Decarboxylation of the DABA Moiety

Figure 5.4 displayed a small mass loss in the free acid that begins at approximately 350 ^oC. To determine if this loss occurs in a free acid film that is annealed using Protocol #1, a free acid film was measured using a TGA program that mimics the annealing protocol, albeit with a slower ramp. The ramp rate was maintained at 5 ^oC/min and the film was heated to 390 ^oC and held at that temperature for 40 minutes. The TGA mass loss for this run is presented in Figure 5.9.

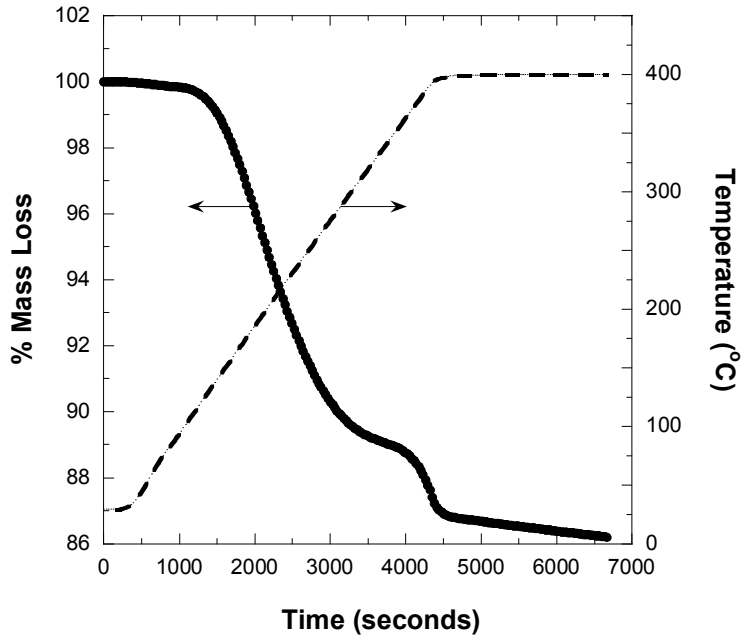

Figure 5.9: % Mass loss and temperature profile of a free acid film to mimic the annealing protocol above T_G

This TGA profile clearly shows a mass loss at 350 ^oC that continues until the 390 ^oC isothermal stage is reached. This temperature falls in the range attributed to decarboxylation as observed in acid containing polymers such as acrylic acid and poly(p-methylacryloyloxy benzoic acid) [17,19]. In the decarboxylation process, CO_2 and/or CO are evolved in gas form. Figures 5.10 and 5.11 display the 3-D IR spectra of gas evolution and IR trace at 2354 cm^{-1} which is associated with CO_2 evolution. No CO evolution was detected by IR as an evolved gas. Again, the large peak at 3200 cm^{-1} is a water peak associated with ice formation on the external IR detector; however, it is still possible that water is evolved during this process and the signal is hidden within this large peak.

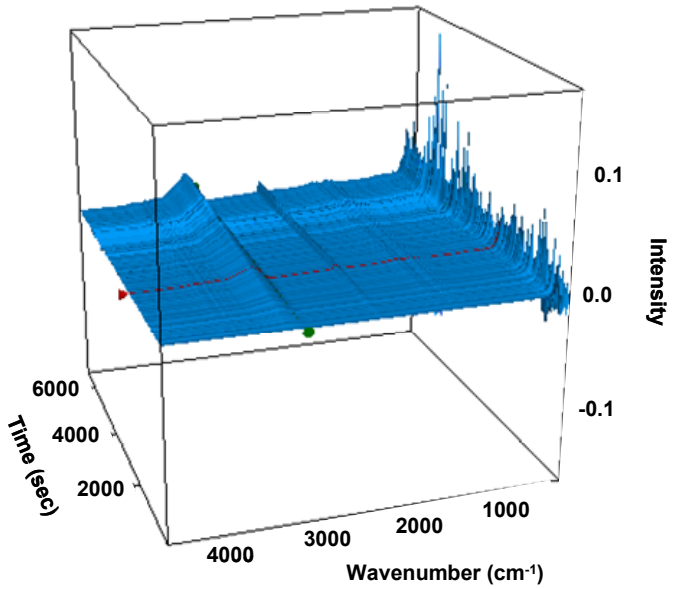

Figure 5.10: 3-D IR spectra of evolved gases corresponding to the TGA run in Figure 5.9

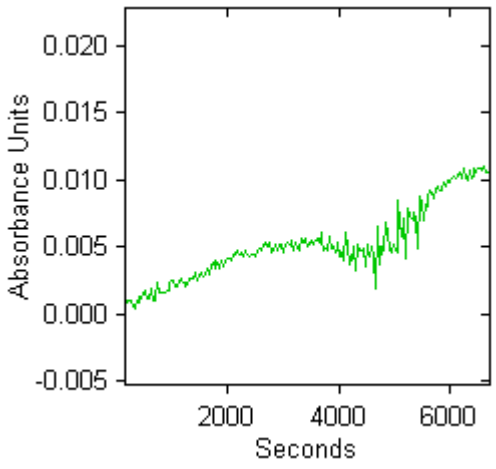

Figure 5.11: IR Trace of 2354 cm^{-1} from the above 3-D IR spectrum

The increase in absorbance during the first 2500 seconds in Figure 5.11 is fully not understood at this time; however, it could be sorbed CO_2 within the polymer that is evolved as temperature increases. However, there is a distinct increase in the

absorbance beginning at ~4500 seconds which corresponds to the significant mass loss that occurs between 4000 and 4500 seconds in Figure 5.9. Therefore, CO_2 is most likely being evolved from the polymer during this portion of the thermal treatment. As a means of confirming that the carboxylic acid group is responsible for this mass loss, a TGA profile of the 6FDA-DAM polymer was conducted, and there is no mass loss prior to the major decomposition of the polymer.

Cervantes et al. concluded that benzoic anhydride is first formed at lower temperatures and the CO_2 evolution that occurs at 353 ^oC is the result of decarboxylation of the anhydride structures [17]. If the free acid polymer followed a similar process, the mass loss associated with removal of the complete anhydride structure from the polymer is 2.16% per 2 repeat units of the free acid (6 6FDA, 4 DAM, 2 DABA). This value takes into account water removal at lower temperatures to form the dianhydride. A first derivative analysis of the TGA data in Figure 5.9 confirms a mass loss of 2.0% at this step. This result substantiates the possibility that the observed mass loss at temperatures just below T_G for the free acid polymer is associated with the decarboxylation of the free acid in the DABA species.

IR spectra of a dried free acid film and a film annealed above T_G also indicate the significant loss of these acid sites. Figure 5.12 displays the high-frequency range for these films, and the broad peaks in the range of 3700 to 3100 cm^{-1} typically associated with OH stretching vibrations have been greatly diminished in the film annealed above T_G. This broad peak range is not just a result of sorbed water in the polymer since the film annealed above T_G was rapidly quenched to room conditions and was not measured with IR for a number of days. Therefore, it would have reached equilibrium with the environment just as the dried free acid film.

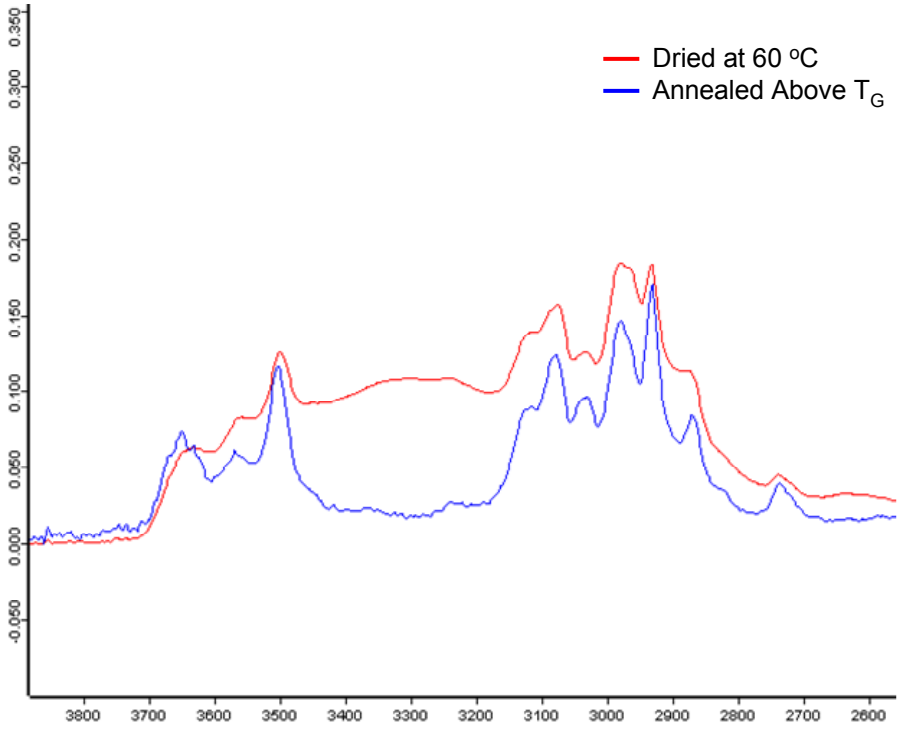

Figure 5.12: High-frequency IR spectra of a dried free acid film and a free acid film annealed above T_G

5.8 Possible Mechanism of Covalent Crosslinking of the Free Acid

Decarboxylation studies of aromatic carboxylic acids have been performed in the past to gain an understanding of how the process occurs and if it can lead to crosslinking during the thermal processing of low rank coals [20-22]. The majority of the studies are conducted in either a base-catalyzed or acid-catalyzed environment, and upon heating to 400 °C, decarboxylation of aromatic acids readily occurs with little resulting crosslinking [20,21]. However, decarboxylation of a model acid was also found to yield a small amount of crosslinked products in a neutral environment. In this case, the model acid formed an aryl linkage at the site of the decarboxylated acid with the solvent, naphthalene. An illustration of this formation is shown in Figure 5.13.

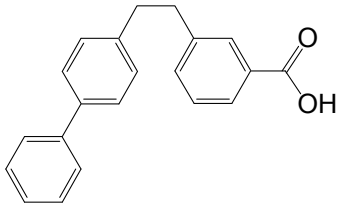

Model Acid

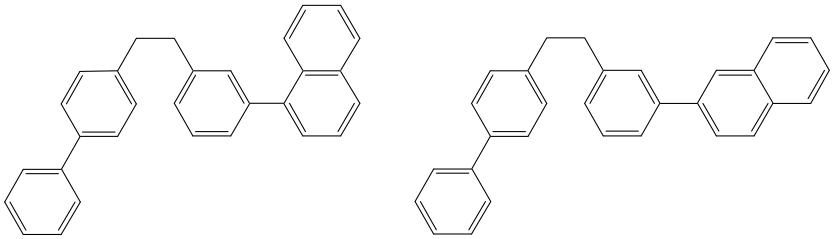

Crosslinked with Naphthalene

Figure 5.13: Structures of model acid and crosslinked structures following decarboxylation [22]

Through an extensive series of systematic tests, Eskay et al. conclude that this crosslinking does not occur through simple hydrogen abstraction and decarboxylation of the acid to form an aryl radical and subsequent arylation with naphthalene. Rather, dianhydride formation must occur as an intermediate product prior to decomposition. In fact, thermolysis of the model dianhydride in naphthalene, yielded 57% crosslinked products with a decomposition rate of 88% hr^{-1} at 400 ^{o}C [22]. Interestingly, there was no crosslinked product created from two model acids forming a bond at the open radical sites. Based on the reaction products and gas byproducts, Eskay et al. concluded that the decomposition of the dianhydride was most likely induced by a radical and not a result of homolysis of the C(=O)-O bond.

As shown in the previous section, the amount of mass loss in the 6FDA-DAM:DABA (2:1) free acid polymer at 350 ^{o}C is slightly below the theoretical amount of

complete removal of the dianhydride formation across two DABA species. With the known pathway to crosslinking shown to occur in the model acid described above, it is reasonable to conclude that the high temperature treatment of the 6FDA-DAM:DABA (2:1) free acid polymer produces a crosslinked polymer in which the acid site of the DABA group is arylated to another portion of the polymer backbone. This crosslinking most likely occurs in a few different places along the backbone. If the proposed induced decomposition pathway of the dianhydride holds true, then a hydrogen must be abstracted from the backbone. The hydrogens in the DAM methyl groups have the lowest bond dissociation energy, and are therefore most likely to be abstracted which then creates a methyl radical and possible crosslinking site [23]. Conversely, even though Eskay et al. did not observe any crosslinked model acids, it may be possible for two radical DABA groups to form linkage and corresponding biphenyl. The structures of these possible crosslinks are shown below in Figure 5.14.

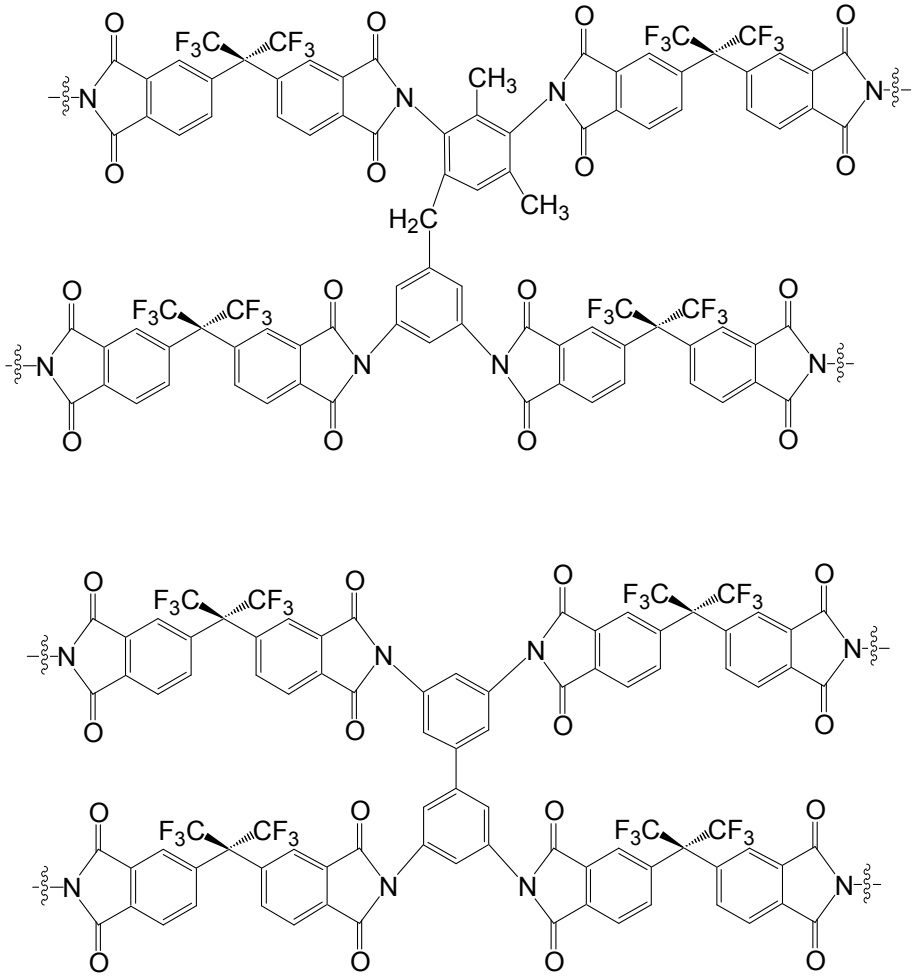

Figure 5.14: Possible crosslinking sites through the diamines in the free acid polymer

One other possibility exists as a potential crosslinking point. The gradual mass loss at 389 ^{o}C from 4500 seconds to 6500 seconds in Figure 5.9 may be the onset of decomposition caused by HCF_3 loss. A similar TGA experiment was conducted with a maximum temperature of 450 ^{o}C. In this run, the gradual mass loss at the isothermal step was slightly enhanced, and the IR spectrum of evolved gases exhibited a small peak at 1149 cm^{-1}. As mentioned before, this is the signature of the first decomposition product HCF_3. Therefore it is possible that a small amount of the CF_3 groups are being

cleaved at 389 °C. The leaving CF_3 group would then provide an available radical site for the following crosslinking structure.

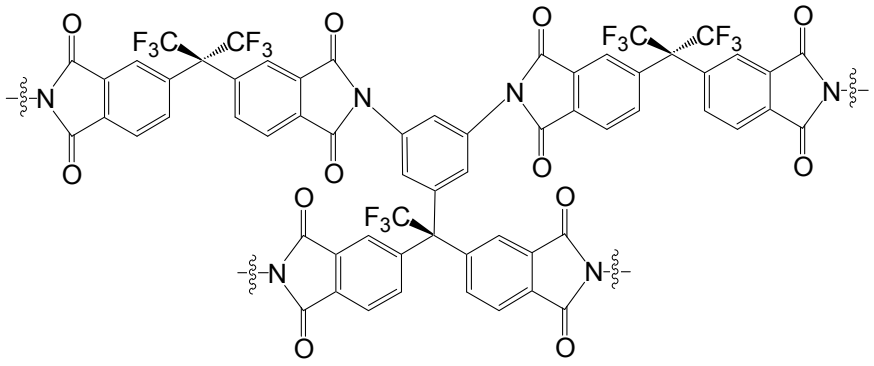

Figure 5.15: Possible crosslinking site through the dianhydride in the free acid polymer

While this structure appears to be too sterically hindered to form, there have been studies conducted with a structurally similar polymer [24,25].

These proposed points of crosslinking would not significantly alter the IR signature of the polymer, which is consistent with what is observed as shown in Figure 5.16. The only substantial difference between these spectra is the diminished peak at 1400 cm^{-1} in the film annealed above T_G. While this peak is not definitively known, it may be the OH in-plane deformation of carboxyl dimers which ranges from 1440-1395 cm^{-1} [18].

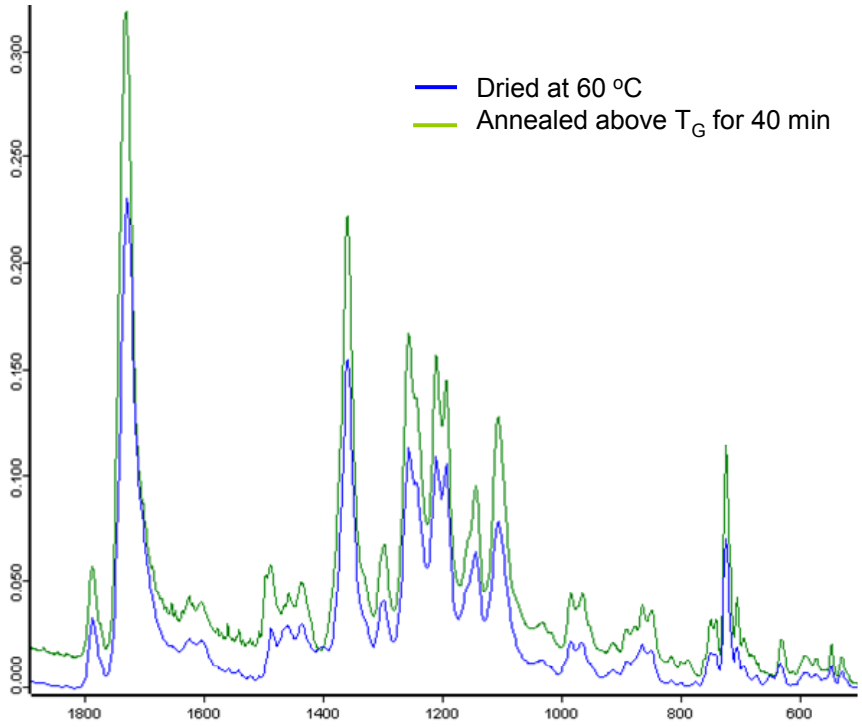

Figure 5.16: IR spectra comparing the free acid before and after annealing above T_G

5.9 C-NMR of the Free Acid

C-NMR was conducted on the free acid polymer to confirm the loss of the carboxylic acid carbon during the heat treatment above T_G. A free acid sample dried at 220 °C was compared to a sample thermally treated using Protocol #2. Because the absolute intensities of these spectra are not equivalent, all data analysis is conducted with respect to the aromatic/CF_3 peaks of the polymer in the range of 150-105 ppm. The peak of interest is the carbonyl carbon band in the range of 170-160 ppm, which comprises the carboxylic acid carbons as well as the imide carbonyl carbons. All chemical shift assignments were determined using ChemDraw® software. Figure 5.17 displays the spectra for the aromatic/CF_3 carbon peaks and the carbonyl carbon peaks.

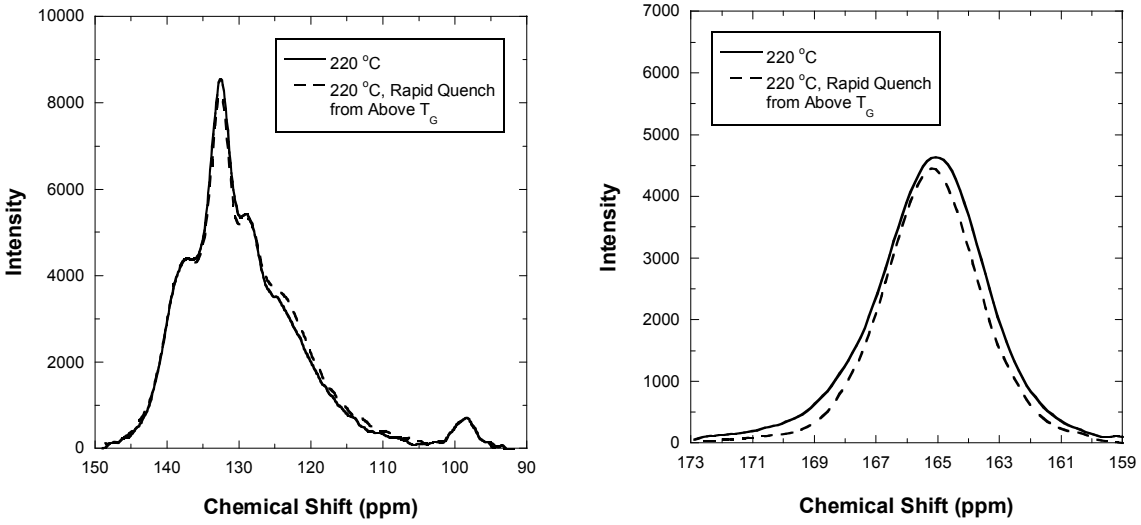

Figure 5.17: C-NMR spectra comparing the free acid before and after annealing above T_G

The small peak at 100 ppm is a side band of the carbonyl carbon peak associated with the 5 kHz spin speed and was not included in the following analysis. While there does not appear to be a large difference in these spectra, an integral analysis of the peaks confirms a reduction in the carbonyl carbon peak following annealing above T_G. To ensure this technique is accurate, peak integral analyses for the quaternary carbon attached to the CF_3 groups and the methyl carbons from the DAM diamine with respect to the aromatic/CF_3 peak were also measured. The quaternary carbon and methyl carbon peaks coupled with side bands in the 5 kHz measurement; therefore, a separate 3.5 kHz measurement was conducted for each sample to allow peak deconvolution. The following table displays these results.

Table 5.2: Ratio of peak areas with respect to the aromatic/CF_3 peak areas

C-NMR Peak	220 ^oC	220 ^oC, Rapid Quench from Above T_G	Percent Change
Carbonyl Carbon (173-160 ppm)	0.192	0.161	16.1%
Quaternary Carbon (69-53 ppm)	0.084	0.083	1.2%
Methyl Carbon (22-2 ppm)	0.300	0.305	-1.6%

Since there is one carboxylic acid carbon and eight imide carbonyl carbons in a repeat unit, the theoretical loss for complete decarboxylation is only 11.1%. While it is not possible to definitively determine the uncertainty associated with this measurement technique, the percent change of the quaternary carbon and methyl carbon peaks sheds some light on the uncertainty of these measurements. At the very least, this technique establishes the fact that a C=O carbon is being removed from the polymer structure when the free acid polymer is annealed above T_G.

5.10 Summary

Upon rapid quenching from above T_G, the free acid polymer exhibits unusual responses for a polymer simply annealed above T_G. The polymer becomes insoluble in strong solvents and exhibits excellent plasticization resistance in CO_2. Fluorescence spectroscopy confirms that charge transfer complexing occurs in the annealed free acid films as well as a structurally similar polyimide, 6FDA-DAM. However, the 6FDA-DAM

polymer is soluble following rapid quenching from above T_G. Therefore, the DABA component of the free acid is most likely responsible for the unusual responses.

The quenched free acid polymer was conditioned in high temperature water to break down possible dianhydride formations, but subsequent CO_2 permeation tests reveal no change in plasticization resistance. TGA-IR measurements confirm the polymer does not undergo decomposition in the temperature range of the annealing protocols; however, there is a small, unexpected mass loss that occurs at high temperatures just below T_G.

This mass loss is further studied with TGA-IR, and it is concluded that decarboxylation of the free acid group in the DABA component occurs at approximately 360 ^oC, just below T_G. This decarboxylation reaction has been shown to form crosslinks in neutral environments, and a few proposed crosslinking mechanisms are presented for the free acid polymer that is annealed above T_G. C-NMR results confirm that the C=O carbon population decreases in the free acid polymer annealed above T_G.

5.11 References

1. Bos, A., et al., “Plasticization-resistant glassy polyimide membranes for CO_2/CH_4 separations”, *Separation and Purification Technology*, **14**(1-3), 27-39 (1998).
2. Barsema, J. N., et al., “Intermediate polymer to carbon gas separation membranes based on Matrimid PI”, *Journal of Membrane Science*, **328**(1-2), 93-102 (2004).
3. Zhou, F. B. & Koros, W. J., “Study of thermal annealing on Matrimid® fiber performance in pervaporation of acetic acid and water mixtures”, *Polymer*, **47**(1), 280-288 (2006).
4. Steel, K. M. & Koros, W. J., “Investigation of porosity of carbon materials and related effects on gas separation properties”, *Carbon*, **41**(2), 253-266 (2003).
5. Steel, K. M. & Koros, W. J., “An investigation of the effects of pyrolysis on gas separation properties of carbon materials”, *Carbon*, **43**(9), 1843-1856 (2005).
6. Vu, D. Q., et al., “High pressure CO_2/CH_4 separation using carbon molecular sieve hollow fiber membranes”, *Industrial & Engineering Chemistry Research*, **41**(3), 367-380 (2002).
7. Liu, Y., et al., “Effects of amidation on gas permeation properties of polyimide membranes”, *Journal of Membrane Science*, **214**(1), 83-92 (2003).
8. Cao, C., et al., “Chemical cross-linking modification of 6FDA-2,6-DAT hollow fiber membranes for natural gas separation”, *Journal of Membrane Science*, **216**(1-2), 257-268 (2003).

9. Shao, L., et al., “Transport properties of cross-linked polyimide membranes induced by different generations of diaminobutane (DAB) dendrimers”, *Journal of Membrane Science*, **238**(1-2), 153-163 (2004).
10. Shao, L., et al., “Polyimide modification by a linear aliphatic diamine to enhance transport performance and plasticization resistance”, *Journal of Membrane Science*, **256**(1-2), 46-56 (2005).
11. Williams, Paul Jason, *Analysis of Factors Influencing the Performance of CMS Membranes for Gas Separation*, Dissertation, Georgia Institute of Technology (2007).
12. Grant, D. G. & Grassie, N., “The thermal decomposition of polymethyacrylic acid”, *Polymer*, **1**(1), 125-134 (1960).
13. McGaugh, M. C. & Kottle, S., “The thermal degradation of poly(acrylic acid)”, *Polymer Letters*, **5**(9), 817-820 (1967).
14. Maurer, J. J., et al., “Thermal characterization of poly(acrylic acid)”, *Macromolecules*, **20**(1), 196-202 (1987).
15. Ho, B. C., et al., “Thermal degradation of polymethacrylic acid”, *Journal of Polymer Science Part A – Polymer Chemistry*, **30**(11), 2389-2397 (1992).
16. Velada, J. L., et al., “A study of the thermal degradation of poly(mono-n-alkylitaconates)”, *Macromolecular Chemistry and Physics*, **196**(10), 3171-3185 (1995).
17. Cervantes-Uc, J. M., et al., “TGA/FTIR study on thermal degradation of polymethacrylates containing carboxylic acid groups”, *Polymer Degradation and Stability*, **91**(12), 3312-3321 (2006).
18. Colthup, N. B., Daly, L. H., Wiberley, S. E., *Introduction to Infrared and Raman Spectroscopy*, San Diego: Academic Press Inc. (1990).

19. Giroux, L., et al., “Application of thermogravimetric Fourier transform infrared spectroscopy (TG-FTIR) to the analysis of oxygen functional groups in coal”, *Energy & Fuels*, **20**(5), 1988-1996 (2006).
20. Eskay, T. P., et al., “Does decarboxylation lead to cross-linking in low-rank coals”, *Energy & Fuels*, **10**(6), 1257-1261 (1996).
21. Manion, J. A., et al., “Decarboxylation and coupling reactions of aromatic acids under coal-liquefaction conditions”, *Energy & Fuels*, **10**(3), 776-788 (1996).
22. Eskay, T. P., et al., “Pyrolysis of aromatic carboxylic acids: Potential involvement of anhydrides in retrograde reactions in low-rank coals”, *Energy & Fuels*, **11**(6), 1278-1287 (1997).
23. McMillen, D. F. & Golden, D. M., “Hydrocarbon bond dissociation energies”, *Annual Review of Physical Chemistry*, **33**, 493-532 (1982).
24. Plummer, C. J., et al., “Microdeformation in thin films of 3FDA/PMDA polyimide and polyimide nanofoams”, *Journal of Polymer Science Part B – Polymer Physics*, **33**(12), 1813-1820 (1995).
25. Hsiao, S. H. & Chen, W. T., “Syntheses and properties of new aromatic polybezoxazoles bearing ether and phenylethylidene or 1-phenyl-2,2,2-trifluoroethylidene linkages”, *Journal of Polymer Science Part A – Polymer Chemistry*, **41**(7), 914-921 (2003).

6.0 SUPERCRITICAL CARBON DIOXIDE CONDITIONING OF THE 6FDA-DAM:DABA (2:1) FREE ACID AND CROSSLINKED DERIVATIVES

6.1 Introduction

This chapter presents research focused on the supercritical carbon dioxide ($scCO_2$) conditioning of the 6FDA-DAM:DABA (2:1) free acid and crosslinked polymers. Pure CO_2 permeation and sorption isotherms are measured to understand the effects that $scCO_2$ has on the polymer. Mixed gas permeation experiments are performed to characterize the polymer for natural gas purification following $scCO_2$ conditioning.

6.2 $scCO_2$ Conditioning of the Free Acid Polymer

6.2.1 Pure Gas Permeation

Figure 6.1 displays the CO_2 permeation isotherm for a 6FDA-DAM:DABA (2:1) free acid polymer film, approximately 50 μm thick, that was annealed at 220 ^oC for 48 hours under vacuum. As mentioned in Chapter 3.6.2, each data point represents 12 ± 1 hours of CO_2 conditioning at that pressure. The CO_2 permeability displays a typical Dual Mode response with decreasing permeability until about 400 psia when there is an upward swing in permeability caused by plasticization. Permeability continues to increase until the film is in the supercritical region of CO_2 when it begins to decline. The film was then maintained at 1500 psia for 10 days, and the permeability continues to decline over that time. During depressurization, the permeability initially increases with

decreasing pressure which is an expected hysteresial response; however, at 1200 psia, the permeability then declines significantly before turning back upward at 950 psia. Finally, after a gradual rise in permeability from 900 to 200 psia, the CO_2 permeability again decreases. This final decline in permeability, however, is key to understanding this CO_2 conditioning process because it reveals that the polymer film completes the conditioning procedure at a lower free volume state than when the initial pressurization begun.

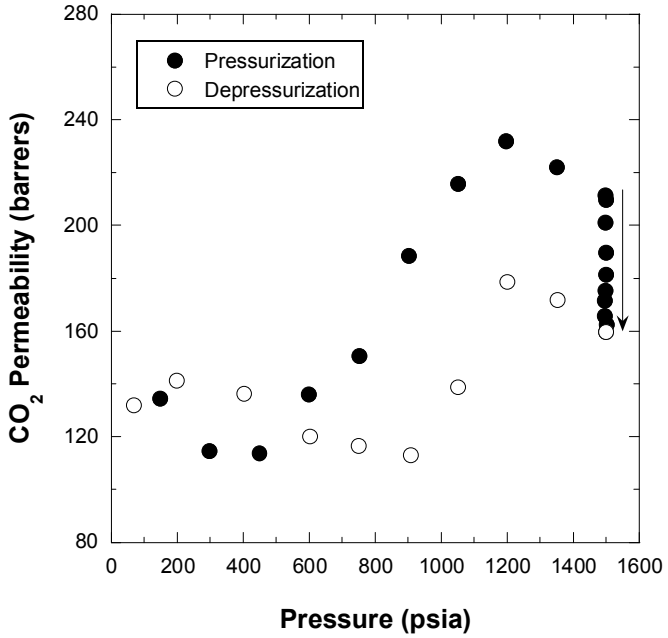

Figure 6.1: CO_2 permeation isotherm for the 6FDA-DAM:DABA (2:1) free acid film conducted at 35 ^oC

Previous work found a similar response using a higher free volume noncrosslinkable polyimide, 6FDA-DAM, and attributed the collapse in permeability to a structural rearrangement of the polymer matrix [1]. This structural rearrangement requires two conditions to occur. A highly sorbing component needs to be present in the polymer coupled with high hydrostatic pressures. Therefore, the highly sorbed species, CO_2 in

this case, appears to act as a “molecular lubricant” for the polymer chains to relax toward an energetically lower configuration state [2]. Previous work has confirmed significant enhancements in polymer self-diffusion in the presence of $scCO_2$ [3,4].

Upon repressurization of the $scCO_2$ conditioned film, presented in Figure 6.2, the typical downward permeability response at low pressures during the pressurization is not observed. Rather, the CO_2 permeability maintains an increasing trend at pressures up to 1350 psia. Also, and more importantly, the CO_2 permeability at the onset of the repressurization cycle is nearly one fourth that of the pressurization cycle. At 200 psia, the CO_2 permeability is only 44 barrers compared to 160 barrers at 150 psia in the pressurization cycle.

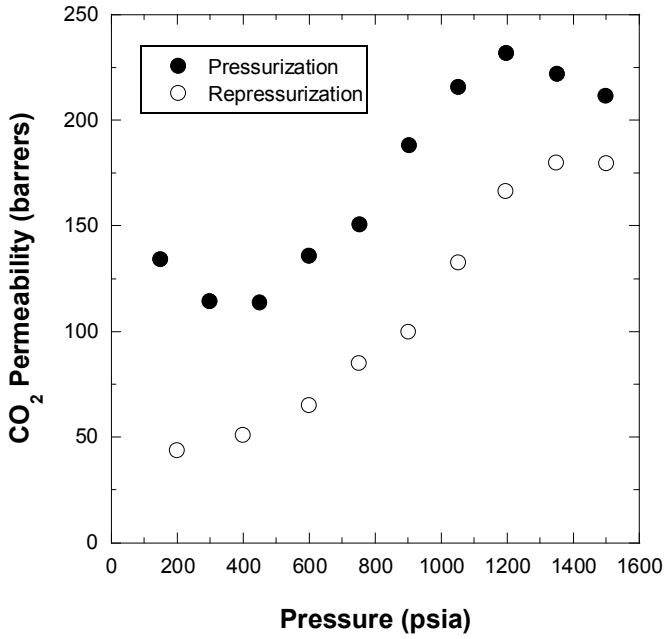

Figure 6.2: CO_2 permeation isotherms of the free acid for the pressurization and repressurization cycles at 35 ^{o}C

The lack of the Dual Mode response at low pressures and the large decrease in CO_2 permeability following $scCO_2$ conditioning indicate that the structural rearrangement

leads to a lower free volume polymer structure with a greatly reduced Langmuir sorption capacity. In fact, the conditioned free acid film is already plasticized at 200 psia as shown by the increasing CO_2 permeability at the onset of repressurization. The permeability continues to increase up to 1500 psia; whereas, in the case of the pressurization cycle, the permeability began to decrease at 1350 psia. Structural rearrangement is occurring between 1200 and 1500 psia, as evident by the reduced increase in permeability; however, there may not be enough CO_2 sorbed within the polymer matrix to cause the larger rearrangement, and more drastic reduction in permeability, as seen in the pressurization cycle.

Once 1500 psia was reached during the pressurization and repressurization cycles, the film was maintained at this pressure for 10 days (or until it failed in the case of the repressurization film). As observed in Figure 6.1, the CO_2 permeability substantially decreased over this 10 day period. This response is better illustrated in Figure 6.3 which displays the CO_2 permeability of the pressurization and repressurization cycles as a function of the time at 1500 psia. The CO_2 permeability during pressurization decreases slowly at the onset, more rapidly after 50 hours, and then finally appears to approach some asymptotic value at longer times. During repressurization, there is an initial increase in permeability before beginning to decrease at 75 hours.

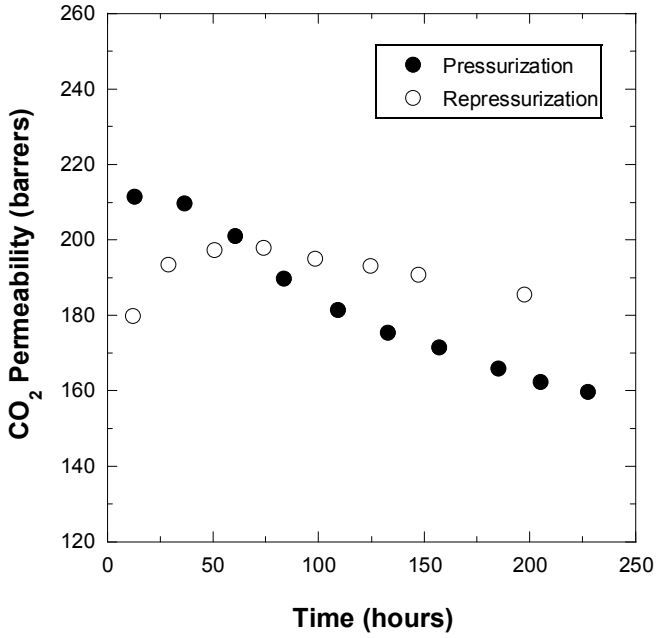

Figure 6.3: CO_2 permeability of the free acid as a function of time at 1500 psia, 35 ^oC

These responses are very similar to a response observed in a previous study in which the sorption of a highly sorbing organic vapor is studied in polymer samples with various thermal histories [5]. In this study, as-received and pre-swollen polystyrene samples were exposed to n-hexane for prolonged periods of time. The results, shown in Figure 6.4, indicate that an ultimate thermodynamic equilibrium is reached at long time scales under these specific conditions. In a similar manner, the free acid film reaches 1500 psia with different histories between the pressurization and repressurization cycles. In other words, for the repressurization cycle, the film has already experienced $scCO_2$ and structural rearrangement which alters the history of the film for subsequent testing. Therefore, for both pressurization cycles, as the film is exposed to $scCO_2$ at 1500 psia over long periods of time, the CO_2 permeability appears to approach an ultimate thermodynamic equilibrium for transport regardless of the film history. This ultimate equilibrium CO_2 permeability value is specific to the conditions of this experiment.

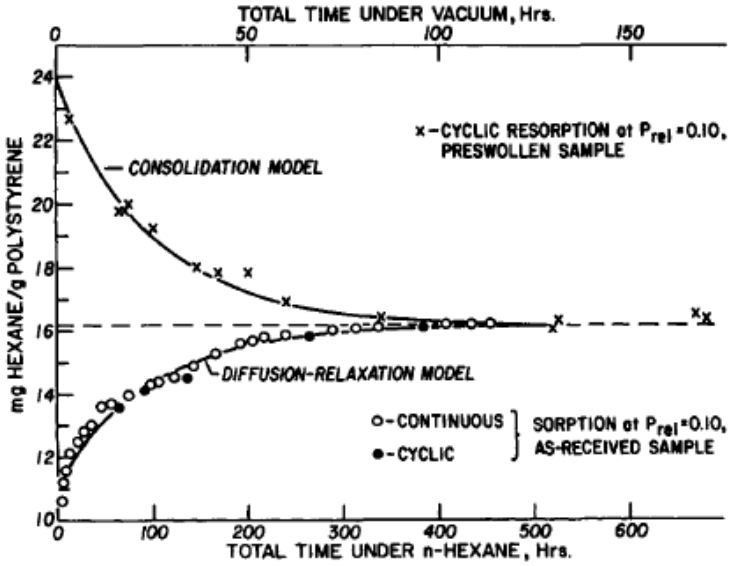

Figure 6.4: Consolidation and swelling of 0.53 μm polystyrene powder at 30 °C as monitored by sorption of n-hexane [5]

6.2.2 CO_2/CH_4 Mixed Gas Permeation

The purpose of this work is to understand the effects $scCO_2$ may have on the polymer for the purification of natural gas. Therefore, prior to $scCO_2$ conditioning and following the first pressurization cycle, the free acid film was probed with a 50/50 CO_2/CH_4 mixed gas feed to examine the effect that this structural rearrangement has on the separation properties of the membrane. Figures 6.5 - 6.7 display the CO_2 and CH_4 permeation isotherms and separation factor for each of these tests.

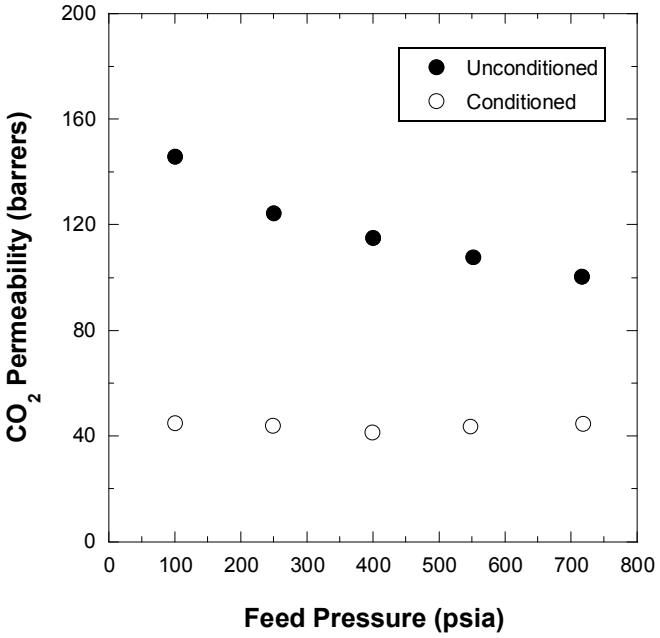

Figure 6.5: CO_2 permeation isotherm for 50/50 CO_2/CH_4 mixed gas feed prior to and after $scCO_2$ conditioning

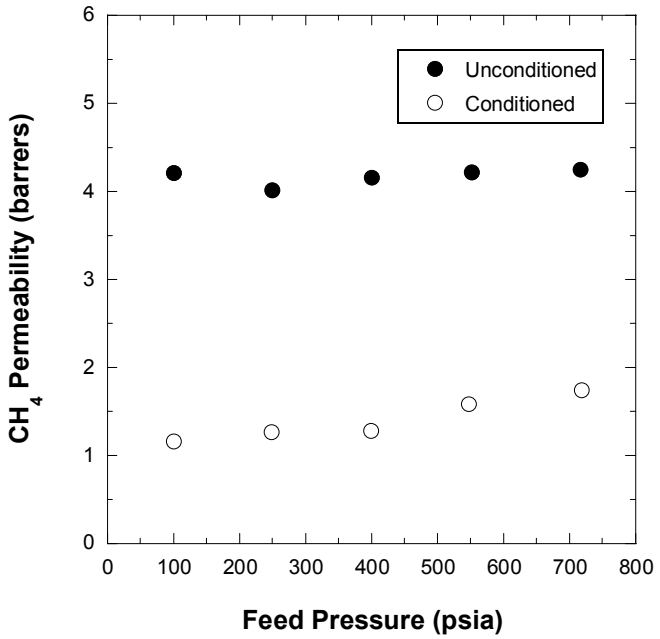

Figure 6.6: CH_4 permeation isotherm for 50/50 CO_2/CH_4 mixed gas feed prior to and after $scCO_2$ conditioning

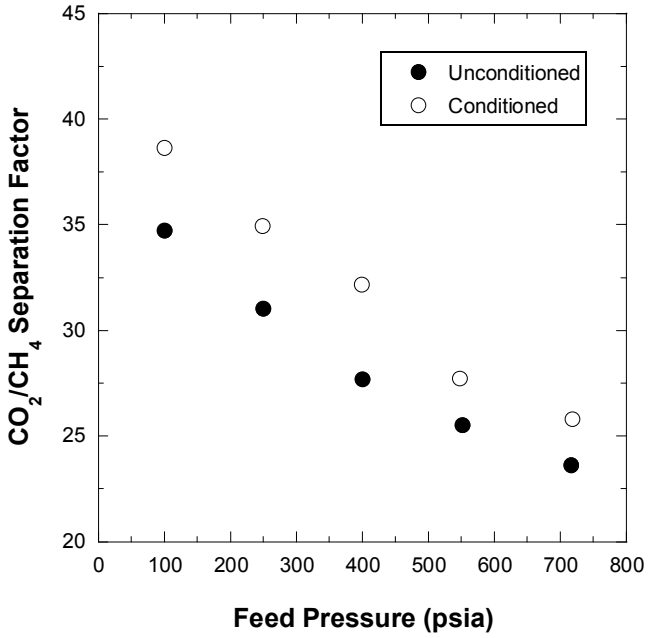

Figure 6.7: CO_2/CH_4 separation factor for 50/50 CO_2/CH_4 mixed gas feed prior to and after $scCO_2$ conditioning

The unconditioned film exhibits a typical binary feed permeation response for both CO_2 and CH_4 when nonideal effects are taken into account. As mentioned in Chapter 2.8, bulk flow and nonideal thermodynamics affect mixed gas permeation and can be detrimental to the overall separation, especially in feeds with large concentrations of both components [6,7]. For this reason the CO_2/CH_4 separation factor decreases with increasing pressure. Consistent with the hypothesis that $scCO_2$ conditioning reduces the Langmuir sorption capacity of the polymer, the CO_2 permeability of the conditioned film is greatly reduced and does not exhibit the typical downswing in permeability associated with Langmuir site filling.

For the purposes of natural gas purification, $scCO_2$ conditioning greatly diminishes the productivity of the free acid membrane as observed by the 55% decrease in CO_2 permeability at 720 psia of the 50/50 CO_2/CH_4 mixed gas feed. However, there was also a corresponding 9% increase in the separation factor.

6.2.3 Gas Sorption

Sorption measurements in $scCO_2$ were measured following the exact protocol used for the CO_2 permeation isotherm in Figure 6.1 (ie 12 hours conditioning at each data point, 10 days of conditioning at 1500 psia), and the results are shown in Figure 6.8. The typical Dual Mode curvature is not observable in this sorption isotherm because the concave curvature from the pressure axis associated with Langmuir site filling occurs at CO_2 pressures lower than 200 psia. At pressures above 200 psia, the sorption of CO_2 remains fairly linear up to 1050 psia as would be expected with the linear response of Henry's Law sorption.

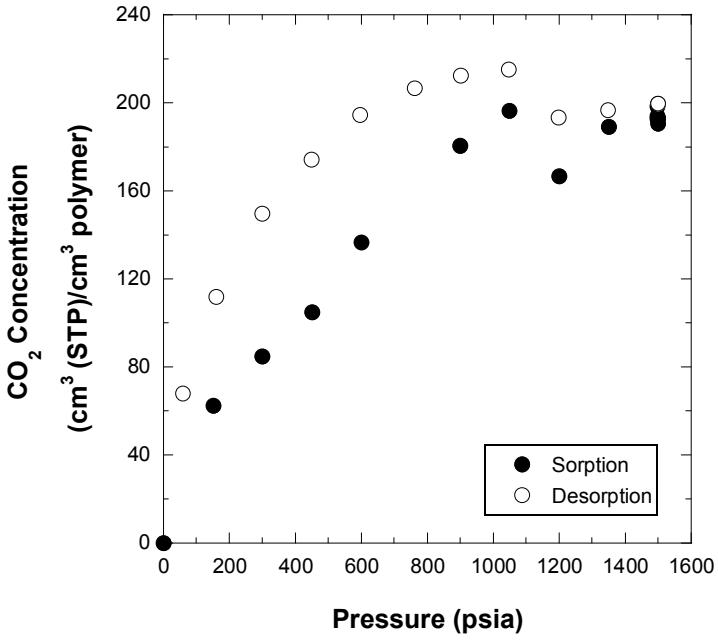

Figure 6.8: CO_2 sorption isotherm for the free acid polymer at 35 ^oC

Interestingly, at 1200 psia, there is a sharp decrease in the CO_2 concentration before rising to stable levels at 1350 and 1500 psia. This response at 1200 psia was also observed in CO_2 sorption in polystyrene samples at 35 ^oC [8]. In this case, the authors confirmed the repeatability of the data point and provided a few possible explanations which revolved around the uncertainty of the measurement due to sensitivity of the CO_2 density in this region.

Unlike the CO_2 permeation isotherm which shows a dramatic decrease in CO_2 permeability over the 10 day conditioning period at 1500 psia, the CO_2 sorption isotherm actually indicates a slight increase in CO_2 concentration over the same time period. This response is counter to the hypothesis that a structural rearrangement of the polymer reduces the overall capacity of the penetrant in the polymer. Furthermore, upon desorption, a typical hysteresis is observed as the desorption curve lies above the sorption curve. Again, there is a significant deviation that occurs at 1200 psia during desorption.

Low pressure CO_2 sorption isotherms were measured before and after the sorption conditioning in $scCO_2$, shown in Figure 6.8, to determine if the conditioning process reduces the overall sorption capacity of the polymer. Figure 6.9 displays these results and Table 6.1 displays the Dual Mode model parameters. Again, the Dual Mode model parameters were fit using Microcal Origin® software.

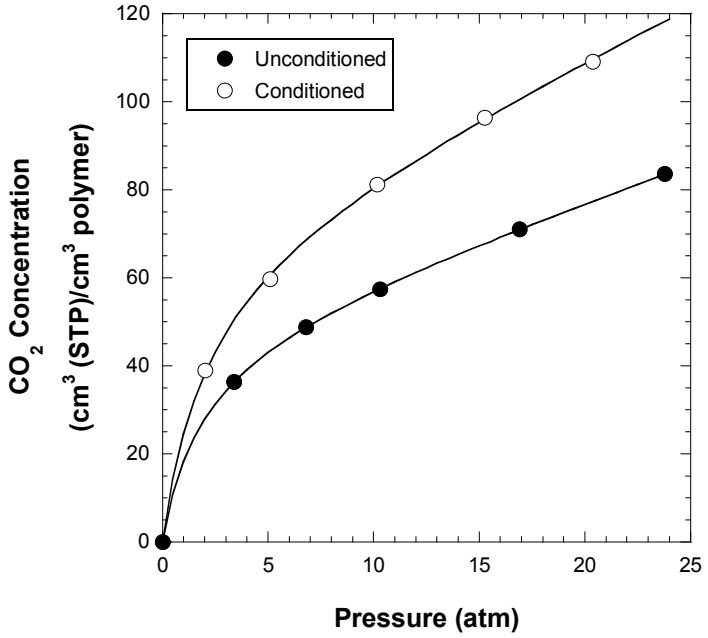

Figure 6.9: CO_2 sorption isotherms for the free acid prior to and after $scCO_2$ conditioning. Lines are the Dual Mode model fit for each data set. (S-30)

Table 6.1: Dual Mode model parameters for the free acid polymer prior to and after $scCO_2$ conditioning at 35 °C

Polymer State	k_D (cm^3 STP/(cm^3-atm))	C_H' (cm^3 STP/cm^3)	b (1/atm)
Prior to $scCO_2$ conditioning	1.64 ± 0.01	48.1 ± 0.4	0.52 ± 0.01
Post $scCO_2$ conditioning	2.28 ± 0.15	69.9 ± 3.6	0.46 ± 0.05

The $scCO_2$ conditioned free acid sorption isotherm clearly has a higher sorption capacity than the unconditioned film. This response is also evident in the Dual Mode sorption parameters which show a large increase in both k_D and C_H' for the conditioned film.

These data confirm that $scCO_2$ conditioning in the sorption chamber does not lead to the structural reorganization of the free acid polymer observed in the permeation isotherm in Figure 6.1 which leads to a lower free volume polymer structure.

The different structural responses observed through permeation and sorption measurements may therefore be a result of the penetrant concentration gradient present in the polymer. In permeation experiments, the CO_2 concentration decreases through the membrane from the upstream side to the downstream side which is under vacuum; whereas, the CO_2 concentration in sorption experiments remains constant through the membrane. This concentration gradient may allow specific polymer configurations of lower energy to be formed and immobilized that might not be possible in a constant concentration CO_2/polymer mixture.

Dilation measurements, as described in Chapter 3.4.2, were taken in conjunction with the above $scCO_2$ conditioning sorption isotherm, and the Dual Mode model presented in Equation 2.11 was used to describe the response. The partial molar volume of CO_2 in the polymer is determined using the sorption and dilation data at each pressure and is described in Appendix B in greater detail. The partial molar volumes of CO_2 are shown in Figure 6.10, and an average value of 26.6 cm^3/mol is used in the Dual Mode model.

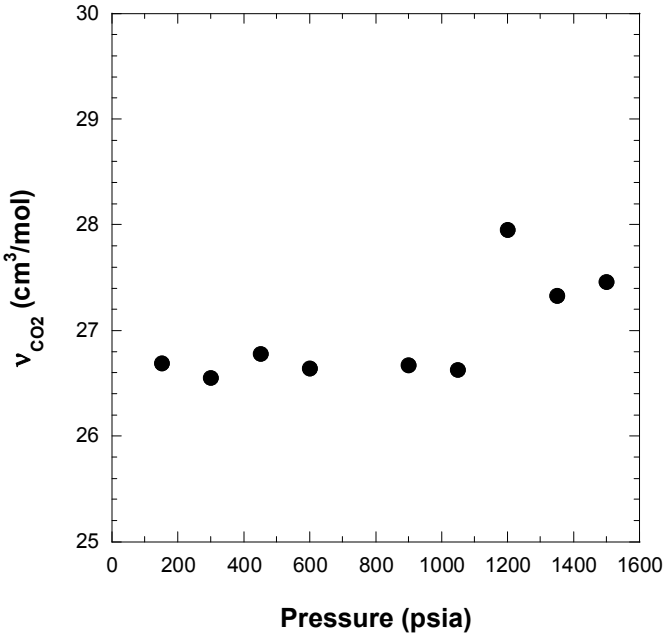

Figure 6.10: Partial molar volumes of CO_2 in the free acid polymer

The Henry's Law constant, k_D, has been shown to increase with increasing pressure, ie polymer swelling, for condensable penetrants in rubbery polymers [9]. Therefore, the k_D value of 1.73 cm^3 STP/(cm^3-atm) in the free acid polymer prior to scCO_2 conditioning in Table 6.1 will most likely underestimate the dilation response since the sorption data in Figure 6.9 was collected at lower CO_2 pressures. Also, the data in Figure 6.9 were collected after 10 time lags (~10 minutes) of equilibration time; whereas, the high pressure sorption and dilation measurements in Figures 6.8 and 6.11 consist of 12 hours conditioning time at each pressure. This CO_2 conditioning results in significantly greater polymer relaxation and swelling, which causes an increase in k_D. A more realistic value of k_D for the Dual Mode model is the post scCO_2 conditioning k_D value of 2.10 cm^3 STP/(cm^3-atm) in Table 6.1. For comparison, both k_D values are used to model the dilation response in Figure 6.11.

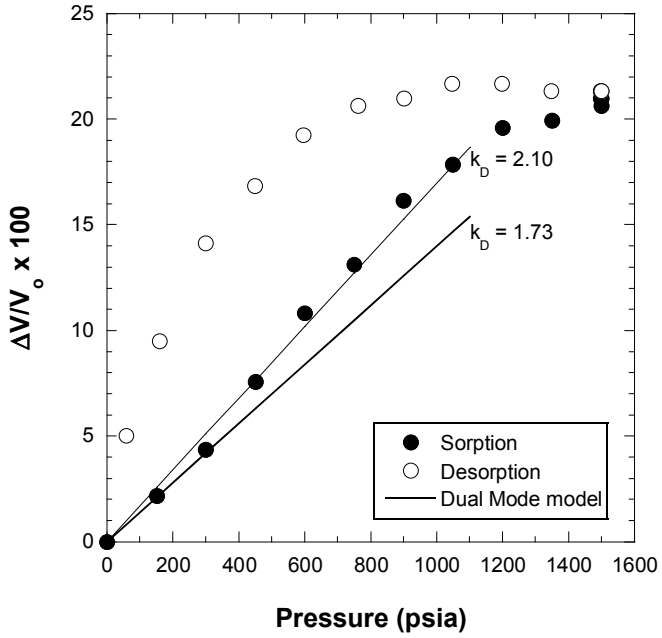

Figure 6.11: Dilation of the free acid polymer in CO_2 at 35 °C. Line is the Dual Mode model fit for dilation.

As can be seen, the Dual Mode dilation model with the post $scCO_2$ conditioning k_D value reasonably describes the dilation response of the free acid polymer up to 1050 psia. As expected, the k_D value of 1.73 cm^3 STP/(cm^3-atm) determined prior to $scCO_2$ conditioning underestimates the free acid dilation. As with the high pressure sorption measurements in Figure 6.8, the dilation measurements exhibit a typical hysteresis upon depressurization.

6.3 $scCO_2$ Conditioning of the Crosslinked Polymers

6.3.1 Pure Gas Permeation

The ethylene glycol crosslinked and 1,4-benzenedimethanol crosslinked polymers were examined in a similar manner as the free acid polymer discussed in the

previous section to probe the effects of crosslinking on polymer stabilization in a $scCO_2$ environment. The film preparations and experimental procedures for the permeation and sorption measurements are identical to the free acid polymer conditions. Figure 6.12 displays the CO_2 permeation isotherms for these two crosslinked films.

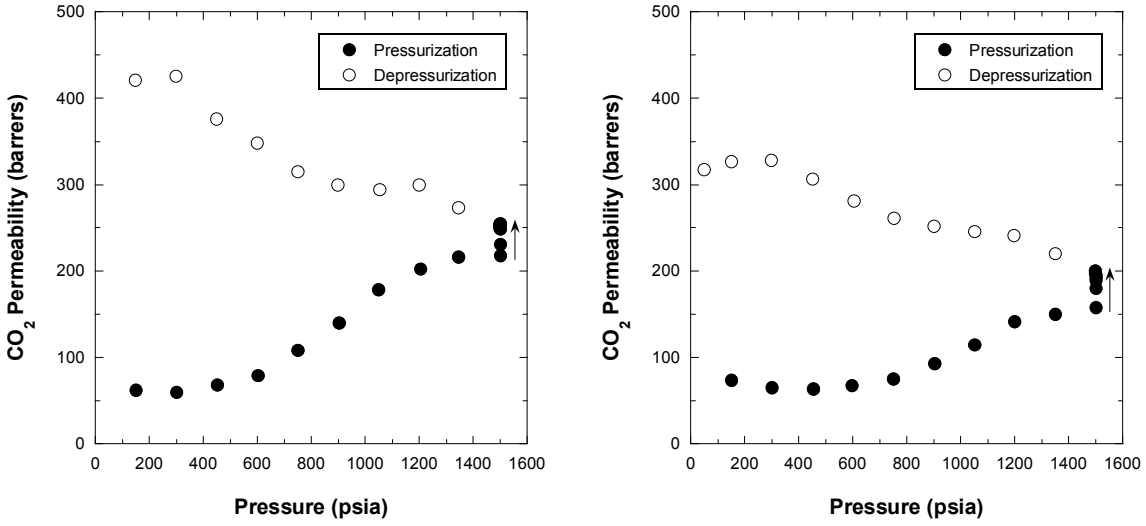

Figure 6.12: CO_2 permeation isotherms of the ethylene glycol crosslinked (left) and 1,4-benzenedimethanol crosslinked (right) films at 35 ^oC

The clear difference between these isotherms and the free acid isotherm, in Figure 6.1, is the lack of the observed structural rearrangement at high pressures in the crosslinked films. Also, these films exhibit a hysteretical response upon depressurization that is typical of glassy polymers. While the larger benzenedimethanol crosslinking agent was expected to prop open the polymer structure and enhance permeability, the CO_2 permeabilities are actually similar to those of the ethylene glycol at lower pressures. Moreover, at higher pressures, the CO_2 permeabilities in the 1,4-benzenedimethanol crosslinked polymer actually remain lower than that of the ethylene glycol crosslinked polymer. Fluorescence spectra were obtained for the two crosslinked polymers to

determine if the aromatic nature of the 1,4-benzenedimethanol crosslinking agent might contribute to the formation of charge transfer complexes, which would facilitate a reduction in polymer chain mobility and gas permeability. As shown in Figure 6.13, the 1,4-benzenedimethanol crosslinked polymer exhibits a lower fluorescence intensity than the ethylene glycol crosslinked polymer indicating the stiff crosslinking agent actually inhibits the formation of charge transfer complexes. Therefore, the reduced CO_2 permeabilities at high CO_2 pressures in the 1,4-benzenedimethanol crosslinked film is solely a result of the crosslinking agent size and rigidity and not of any interactions the crosslinking agent may have with the polymer backbone.

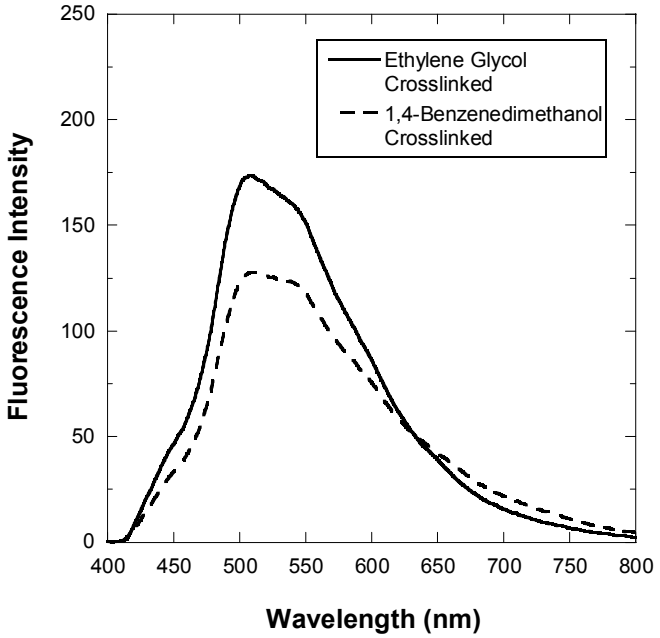

Figure 6.13: Fluorescence spectra of the crosslinked polymers

Ultimately, the 1,4-benzenedimethanol crosslinked film is more stabilized in the $scCO_2$ environment, as revealed by the lower CO_2 permeability at 1500 psia, and returns to a

lower free volume state upon depressurization as compared to the ethylene glycol crosslinked film.

The repressurization permeation isotherms for both crosslinked films are presented in Figure 6.14. Again, the 1,4-benzenedimethanol crosslinked film exhibits greater stability than the ethylene glycol crosslinked film upon repressurization as shown by the lower CO_2 permeability at 1500 psia. Neither film exhibits the large decline in CO_2 permeability at the onset of repressurization indicative of structural rearrangement as observed in Figure 6.1; however, both crosslinked films have reduced plasticization pressures indicating that some level of the structural reorganization has occurred. Surprisingly, $scCO_2$ conditioning on the ethylene glycol crosslinked film during repressurization has a less substantial effect than the during pressurization which is evident by the lower CO_2 permeability at 1500 psia. Conversely, the 1,4-benzenedimethanol crosslinked film exhibits an expected response for a crosslinked stabilized film in that the CO_2 permeability at higher pressures during repressurization is similar to that during pressurization.

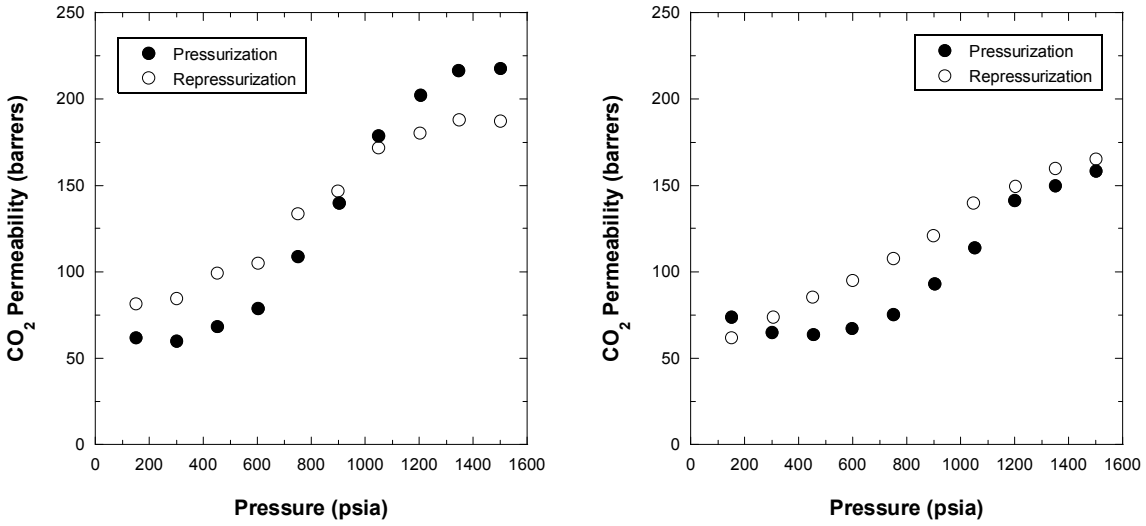

Figure 6.14: CO_2 permeation isotherms of the ethylene glycol crosslinked (left) and 1,4-benzenedimethanol crosslinked (right) films for the pressurization and repressurization cycles at 35 ^oC

Even though the ethylene glycol crosslinked film appears to be more stabilized during repressurization, the film returns to the same equilibrium state when conditioned at 1500 psia. This response is presented in Figure 6.15 where the CO_2 permeability at 1500 psia following repressurization increases to match the pressurization CO_2 permeability level before the film breaks. Therefore, the ethylene glycol crosslinked film ultimately maintains its stability throughout the $scCO_2$ conditioning process for the time scale of these experiments. Conversely, the 1,4-benzenedimethanol crosslinked film has nearly identical CO_2 permeabilities at 1500 psia for both pressurization and repressurization cycles indicating this crosslinked film possesses the best overall stability in the presence of $scCO_2$.

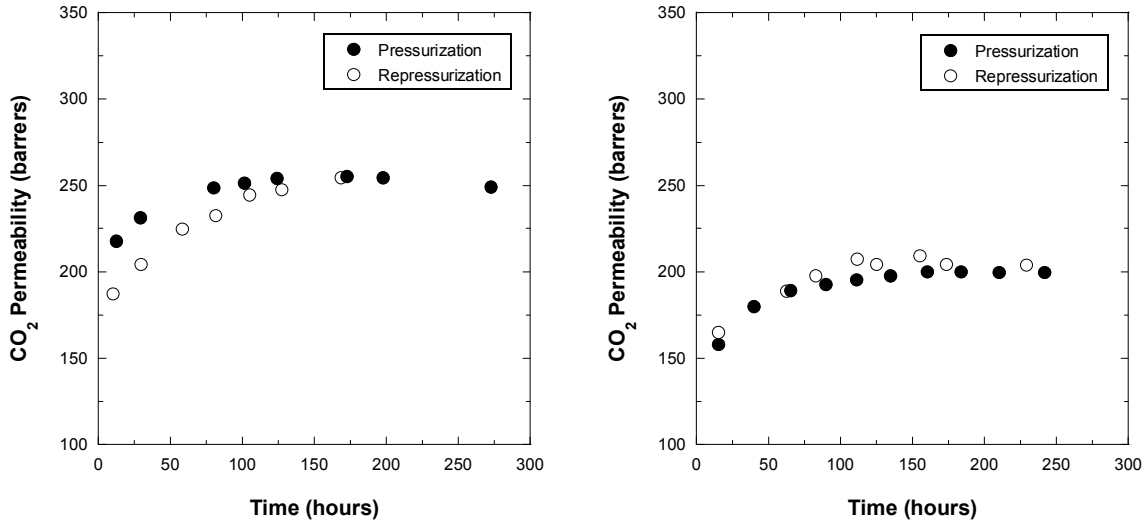

Figure 6.15: CO_2 permeability of the ethylene glycol crosslinked (left) and 1,4-benzenedimethanol crosslinked (right) films as a function of time at 1500 psia, 35 ^oC

6.3.2 CO_2/CH_4 Mixed Gas Permeation

As with the free acid polymer, the ethylene glycol crosslinked and 1,4-benzenedimethanol crosslinked films were examined with a 50/50 CO_2/CH_4 mixed gas feed prior to and after the $scCO_2$ conditioning in Figure 6.12. These results are presented in Figure 6.16. Both crosslinked films exhibit similar responses to the free acid film in that the CO_2 permeability remains relatively constant and the CH_4 permeability increases with increasing pressure. However, where the free acid film experienced a significant reduction in the CO_2 and CH_4 gas permeabilities following $scCO_2$ conditioning, the crosslinked film gas permeabilities generally increased compared to the unconditioned values suggesting that additional free volume was trapped in the polymer following the $scCO_2$ conditioning cycle. This result was expected considering the typical hystereses that both crosslinked films exhibited during depressurization.

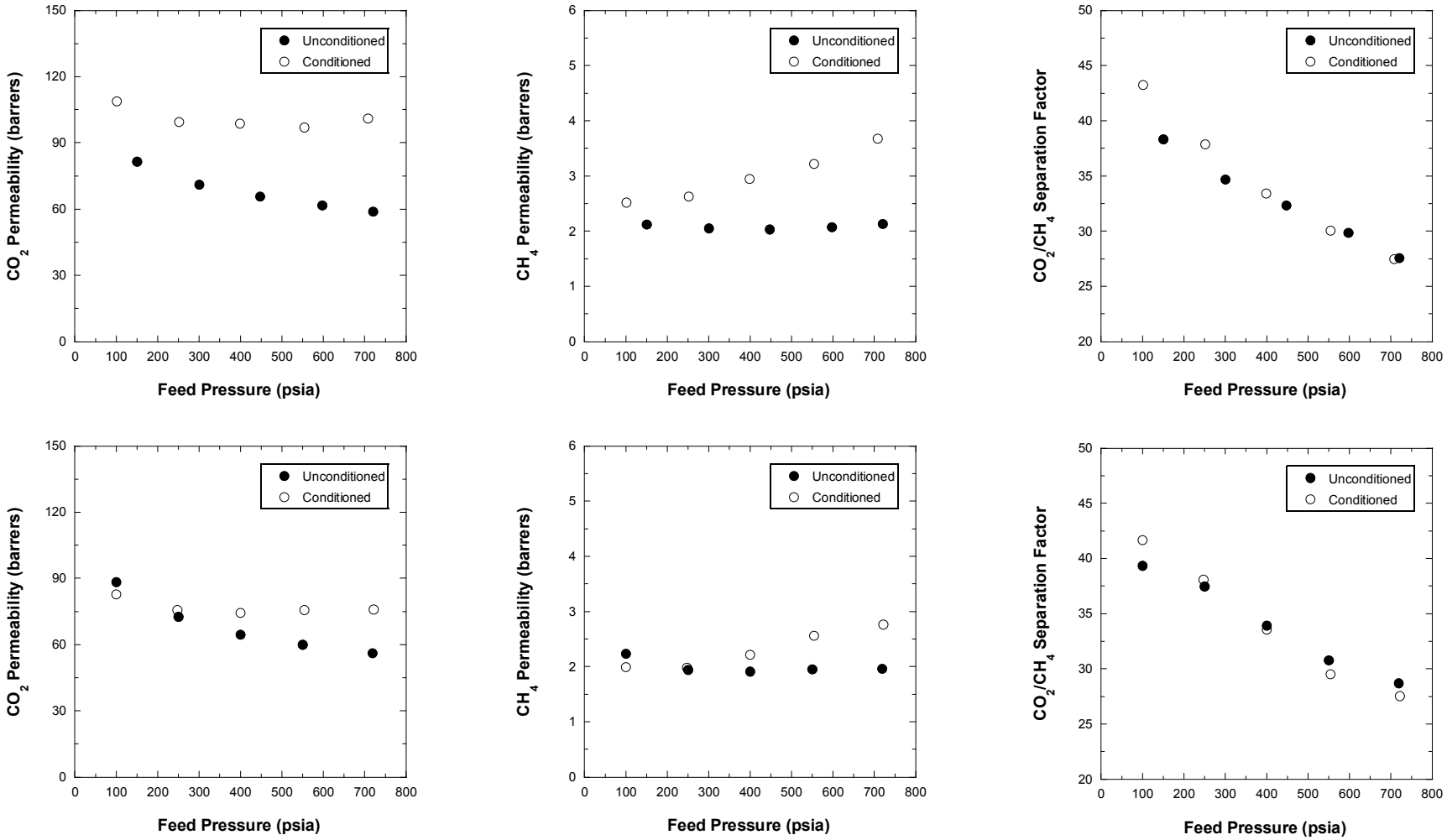

Figure 6.16: 50/50 CO_2/CH_4 mixed gas permeation results before and after $scCO_2$ conditioning for the ethylene glycol crosslinked (top) and 1,4-benzenedimethanol crosslinked (bottom) polymers

Following $scCO_2$ conditioning, the ethylene glycol crosslinked film CO_2 permeability increases 70% at 720 psia of the 50/50 CO_2/CH_4 mixed gas feed, whereas the 1,4-benzenedimethanol crosslinked film CO_2 permeability only increases 35%. Surprisingly, the separation factors for both films remained relatively unchanged. Even though the additional free volume enhances the overall gas transport, the crosslinked nature of the polymer maintains the size-discriminating ability by restricting segmental mobility of the polymer.

For the purposes of natural gas purification, these crosslinked 6FDA-DAM:DABA (2:1) polymers are more suitable than the free acid polymer due to their ease of forming asymmetric hollow fibers in aqueous quench. Furthermore, these crosslinked polymers are more ideal due to their increased stability in the presence of $scCO_2$ and higher gas permeabilities and selectivities following $scCO_2$ conditioning. Between the two crosslinked polymers, the ethylene glycol crosslinked polymer appears to be the most feasible option since it has the highest gas throughput while maintaining the separation efficiency of the membrane.

6.3.3 Gas Sorption

The $scCO_2$ conditioning sorption isotherms for the crosslinked polymers are presented in Figure 6.17. Again, both films exhibit the same linear response up to 1050 psia, and then display the same reduction at 1200 psia that was observed in the free acid film. Upon reaching 1500 psia and following 10 days of $scCO_2$ conditioning, the 1,4-benzenedimethanol crosslinked polymer has a lower sorption capacity than the ethylene glycol crosslinked polymer. Unfortunately, the 1,4-benzenedimethanol crosslinked desorption curve ends at 900 psia due to a leak that drained the system;

however, it appears to be following a similar hysteretical path as the ethylene glycol crosslinked film.

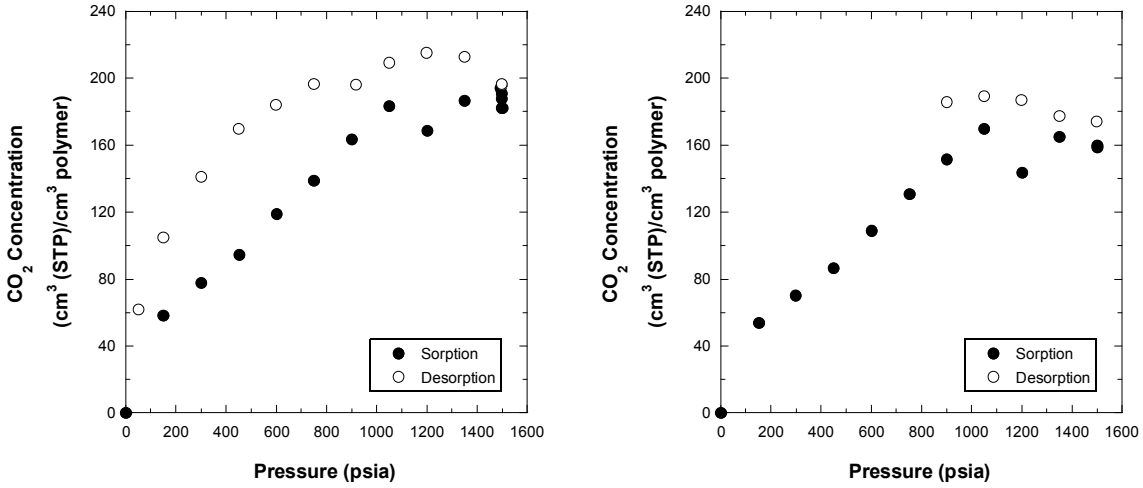

Figure 6.17: CO_2 sorption isotherm for the ethylene glycol crosslinked (left) and 1,4-benzenedimethanol crosslinked (right) polymers at 35 ^oC

These sorption curves and the permeation isotherms in Figure 6.12 allow determination of the diffusion coefficients for the crosslinked polymers, which are shown in Figure 6.18. At higher pressures, the 1,4-benzenedimethanol crosslinked polymer has a higher diffusion coefficient than the ethylene glycol crosslinked polymer. Therefore, the lower CO_2 permeabilities for this crosslinked polymer in Figure 6.12 are a combined result of lower sorption capacity and lower diffusivity. At low pressures before plasticization occurs, the diffusion coefficient is expected to be relatively constant; however, as can be seen, the diffusion coefficients for both crosslinked polymers increase across all pressures. This result indicates that the 12 hours of conditioning at each pressure interval actually swells the polymer to some extent, even at pressures below the plasticization pressure. The reduced slope of the 1,4-benzenedimethanol crosslined

polymer confirms this polymer is more stable under CO_2 conditioning than the ethylene glycol crosslinked polymer.

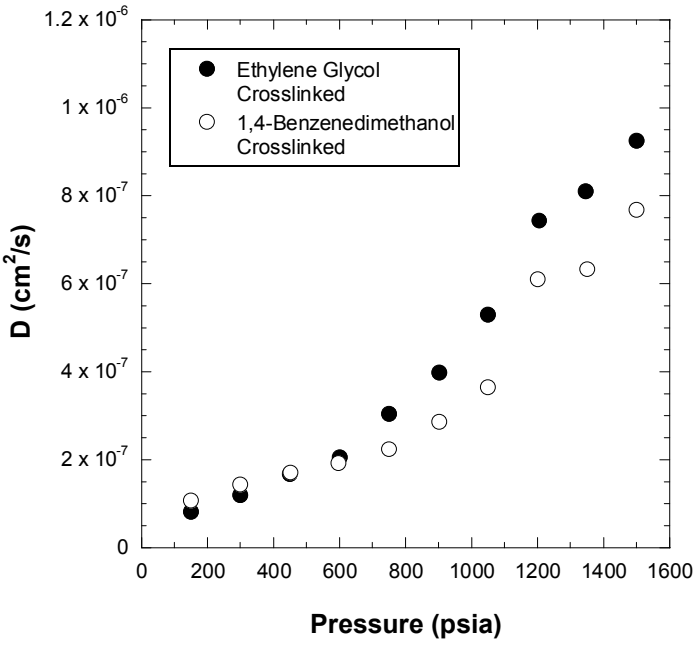

Figure 6.18: Diffusion coefficients for the crosslinked polymers

The low pressure CO_2 sorption isotherms from before and after the $scCO_2$ sorption conditioning and the corresponding Dual Mode parameters are presented in Figure 6.19 and Table 6.2. These data reveal that prior to $scCO_2$ conditioning, both crosslinked polymers have similar CO_2 sorption capacities; however, following $scCO_2$ conditioning, the sorption capacity of the ethylene glycol crosslinked polymer is enhanced more than the 1,4-benzenedimethanol polymer. This result is consistent with the mixed gas results for the ethylene glycol crosslinked film which exhibits a greater increase gas permeabilities following $scCO_2$ conditioning. The Dual Mode parameters confirm this sorption enhancement with a 57% and 60% increase in k_D and C_H',

respectively. Conversely, the 1,4-benzenedimethanol crosslinked polymer only exhibits a 38% and 50% increase in k_D and C_H'.

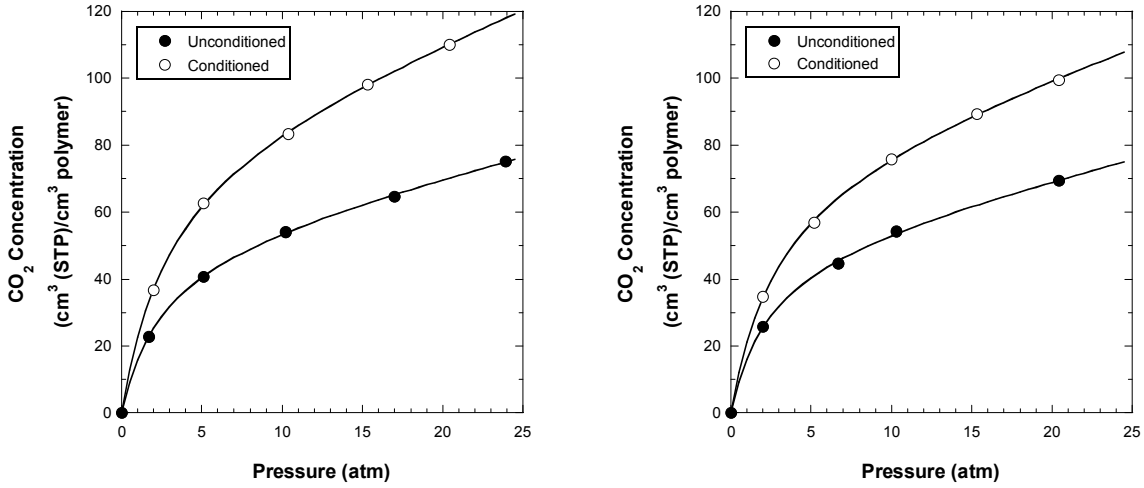

Figure 6.19: CO_2 sorption isotherms for the ethylene glycol crosslinked (left) and 1,4-benzenedimethanol crosslinked (right) polymers prior to and after $scCO_2$ conditioning. Lines are the Dual Mode model fit for each data set.

Table 6.2: Dual Mode model parameters for the crosslinked polymers prior to and after $scCO_2$ conditioning at 35 ^oC

Polymer State	k_D (cm^3 STP/(cm^3-atm))	C_H' (cm^3 STP/cm^3)	B (1/atm)
Ethylene Glycol Crosslinked Pre-$scCO_2$	1.15 ± 0.07	52.5 ± 1.9	0.39 ± 0.03
Ethylene Glycol Crosslinked Post-$scCO_2$	1.81 ± 0.13	84.1 ± 3.6	0.33 ± 0.03
1,4-Benzenedimethanol Glycol Crosslinked Pre-$scCO_2$	1.15 ± 0.15	51.5 ± 3.7	0.41 ± 0.06
1,4-Benzenedimethanol Glycol Crosslinked Post-$scCO_2$	1.59 ± 0.13	77.1 ± 3.4	0.34 ± 0.03

Dilation measurements were also taken in conjunction with the $scCO_2$ sorption measurements of the crosslinked polymers. As with the sorption isotherms, the dilation measurements indicate the 1,4-benzenemethanol crosslinked polymer is more stable with a maximum dilation of only 20%. The determined average partial molar volumes of CO_2 in the crosslinked polymers are 29.6 cm^3/mol and 28.9 cm^3/mol for the ethylene glycol and 1,4-benzenedimethanol crosslinked polymers respectively. These values are larger than the free acid value of 26.6 cm^3/mol indicating that the crosslinked polymers can withstand a larger percentage of the penetrant in the polymer matrix while maintaining the separating efficiency as shown in Figure 6.16. The post $scCO_2$ values of k_D in Table 6.2 are used in conjunction with the average partial molar volumes to model

the dilation of the crosslinked polymers. The dilation measurements with the Dual Mode model are presented in Figure 6.20.

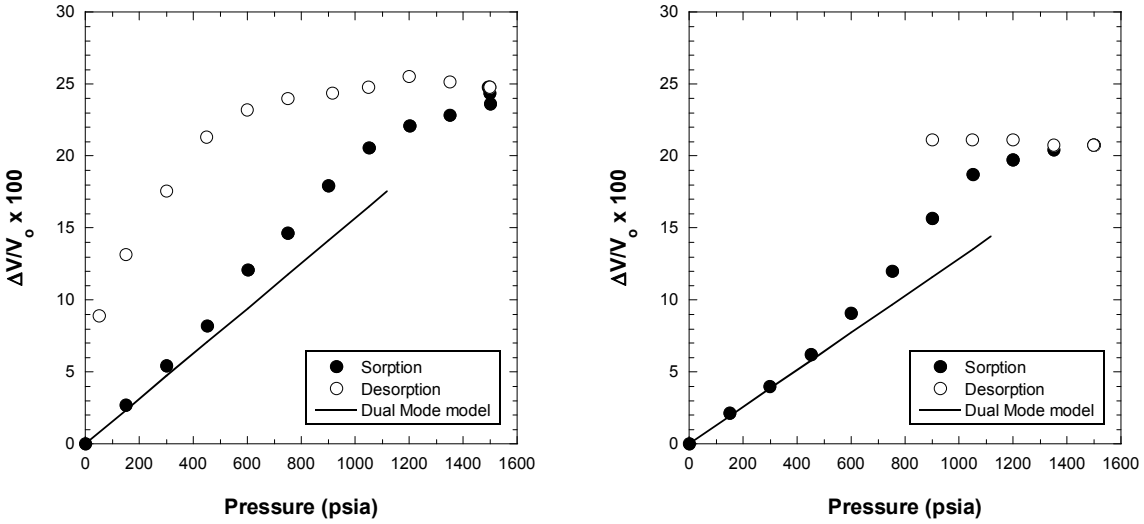

Figure 6.20: Dilation of the ethylene glycol crosslinked (left) and 1,4-benzenedimethanol crosslinked (right) polymers in CO_2 at 35 ^oC. Lines are the Dual Mode model fit for dilation.

Interestingly, the dilation measurements follow the Dual Mode model at low pressures and then deviate to higher degrees of swelling at higher pressures. This response indicates the crosslinked polymers tend to lose their enhanced stability when conditioned at high CO_2 pressures. However, as mentioned earlier, the separation efficiency is not greatly affected by this additional swelling.

6.4 Summary

$scCO_2$ conditioning of the 6FDA-DAM:DABA (2:1) free acid polymer exhibits a large reduction in CO_2 permeability at pressures in the supercritical region. This reduction can be attributed to a structural rearrangement of the polymer matrix to a lower

energy configuration. The 50/50 CO_2/CH_4 mixed gas permeation measurements confirm reductions in excess free volume and enhanced separating efficiency of the membrane following $scCO_2$ conditioning. Surprisingly, $scCO_2$ sorption measurements and pre/post sorption isotherms do not show this structural rearrangement in the free acid polymer. Corresponding dilation measurements are reasonably modeled by the Dual Mode model.

$scCO_2$ conditioning of the ethylene glycol crosslinked and 1,4-benzenedimethanol crosslinked polymers yield typical results and hystereses upon depressurization. The 1,4-benzenedimethanol crosslinked polymer is more stable under the $scCO_2$ conditions; however, the ethylene glycol crosslinked polymer possesses a higher CO_2 permeability while maintaining the separating efficiency of the polymer following $scCO_2$ conditioning, which is ideal for natural gas purification processes. Sorption measurements with $scCO_2$ and pre/post sorption isotherms confirm the greater stability of the 1,4-benzenedimethanol crosslinked polymer. Corresponding dilation measurements show additional swelling of the crosslinked polymers above the Dual Mode prediction; however, as mentioned earlier, the separation efficiency is maintained.

6.5 References

1. Damle, Shilpa, *Membrane Based Separations of Carbon Dioxide and Phenol Under Supercritical Conditions*, Dissertation, University of Texas-Austin (2004).
2. Fleming, O. S., et al., "Confocal raman study of poly(ethylene terephthalate) fibres dyed in supercritical carbon dioxide: dye diffusion and polymer morphology", *Polymer*, **46**(9), 2943-2949 (2005).
3. Gupta, R. R., et al., "Self-diffusion of polystyrene in a CO_2-swollen polystyrene matrix: a real time study using neutron reflectivity", *Macromolecules*, **36**(2), 346-352 (2003).
4. Fleming, O. S., et al., "High-pressure CO_2-enhanced polymer interdiffusion and dissolution studied with in situ ATR-FTIR spectroscopic imaging", *Polymer*, **47**(13), 4649-4658 (2006).
5. Berens, A. R. & Hopfenberg, H. B., "Induction and measurement of glassy-state relaxations by vapor sorption techniques", *Journal of Polymer Science – Polymer Physics*, **17**(10), 1757-1770 (1979).
6. Kamaruddin, H. D. & Koros, W. J., "Some observations about the application of Fick's first law for membrane separation of multicomponent mixtures", *Journal of Membrane Science*, **135**(2), 147-159 (1997).
7. Wind, J. D., Staudt-Bickel, C., et al., "The effects of crosslinking chemistry on CO_2 plasticization of polyimide gas separation membranes", *Industrial & Engineering Chemistry Research*, **41**(24), 6139-6148 (2002).
8. Zhang, Y., et al., "Sorption and swelling of block copolymers in the presence of supercritical fluid carbon dioxide", *Journal of Supercritical Fluids*, **11**(1-2), 115-134 (1997).

9. Pope, D. S., et al., “Statistical thermodynamics interpretation of sorption/dilation behavior of gases in silicone rubber”, *Macromolecules*, **24**(8), 1779-1783 (1991).

7.0 PHYSICAL AGING OF FLUORINE-CONTAINING POLYIMIDES

7.1 Introduction

This chapter examines the effects of long term physical aging of fluorine-containing polyimides. Structural differences in the dianhydride and diamine reveal the effects of bulky, CF_3 groups and symmetry of the phenylene linkage to changes in density and gas permeation through physical aging. Sorption isotherms are obtained following gas permeation to characterize the effects of physical aging on the sorption and diffusion coefficients; however, CO_2 exposure during gas permeation reverses the effects of physical aging.

7.2 Polymer Free Volume

The long term physical aging of fluorine-containing polyimides can be directly measured through comparison of the original and aged polymer densities. The fractional free volume can then be determined through the known density and a group contribution model which estimates the occupied volume of the polymer. Table 7.1 displays the initial density and fractional free volume (f) of the polyimides as measured some time between 1989 and 1991. The occupied volumes of the polymers were estimated using using the group contribution method of Van Krevelen [1].

Table 7.1: Initial density and fractional free volume measurements for the polyimides [2]

Polymer	Density (g/cm^3)	f
6FDA-6FpDA	1.466	0.190
6FDA-6FmDA	1.493	0.175
BPDA-6FpDA	1.417	0.161

Density measurements were conducted on aged cast films found along with the aged masked films for gas permeation. The following table displays the densities, factional free volumes, and the change in fractional free volume of the aged polymers as a result of physical aging. The same method described above is used to determine the occupied volume of each polymer to ensure direct comparisons of the fractional free volumes.

Table 7.2: Aged density and fractional free volume measurements for the polyimides

Polymer	Density (g/cm^3)	f	Change in f
6FDA-6FpDA	1.4833 ± 0.0004	0.181	4.7%
6FDA-6FmDA	1.502 ± 0.002	0.170	2.9%
BPDA-6FpDA	1.4220 ± 0.0004	0.158	1.8%

As would be expected with the physical aging process, the densities increased and the fractional free volumes decreased after approximately 18 years of aging. Also, the change in the fractional free volume scales with the original amount of free volume within

the polymer. 6FDA-6FpDA, which contains the highest fractional free volume, has the largest decrease in free volume; whereas, BPDA-6FpDA displays the smallest decrease in fractional free volume. These relative changes in free volume are consistent with the notion that physical aging is a self-retarding process as discussed in Chapter 2.5.

7.3 Effects of Physical Aging on Gas Permeation

In 1991, Robeson compiled a literature review of both glassy and rubbery polymers to examine the trade-off between gas permeability and gas pair selectivity [3]. From this compilation, an "upper bound" limit was determined for a number of gas pairs in which no polymers exhibited separation properties beyond that limit. Figures 7.1 - 7.3 display the gas permeabilities and gas pair selectivities for the original and aged polyimide samples with respect to the Robeson upper bound for each gas pair. Figure 7.3 does not display this upper bound because it was not examined by Robeson; however, the N_2/CH_4 separation has proven to be an important separation for natural gas denitrogenation [4]. The aged polymers probed through gas permeation came from aged masked films which were originally examined through permeation. However, it was not possible to ensure that each aged film corresponded to the original permeation data. In these figures, the solid data points are the original gas measurements and the hollow data points are the aged gas measurements. CO_2, CH_4, and N_2 were probed at 10 atm and O_2 was probed at 2 atm to match the original measurements. Because only one aged film was examined per polymer, a statistical analysis could not be performed to determine sample variance. However, a propagation of errors analysis was performed for gas permeabilities using measurement error in the dP/dt, sample volume, temperature, film thickness, film area, and upstream pressure [5]. All resulting uncertainties for both permeability and selectivity were smaller than the aged data points

in Figure 7.1 - 7.3. In fact, the uncertainty associated with gas selectivity is significantly less than that of gas permeability since temperature, sample volume, film area, and film thickness can be eliminated from the ratio. As expected with physical aging, the general trend for each polymer is a decrease in gas permeability and an increase in gas pair selectivity. However, for the most part, the changes resulting from physical aging run parallel to the Robeson limit and, therefore, do not do transcend this upper-bound limit for polymer membrane gas separations.

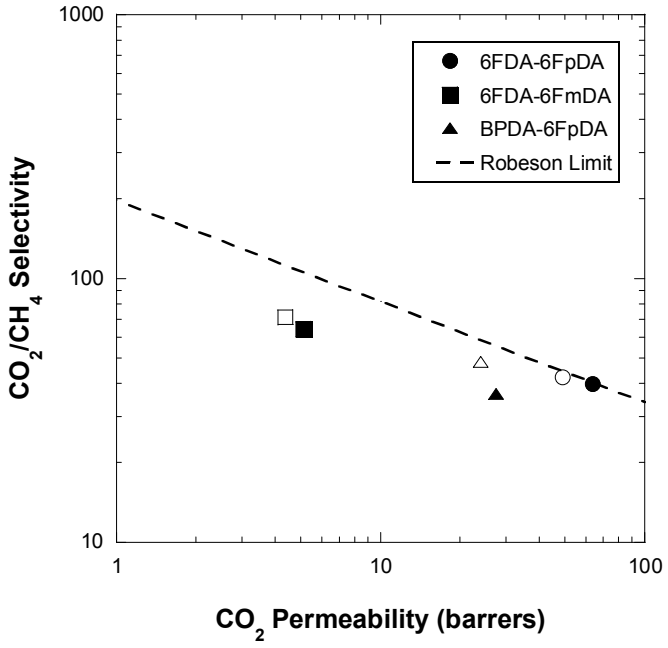

Figure 7.1: CO_2/CH_4 separation properties of original (solid data points) and aged (hollow data points) polymers

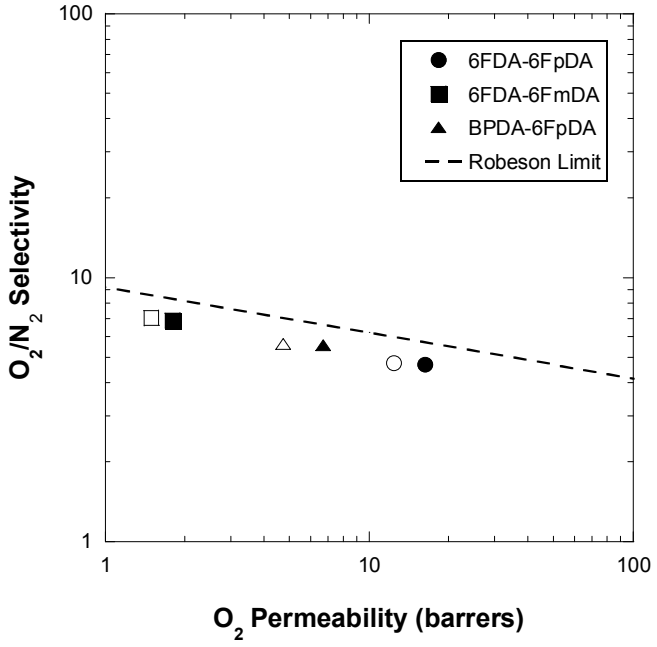

Figure 7.2: O_2/N_2 separation properties of original (solid data points) and aged (hollow data points) polymers

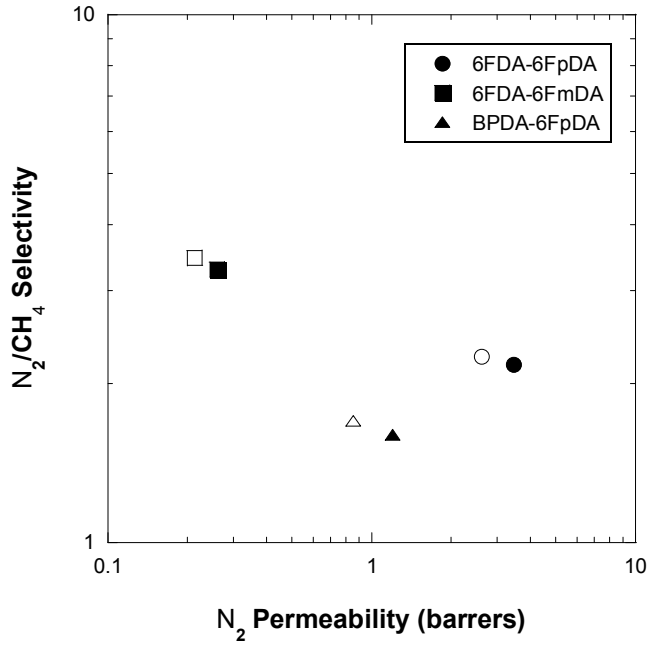

Figure 7.3: N_2/CH_4 separation properties of original (solid data points) and aged (hollow data points) polymers

7.3.1 Dianhydride Comparison

As shown in Figure 3.3, the structural difference between the BPDA and 6FDA dianhydrides is the lack of CF_3 groups between the aromatic groups. These bulky, CF_3 groups disrupt chain packing and increase the excess free volume within the polymer as shown by the enhanced fractional free volume for 6FDA-6FpDA in Table 7.1. This disruption in the chain packing also leads to a lower T_G for the 6FDA-6FpDA polymer [2]. As would be expected with a higher fractional free volume polymer of a similar structure, gas permeabilites are higher in 6FDA-6FpDA as compared to BPDA-6FpDA. The higher CO_2/CH_4 and N_2/CH_4 selectivities in the 6FDA-6FpDA polymer are not products of the higher fractional free volume of the polymer, but likely the result of differences in the distribution of the excess free volume [2].

Since 6FDA-6FpDA displayed the larger change in fractional free volume following approximately 18 years of physical aging, it is expected that this polymer would also exhibit the largest decrease in gas permeability. However, as shown in Table 7.3, the BPDA-6FpDA polymer actually exhibits larger relative decreases for all gas permeabilities except CO_2.

Table 7.3: Percent reduction of gas permeabilities of aged polymers: dianhydride comparison

Polymer	CO_2	O_2	N_2	CH_4
6FDA-6FpDA	23.1% ± 0.3	23.6% ± 0.3	24.4% ± 0.3	27.1% ± 0.3
BPDA-6FpDA	12.3% ± 0.1	28.9% ± 0.3	29.6% ± 0.3	33.8% ± 0.3

Within each polymer, the relative reduction in gas permeability scales with penetrant size. This is the expected response as physical aging can narrow the free volume distribution in a polymer as discussed in Chapter 4.4.6. Interestingly, the CO_2 permeability for BPDA-6FpDA exhibits a smaller decrease than expected which greatly enhances the CO_2/CH_4 selectivity associated with physical aging. The larger reductions in gas permeability, with the exception of CO_2, associated with BPDA-6FpDA may be a result of charge transfer formations. The lack of bulky, CF_3 groups coupled with the relatively straight, flat structure of BPDA should allow for more overlapping of electron-donating and electron-accepting portions of the backbone as discussed in Chapter 4.4.6. This response is observed through fluorescence spectroscopy measurements in Figure 7.4 which show a significantly higher spectrum intensity in the BPDA-6FpDA polymer as compared to the 6FDA-based polymers. Therefore, the increased charge transfer density likely causes the larger reductions in gas permeability as polymer chain mobility is further reduced.

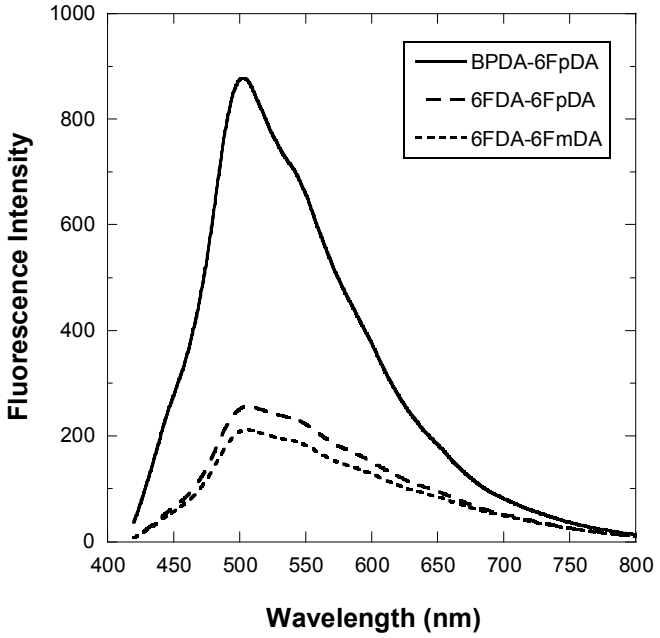

Figure 7.4: Fluorescence spectra of the polyimides

In order to confirm the measured permeabilities of the BPDA-6FpDA polymer, a sample from an aged cast film (ie not an aged masked film) was masked and examined through gas permeation. Table 7.4 presents the results of these two films and confirms the atypical CO_2 response of the aged BPDA-6FpDA polymer.

Table 7.4: Gas permeability comparison of two different aged BPDA-6FpDA films

Sample	CO_2 (Barrers)	O_2 (Barrers)	N_2 (Barrers)	CH_4 (Barrers)
Aged Masked Film	24.0 ± 0.2	4.7 ± 0.1	0.84 ± 0.02	0.50 ± 0.02
Aged Cast Film	23.5 ± 0.3	4.6 ± 0.1	0.82 ± 0.02	0.48 ± 0.01

A possible explanation for this small reduction in CO_2 permeability can be found in the distribution of free volume of this polymer. As the polymer ages, the narrowing of the free volume distribution may be more drastic with the larger free volume packet sizes. Therefore, the free volume accessible to CO_2 may experience a much smaller change than the larger gas molecules, as demonstrated in Figure 7.5. This is clearly a speculation, but it appears to explain the observed trends in the data. Modeling of the aging process might probe and test this speculative explanation.

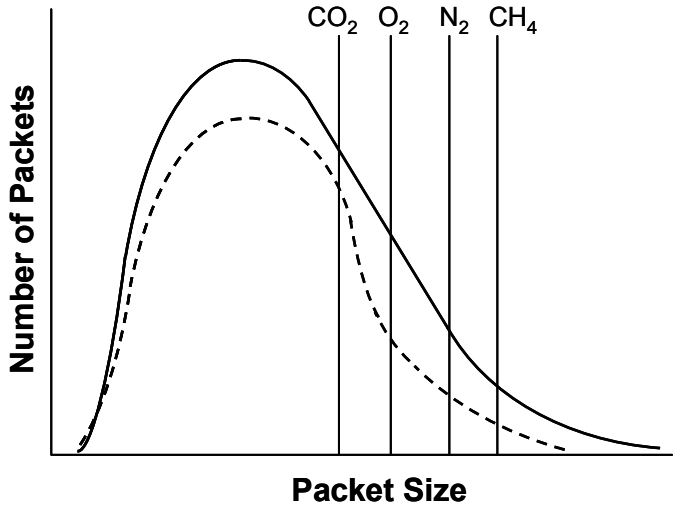

Figure 7.5: Possible change in free volume distribution of BPDA-6FpDA: original film (—) and aged film (---)

Table 7.5 presents the corresponding selectivity enhancements resulting from physical aging. Since a likely result of physical aging is a narrowing of the free volume distribution, a lower fractional free volume polymer will have greater relative changes in available excess free volume between gas pairs which results in relatively higher selectivities than a higher fractional free volume polymer of similar structure. This phenomenon is observed in the following table where the BPDA-6FpDA polymer exhibits

larger increases in selectivity than 6FDA-6FpDA. The significantly larger CO_2/CH_4 selectivity for BPDA-6FpDA is a result of the small reduction in CO_2 permeability of this polymer discussed above.

Table 7.5: Percent increase of selectivities of aged polymers: dianhydride comparison. All uncertainties are less than 0.01%.

Polymer	CO_2/CH_4	O_2/N_2	N_2/CH_4
6FDA-6FpDA	5.6%	0.97%	3.8%
BPDA-6FpDA	32.5%	1.08%	6.3%

7.3.2 Diamine Comparison

The structural difference between the 6FpDA and 6FmDA diamines is the position of the phenylene linkage of the diamine to the dianhydride, para vs meta. 6FDA-6FmDA is known to have a more tightly packed chain density as shown by the lower d-spacing value and fractional free volume than 6FDA-6FpDA [6]. For this reason, the 6FDA-6FmDA isomer has significantly lower gas permeabilities and higher gas selectivities. Surprisingly, the 6FDA-6FmDA isomer has a lower T_G than 6FDA-6FpDA, which would suggest higher gas permeabilities due to enhanced polymer segmental mobility; however, many studies have concluded that no correlation exists between gas permeabilities and the glass transition temperature [2,7-11].

Table 7.6 presents the relative reductions in gas permeability for the polyimide isomers, 6FDA-6FpDa and 6FDA-6FmDA. In this case, there is a larger reduction in permeability for all gases in the 6FDA-6FpDA polymer than 6FDA-6FmDA. Therefore, as expected, physical aging of the higher fractional free volume isomer with the para

conformation causes greater reductions in excess free volume than the meta conformation. As with the dianhydride comparison, the relative reductions in gas permeability scales with penetrant size.

Table 7.6: Percent reduction of gas permeabilities of aged polymers: diamine comparison

Polymer	CO_2	O_2	N_2	CH_4
6FDA-6FpDA	23.1% ± 0.3	23.6% ± 0.3	24.4% ± 0.3	27.1% ± 0.3
6FDA-6FmDA	14.1% ± 0.8	16.7% ± 1.0	18.5% ± 1.1	22.6% ± 1.5

Similar to the dianhydride comparison discussed above, the lower fractional free volume polymer should exhibit larger relative increases in gas selectivity. In this case, 6FDA-6FmDA exhibits relative selectivity enhancements approximately twice that of 6FDA-6FpDA.

Table 7.7: Percent increase of selectivities of aged polymers: diamine comparison. All uncertainties are less than 0.01%.

Polymer	CO_2/CH_4	O_2/N_2	N_2/CH_4
6FDA-6FpDA	5.6%	0.97%	3.8%
6FDA-6FmDA	10.9%	2.22%	5.2%

7.4 Effects of Physical Aging on Gas Sorption

Following gas permeation measurements, the polymer samples were removed from the permeation masks and examined through gravimetric sorption. Therefore, all aged sorption measurements for each polymer have been conducted on the same sample as permeation. These sorption isotherms, presented in Figures 7.6 - 7.8, coupled with the gas permeabilities will then reveal the effects of physical aging on the kinetic and thermodynamic contributions to gas permeation using Equation 2.7. The CO_2 sorption isotherms for all polymers exhibit little change in the aged measurements as compared to the original measurements. Surprisingly, in the lower fractional free volume polymers, the N_2 and CH_4 isotherms of the aged polymer are actually enhanced compared to the original measurements. The N_2 and CH_4 isotherms for the aged 6FDA-6FpDA exhibit little change. These results are counter to previous work which found physical aging to reduce the overall sorption capacity of another polyimide [12]. It is believed that the 10 atm of CO_2 exposure and subsequent depressurization, albeit a slow one, for the CO_2 permeability measurement prior to the sorption measurements "puffed up" the polymer structure and reversed the effects of physical aging.

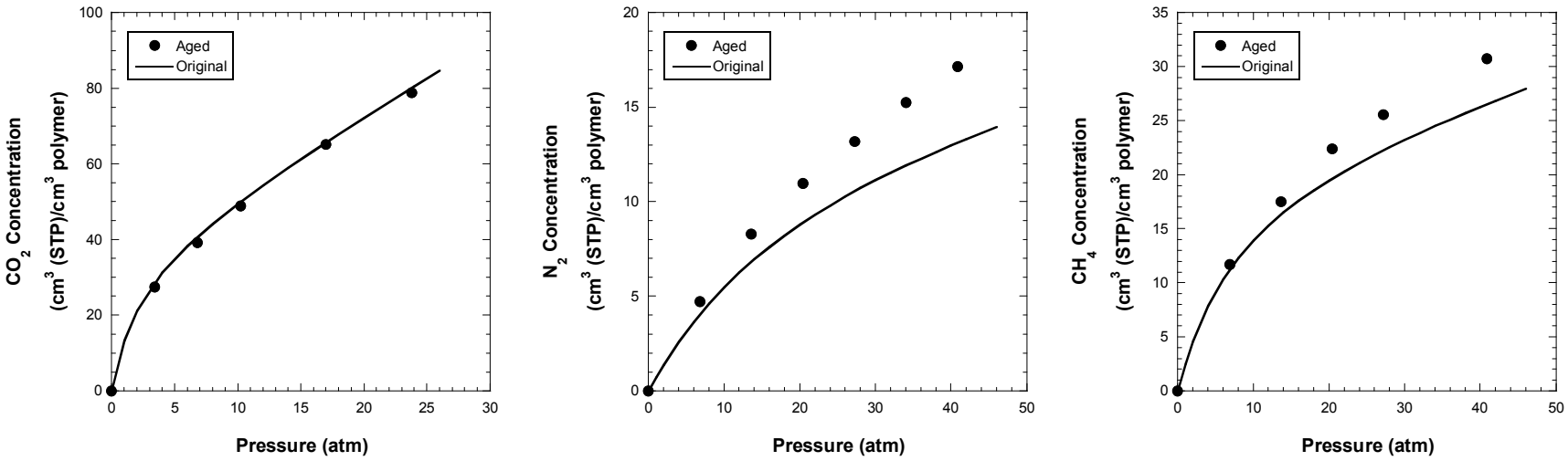

Figure 7.6: Sorption isotherms of the aged and original BPDA-6FpDA polymer conducted at 35 ^{o}C [2]
*Note – Enhanced sorption of aged film caused by CO_2 exposure during permeation measurements

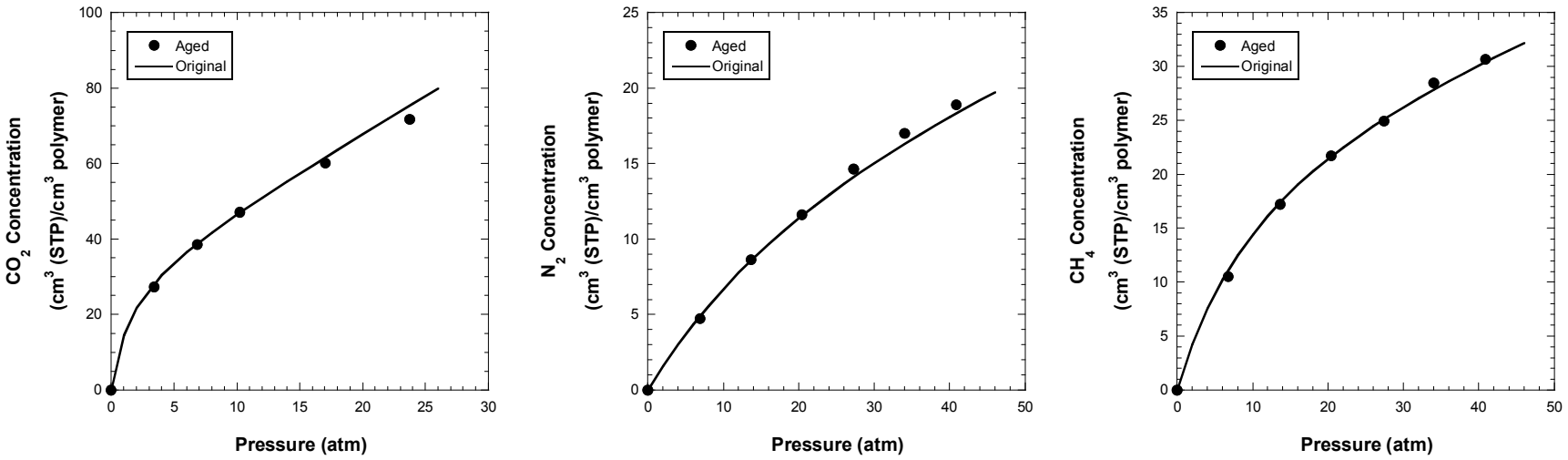

Figure 7.7: Sorption isotherms of the aged and original 6FDA-6FpDA polymer conducted at 35 ^{o}C [2]
*Note – Enhanced sorption of aged film caused by CO_2 exposure during permeation measurements

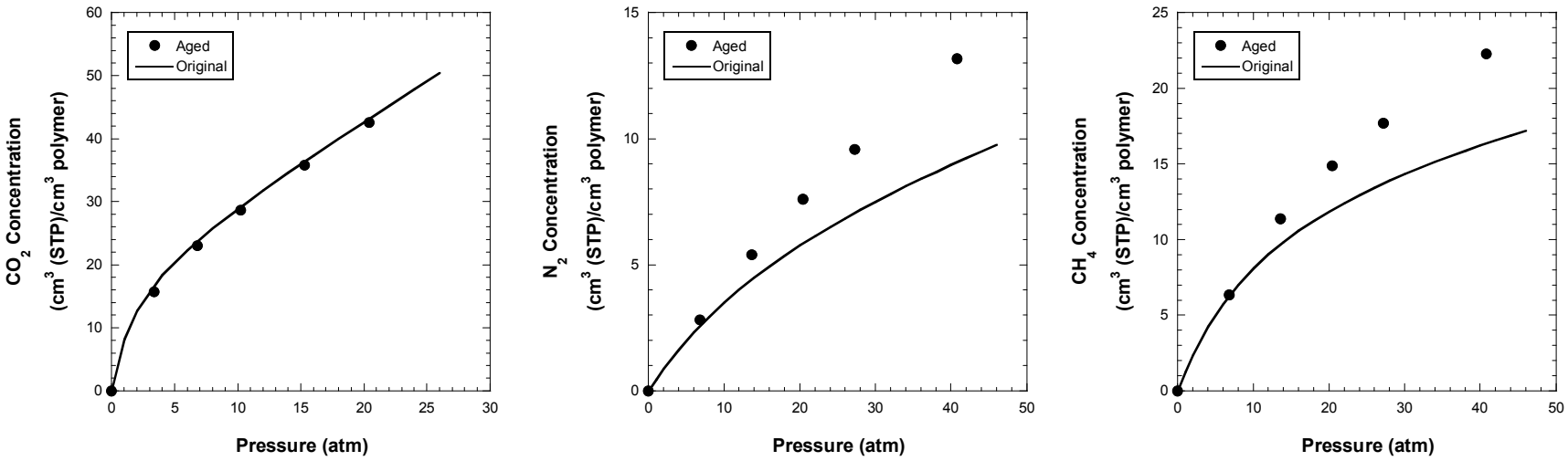

Figure 7.8: Sorption isotherms of the aged and original 6FDA-6FmDA polymer conducted at 35 ^oC [2]
*Note – Enhanced sorption of aged film caused by CO_2 exposure during permeation measurements

To test this hypothesis, aged polymer from the same film was needed that was not exposed to CO_2 during gas permeation measurements. Therefore, it was attempted to retrieve pieces of the film that were sandwiched between the aluminum tape mask; however, it was not possible to separate the aluminum tape mask and the adhesive from the polymer without damaging the polymer beyond the point of use. In another effort to determine the effect of CO_2 exposure on these polymer films, the 6FDA-6FpDA film used for sorption was remasked and re-examined through gas permeation, as shown in Figure 7.9. The permeability and selectivity uncertainties for the "Aged" and "Post CO_2 Exposure" data are smaller than the actual data point.

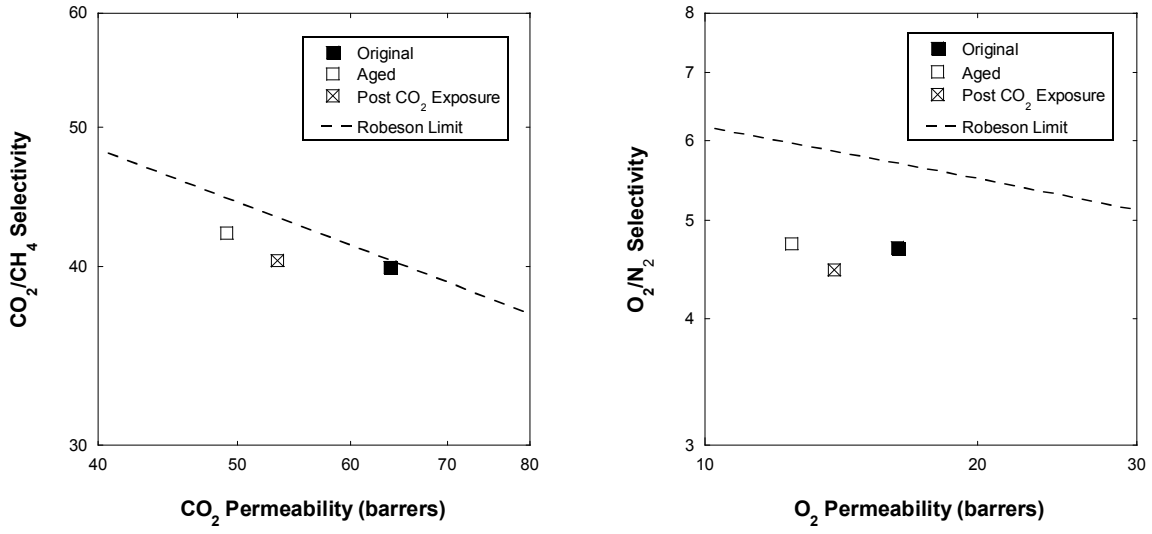

Figure 7.9: CO_2 exposure response to the aged 6FDA-6FpDA polymer film

Unfortunately, these results show that CO_2 permeation at 10 atm altered the state of the aged film and essentially reversed the effects of physical aging. CO_2 exposure also appears to have a greater effect on the slow gas permeability as evident by the substantial decreases in selectivity. Therefore, the sorption isotherms measured on the

permeation films can not be used to determine changes in the diffusion and sorption coefficients resulting from physical aging.

7.5 Summary

Density measurements along with the corresponding fractional free volumes reveal the effects of physical aging on fluorine-containing polyimides. As expected, the relative change in fractional free volume scaled with the original amount of free volume present in the polymer. Following approximately 18 years of physical aging under ambient conditions, the changes in fractional free volume of 6FDA-6FpDA, BPDA-6FpDA, and 6FDA-6FmDA are 4.7%, 2.9%, and 1.8% respectively.

Gas permeation results show an expected general decrease in permeability coupled with an increase in selectivity. Contrary to the relative changes in fractional free volume, BPDA-6FpDA actually exhibits larger reductions in gas permeability than 6FDA-6FpDA. A significant increase in the fluorescence intensity of this polymer suggests the higher charge transfer density plays a role in further reducing chain mobility and gas permeability. Permeation results comparing the 6FDA-based isomers confirm a typical aging response in that the lower fractional free volume polymer exhibits smaller relative changes in permeability and larger relative changes in selectivity.

Sorption isotherms were measured on the same films in which gas permeation measurements were performed to determine the effects of physical aging on the diffusion coefficients. However, CO_2 exposure during the permeation test along with the subsequent depressurization reversed the effects of physical aging.

7.6 References

1. Van Krevelen, D. W., *Properties of Polymers*, Amsterdam: Elsevier (1990).
2. Coleman, Maria, *Isomers of Fluorine-Containing Polyimides For Gas Separation Membranes*, Dissertation, University of Texas-Austin (1992).
3. Robeson, L. M., "Correlation of separation factor versus permeability for polymeric membranes", *Journal of Membrane Science*, **62**(2), 165-185 (1991).
4. Lokhandwala, Kaaeid A., et al., "Nitrogen removal from natural gas using membranes", NETL, 1997 Conference Proceedings, Session 8.2.
5. Vu, De, *Formation and Characterization of Asymmetric Carbon Molecular Sieve and Mixed Matrix Membranes for Natural Gas Purification*, Dissertation, University of Texas-Austin (2001).
6. Fuhrman, C., et al., "Effect of thermal hysteresis on the gas permeation properties of 6FDA-based polyimides", *Journal of Applied Polymer Science*, **91**(2), 1174-1182 (2004).
7. Aitken, C. L., et al., "Effect of structural symmetry on gas transport properties of polysulfones", *Macromolecules*, **25**(13), 3424-3434 (1992).
8. Aitken, C. L., et al., "Gas transport properties of biphenyl polysulfones", *Macromolecules*, **25**(14), 3651-3658 (1992).
9. McHattie, J. S., et al., "Gas-transport properties of polysulfones – 1. Role of symmetry of methyl-group placement on bisphenol rings", *Polymer*, **32**(5), 840-850 (1991).
10. McHattie, J. S., et al., "Gas-transport properties of polysulfones – 2. Effect of bisphenol connector groups", *Polymer*, **32**(14), 2618-2625 (1991).

11. McHattie, J. S., et al., “Gas-transport properties of polysulfones – 3. Comparison of tetramethyl-substituted bisphenols”, *Polymer*, **33**(8), 1701-1711 (1992).

12. Punsalan, D. & Koros, W. J., “Thickness-dependent sorption and effects of physical aging in a polyimide sample”, *Journal of Applied Polymer Science*, **96**(4), 1115-1121 (2005).

8.0 SUMMARY & RECOMMENDATIONS FOR FUTURE WORK

8.1 Summary

The primary goal of this research was to study the effects of sample dimension and covalent crosslinking on physical aging of a state-of-the-art polyimide membrane for natural gas purification. Crosslinkable derivatives of the 6FDA-DAM:DABA (2:1) polyimide were prepared with a small (ethylene glycol) and large, rigid (1,4-benzenedimethanol) crosslinking agents. These crosslinked polymers along with the "noncrosslinkable" precursor (free acid) were annealed above T_G to erase the thermal history of the film and create a common starting point for the physical aging studies. During the high-temperature anneal above T_G, the free acid polymer was found to undergo a decarboxylation reaction that resulted in a crosslinked polymer. Therefore, the physical aging studies of the thick films (50 um) and thin films (600-700 nm) of these polymers actually examines two crosslinked polymers through glycol esterification of the carboxylic acid sites and a crosslinked polymer resulting from decarboxylation of the acid sites.

Physical aging of these crosslinked polymers was primarily probed through gas permeation measurements at low pressure. Thick film gas permeabilities declined between 6% and 24%, depending on the gas, coupled with a 10% increase in the CO_2/CH_4 selectivity and a 20% increase in the He/CH_4 selectivity over 1000 hours of physical aging. Thin film gas permeabilities declined between 70% and 87% with corresponding selectivity enhancements of 25% and 130% for CO_2/CH_4 and He/CH_4 over 1000 hours of physical aging. Surprisingly, there was very little difference in the rates of physical aging for the three crosslinked polymers, even in the thin films which

experience these large reductions in gas permeability. Comparison of the thick film and thin film physical aging responses through gas permeation revealed physical aging to be a complex process involving both lattice contraction and diffusion of free volume. The formation of charge transfer complexes throughout the aging process also indicated that these complexes may contribute to physical aging and facilitate the reduction in gas permeabilities and corresponding enhancement in gas selectivities. CO_2 sorption of the free acid thin films enabled determination of the effects of physical aging on gas solubility and diffusivity in the polymer. Over 1000 hours of aging, CO_2 uptake only decreased 6%; whereas, the CO_2 diffusion coefficient decreased by nearly an order of magnitude from $2x10^{-7}$ cm^2/s to $3x10^{-8}$ cm^2/s. Refractive index measurements of the thin films to monitor the effects of physical aging on the fractional free volume present in the polymer confirm the removal of excess free volume; however, the Free Volume model results yielded unusually high values for the model constants, A and B. Finally, wide angle X-ray diffraction measurements of aged thick films exhibited larger d-spacing values for the aged films indicating the use of this technique to monitor physical aging to be invalid.

When annealed above T_G, the free acid polymer becomes insoluble in all solvents used in this work, even boiling NMP, and exhibits excellent plasticization resistance in CO_2 up to 700 psia. These responses indicate a high degree of crosslinking has occurred in the polymer; however, this free acid polymer does not contain a diol crosslinking agent. Fluorescence spectroscopy measurements of annealed 6FDA-DAM:DABA (2:1) and 6FDA-DAM polymers revealed formation of charge transfer complexes in both polymers; however, the 6FDA-DAM polymer remained soluble in THF and NMP following rapid quench from above T_G. Therefore, charge transfer complexes, which have been shown to stabilize polyimides as a sort of physical crosslink, are not responsible for the polymer insolubility. Furthermore, this test

revealed the DABA moiety to be the cause for these unusual responses when annealed above T_G. To eliminate the possibility of small chain oligomers present in the bulk polymer from forming crosslinks across the imide, a batch of the free acid polymer was placed in a near-theta solvent to dissolve the low molecular weight material. The remaining high molecular weight material was thermally treated above T_G and still exhibited the crosslinked nature discussed earlier. TGA-IR measurements confirmed decomposition of the free acid polymer does not occur until ~470 ^oC, well above the 390 ^oC annealing temperature. However, this measurement illuminated a small mass loss that occurs at 360 ^oC which corresponds to decarboxylation of the DABA carboxylic acid. Further TGA-IR measurements confirm the release of CO_2 at this temperature and a mass loss just below that of the theoretical limit for complete decarboxylation. C-NMR measurements confirm the loss of C=O carbons from the polymer structure. Decarboxylation of the acid yields a free radical phenyl group that attacks other portions of the polymer backbone to form a fully crosslinked polymer. Multiple crosslinking sites are proposed. Therefore, at temperatures just below the T_G of the 6FDA-DAM:DABA (2:1) polymer, this polymer undergoes a thermally induced decarboxylation reaction which results in a crosslinked polymer. This type of crosslinking has the potential to be much more stable in aggressive separations than the esterification crosslinking process.

The uncrosslinked free acid, ethylene glycol crosslinked, and 1,4-benzenedimethanol crosslinked polymers were conditioned using supercritical CO_2. The free acid polymer exhibited a significant reduction in CO_2 permeability at 1500 psia which resulted in reduced CO_2 permeabilities upon depressurization. Upon repressurization, CO_2 permeabilities were significantly lower than during pressurization which suggests a possible structural rearrangement occurred as a result of the large uptake of CO_2 coupled with high hydrostatic pressure. This structural rearrangement is confirmed with CO_2/CH_4 mixed gas permeability measurements which show more than

50% reduction gas permeabilities at 720 psia and a nearly 10% enhancement in the separation factor. Corresponding sorption measurements with supercritical CO_2 do not exhibit this structural rearrangement which is likely a result of the differences in the CO_2 concentration gradient between gas permeation and sorption. Sorption and dilation measurements are used to determine an average partial molar volume of CO_2 of 26.6 cm^3/mol in the free acid polymer which, when used in the Dual Mode dilation model, reasonably models the dilation measurements.

Supercritical CO_2 conditioning of the crosslinked polymers yields an expected response at 1500 psia with slightly increasing permeabilities over time. Upon depressurization, a typical hysteretical response is observed in which CO_2 permeabilities remain higher than the corresponding pressurization permeabilities. The stability of the crosslinked polymers is observed in the CO_2/CH_4 mixed gas permeability measurements which exhibit smaller changes in permeability while maintaining the separation factor prior to supercritical CO_2 exposure. Corresponding sorption measurements, coupled with the permeation measurements, show that conditioning in CO_2 actually increases the diffusion coefficient of crosslink stabilized polymers even at pressures below the plasticization pressure. The average partial molar volumes of CO_2 in the ethylene glycol crosslinked and 1,4-benzenedimethanol crosslinked polymers are 29.6 and 28.9 cm^3/mol respectively. The Dual Mode dilation model using these values reasonably models the dilation measurements at low pressures. Interestingly, the dilation responses deviate from linearity at higher pressures indicating additional swelling, even though the separating efficiency is maintained. For the purposes of natural gas purification, the crosslinked polymers are more stable, productive, and efficient following supercritical CO_2 conditioning than the free acid polymer.

Physical aging of the fluorine-containing polyimides was characterized through density and gas permeation and sorption measurements. Comparison of the BPDA and

6FDA dianhydrides revealed that the lower fractional free volume polymer, BPDA-6FpDA, actually exhibited larger relative reductions in gas permeability as a result of physical aging. This response can be explained through the significant increase in charge transfer density compared to the aged 6FDA-6FpDA polymer which further reduces polymer chain mobility. As expected with a lower fractional free volume polymer, the aged BPDA-6FpDA polymer exhibited larger relative increases in gas selectivity. Comparison of the diamine isomers yielded the expected results. The lower free volume meta conformation exhibited smaller relative reductions in gas permeability with larger relative increases in gas selectivity. Corresponding sorption measurements were not useful for the determination of diffusion and sorption coefficients due to the conditioning effect of CO_2 exposure on the polymer films.

8.2 Recommendations for Future Work

The crosslinking chemistry used in this work results in ester linkages through the carboxylic acid on the DABA diamine. These esters can potentially be hydrolyzed in aggressive feed streams, thus eliminating the added stability of crosslinking. The discovering of the thermally induced crosslinking in the free acid polymer, which yields a covalently crosslinked polymer absent of these vulnerable ester linkages, opens many avenues of further research.

First and foremost, the decarboxylation crosslinking mechanism needs to be fully characterized. Solid-state proton NMR can be a useful tool to determine which part of the polymer is being attacked by the phenyl radical created through decarboxylation of the DABA group. Also, the thermally induced crosslinked polymer should be characterized through gas permeation and sorption to reveal the full potential of this new crosslinking mechanism.

Asymmetric hollow fiber membranes are the morphology and form of choice for most gas separations. However, the hydrophilic nature of the 6FDA-DAM:DABA (2:1) free acid polymer makes spinning defect-free hollow fibers difficult. In order to utilize this new crosslinking method, a process needs to be developed to spin the free acid polymer into non-defective asymmetric hollow fibers. Also, previous work found that esterified crosslinked hollow fiber membranes tend to lose their separating efficiency when annealed at temperatures above 200 ^{o}C [1]. When annealed to temperatures above 250 ^{o}C, the asymmetric morphology of the hollow fiber begins to break down and the fiber becomes defective. Therefore, once free acid hollow fibers have been spun, the effects of high temperature annealing on the fiber substructure and selective layer should be examined. If high temperature annealing of the hollow fibers proves detrimental for gas separations, a low temperature pathway for decarboxylation needs to be explored in order to preserve the delicate morphology of the hollow fibers.

Finally, in order to characterize the esterified crosslinked and decarboxylated crosslinked polymers for “real world” applications, hollow fiber membranes should be examined using a variety of feed streams. A CH_4/CO_2 mixed gas feed with small concentrations of condensable hydrocarbons can be used to probe the membrane’s robustness in the presence of contaminants. Also, a high CO_2 concentration mixture of CH_4/CO_2 with pressures allowing the CO_2 to reach the supercritical state will allow characterization of these membranes for use in enhanced gas recovery processes.

8.3 References

1. Wallace, David, *Crosslinked Hollow Fiber Membranes for Natural Gas Purification and Their Manufacture from Novel Polymers*, Dissertation, University of Texas-Austin (2004).

APPENDIX A: REFRACTIVE INDEX MEASUREMENTS IN THIN FILMS

As a means of confirming the removal of free volume and subsequent densification of the thin films as a result of physical aging, refractive index measurements were taken over time on prepared samples. These samples were prepared in the same manner as the samples used for fluorescence spectroscopy measurements in Chapter 4.4.6. A 3mm x 3mm area was marked off for consistent measurements of the film. The refractive index of glassy polymers has been shown to be dependent on the relative humidity of the sample environment [1]. Therefore, a controlled-environment chamber was purged with N_2 until the relative humidity reached 5.0% before each measurement was taken. Two or three measurements were taken at each aging time, and the sample was removed from the chamber and replaced to measure the same marked spot between each measurement. The windows of the control chamber were taken into account during the sample analysis by calibrating the delta offset parameters using a known sample and fixing the offsets at the calibrated values for subsequent analysis. The measurements were taken in the spectral range of 400 to 900 nm, with the refractive index determined at 632 nm. Further details of the measurements can be found elsewhere [2].

In order to use the Free Volume model presented in Chapter 2.4, thick film densities and refractive indices are required to first determine the material constant of the Lorentz-Lorenz relationship in Equation 2.14. The rapidly quenched thick film densities were determined from three different samples using the density gradient column, and the refractive indices were determined from three measurements on each

thick film sample using the prism coupler. The refractive indices from the prism coupler were determined at a wavelength of 632 nm as well. The following table presents the average value results of these measurements.

Table A.1: Densities and refractive indices of rapidly quenched thick films

Polymer Film	Density (g/cm^3)	Refractive Index
Free Acid	1.3707	1.5501
Ethylene Glycol Crosslinked	1.3716	1.5510
1,4-Benzenedimethanol Crosslinked	1.3685	1.5530

Figures A.1 and A.2 display the refractive indices and corresponding fractional free volumes of the free acid, ethylene glycol crosslinked, and 1,4-benzenedimethanol crosslinked thin films as functions of aging time. To determine the fractional free volume of each film, the density was determined using the Lorentz-Lorenz relationship and the occupied volumes of the free acid and crosslinked derivatives were determined using a group contribution method [3]. It should be noted that achieving reproducible and consistent data, even in a controlled environment, was difficult, as demonstrated by the scatter in the ethylene glycol and 1,4-benzenedimethanol crosslinked films. Also, the rate of change of the free acid polymer is significantly lower than that reported in literature [4].

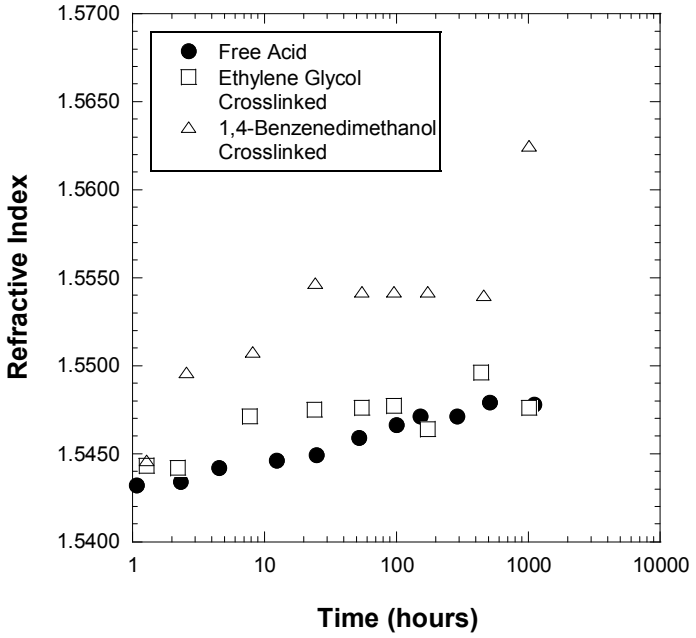

Figure A.0.1: Refractive index measurements of the free acid (680 nm), ethylene glycol crosslinked (590 nm), and 1,4-benzenedimethanol crosslinked (670 nm) thin films

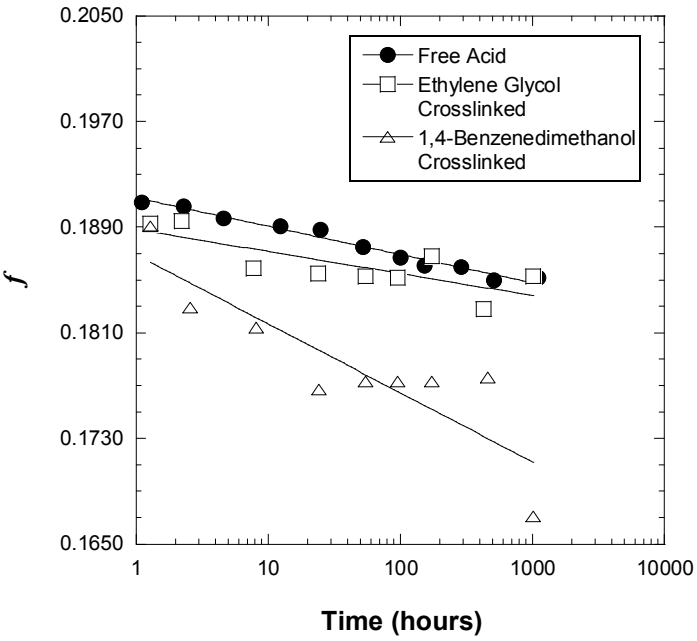

Figure A.0.2: Fractional free volume of the thin films as determined by refractive index measurements. Lines are to guide the eye.

As expected with physical aging, the refractive indices gradually increase over time as the removal of excess free volume enhances polymer chain packing and increases the density of the film. This density increase then corresponds to a reduction in the fractional free volume of the thin film as shown in Figure A.2. However, as mentioned earlier, even though each data point is an average of two, or in most cases, three data points, there is still a considerable amount of scatter associated with this measurement technique that is not present in comparable measurements in literature [4,5].

Of the three data sets presented above, only the free acid data set proves useful for modeling with the Free Volume model; therefore, all subsequent analysis is only performed using the free acid refractive indices. The change in fractional free volume with aging time enables use of the Free Volume model to determine the relationship between gas permeability and fractional free volume of the polymer. Since the refractive index and permeability data were collected at different times, the fractional free volume data was interpolated to aging times that match the permeation data in Figure 4.13. Figure A.3 displays a representative plot for CH_4 of the natural log of the permeability coefficient vs the inverse of the fractional free volume. The Free Volume model constants, A and B, can then be determined from the slope and intercept of plotted data.

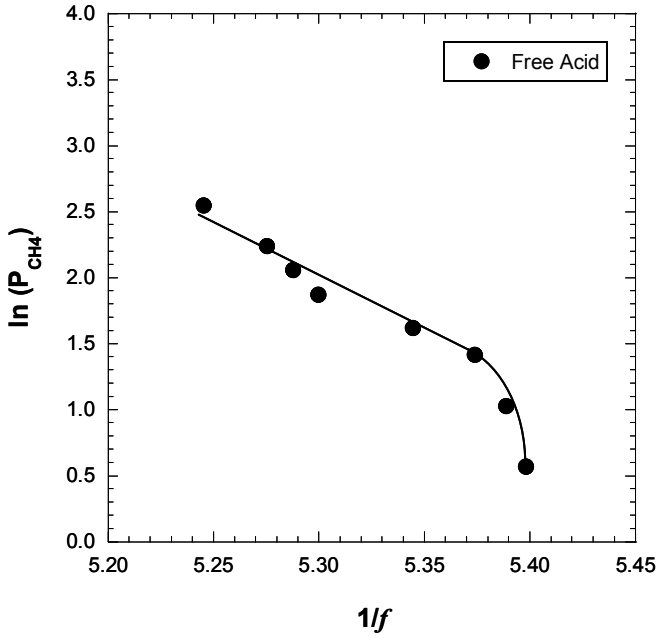

Figure A.0.3: Free Volume model determination of CH_4 constants for the free acid thin film. Lines are to guide the eye.

Interestingly, the trend for the free acid film deviates from linearity at higher $1/f$ values, which corresponds to longer aging times. This response mirrors the slight enhancement observed in the He/CH_4 selectivities which results from either charge transfer complexing or changes in the free volume distribution discussed in Chapter 4.4.6. The Free Volume model parameters, presented in Table A.2, are determined using the lower $1/f$ values and exclude the final two values from each film that deviate from linearity at higher $1/f$ values.

Table A.2: Values for the Free Volume model parameters for the free acid thin film. Parameter 'A' has units of Barrers.

Gas	A	B
CO_2	2.5×10^{20}	7.8
CH_4	5.9×10^{20}	8.6
He	7.6×10^{13}	5.0

There are several issues that need to be addressed in the above data analysis. First, small changes in the rate of change of the refractive index measurements can have a large impact in determining the order of magnitude of the Free Volume model parameters. Therefore, any errors associated with the refractive index measurements are greatly magnified in the Free Volume model analysis. Also, there is an enormous range for the Free Volume model parameters as reported in literature. For polyimides, an example of this is the N_2 parameter values which range from 101 to 4.7×10^{18} (A) and 0.624 to 7.15 (B) [4,6,7]. Consequently, the determined Free Volume model parameters are not good indicators for comparing the effect of free volume on gas permeability between different studies.

As a check to determine if annealing the polymer films above T_G is responsible for the inconsistent data, refractive indices of "as-spun" films were monitored over time. In this case, a thin free acid film was spun onto a wafer and time zero was taken to be the time of spinning; therefore, the films did not receive any high-temperature thermal treatment. In addition to this, one sample was removed as a free standing film and replaced onto a silicon wafer for measurements; whereas, the second sample is the original "as-spun" film on the wafer to determine if film removal played a role in the inconsistent data. Figure A.4 presents the results from these measurements.

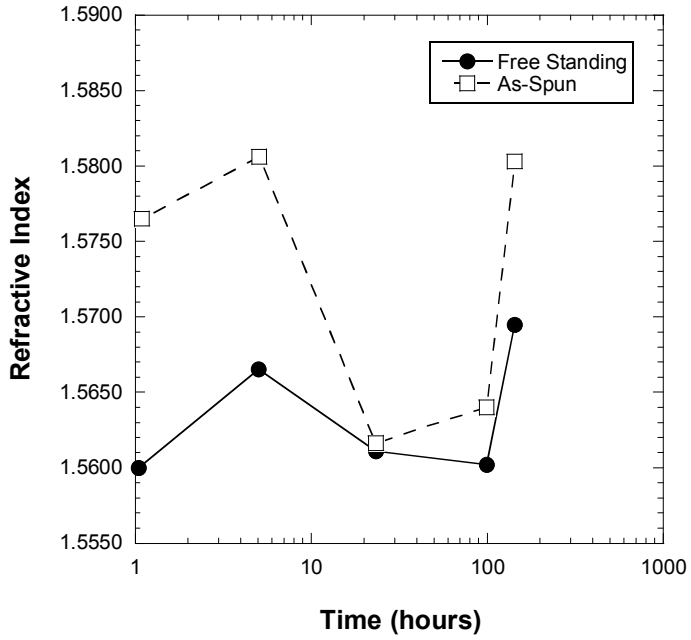

Figure A.4: Refractive indices for the free acid polymer without annealing above T_G

The first data points can be disregarded due to remaining solvent that is most likely present in the film. Storage at 35 ^{o}C and vacuum should have completely removed the cyclohexanone solvent for all subsequent measurements. Even though the data is still quite inconsistent, there is a general trend between the two samples. This data indicates that standard spectroscopic ellipsometer measurements need to be taken on a known, unchanging sample over a minimum of 1000 hours to determine if the instrument is the cause of these data fluctuations.

Due to the inconsistent data within each set and the difficulty in achieving reproducible data, monitoring the free volume state of thin polymer films through changes in refractive index has not proven to be useful in this work.

References

1. Rowe, B. W., et al., “Effect of sorbed water and temperature on the optical properties and density of thin glassy polymer films on a silicon substrate”, *Macromolecules*, **40**(8), 2806-2813 (2007).
2. Huang, Y. & Paul, D. R., “Experimental methods for tracking physical aging of thin glassy polymer films by gas permeation”, *Journal of Membrane Science*, **244**(1-2), 167-178 (2004).
3. Park, J. Y. & Paul, D. R., "Correlation and prediction of gas permeability in glassy polymer membrane materials via a modified free volume based group contribution method", *Journal of Membrane Science*, **125**(1), 23-39 (1997).
4. Kim, J. H., et al., “Physical aging of thin 6FDA-based polyimide membranes containing carboxyl acid groups. Part 1. Optical properties”, *Polymer*, **47**(9), 3104-3111 (2006).
5. Huang, Y. & Paul, D. R., “Physical aging of thin glassy polymer films monitored by optical properties”, *Macromolecules*, **39**(4), 1554-1559 (2006).
6. Huang, Y., et al., “Physical aging of thin glassy polymer films: Free volume interpretation”, *Journal of Membrane Science*, **277**(1-2), 219-229 (2006).
7. Miyata, S., et al., “Relationship between gas transport properties and fractional free volume determined from dielectric constant in polyimide films containing the hexafluoroisopropylidene group”, *Journal of Applied Polymer Science*, **107**, 3933-3944 (2007).

APPENDIX B: DETERMINATION OF THE PARTIAL MOLAR VOLUME

The thermodynamic definition of the partial molar volume of a penetrant in a polymer is [1]:

$$\bar{v}_1 = \left.\frac{\partial V}{\partial n_1}\right|_{T,p,n_2}$$

V is the total volume of the system, n is the number of moles of a species, and 1 and 2 refer to the penetrant and polymer. After converting to a mass-based relationship, this expression can be rearranged to give the following expression:

$$\bar{\nu}_1 = \nu_T + (1-\omega_1)\left[\left.\frac{\partial \nu_T}{\partial \omega_1}\right|_T + \nu_T \beta \left.\frac{\partial p}{\partial \omega_1}\right|_T\right]$$

ν_T is the total specific volume of the system, ϖ_1 is the weight fraction of the penetrant in the polymer, and β is the isothermal compressibility. The second term in the brackets can be neglected due to the rigidity of the polymers in this study [2]. The partial specific volume of the penetrant, ν_1, can then be converted to the partial molar volume through the following expression where MW_1 is the molecular weight of the penetrant:

$$\bar{v}_1 = \bar{\nu}_1 * MW_1$$

References

8. Prausnitz, J. M., Lichtenthaler, R. N., de Azevedo, E. G., *Molecular Thermodynamics of Fluid-Phase Equilibria*, New Jersey: Prentice Hall PTR (1999).
9. Punsalan, David, *A Sorption and Dilation Investigation of Amorphous Glassy Polymers and Physical Aging*, Disseration, University of Texas-Austin (2001).

VITA

Adam Michal Kratochvil was born on November 4, 1978 to Gary and Linda Kratochvil in Killeen, Texas. He graduated from Clear Lake High School in Houston, Texas in 1996. In December of 2000, he received his Bachelor of Science degree in Chemical Engineering from the University of Texas at Austin. After working for two years in the semiconductor industry, he enrolled in the doctorate program at the Georgia Institute of Technology under the supervision of Dr. William J. Koros. In April 2008, he fulfilled the requirements for a Doctorate of Philosophy in Chemical & Biomolecular Engineering. Following graduation, he started working for Air Products and Chemicals, Inc. in St. Louis, Missouri.

Permanent Address: 243 W. Woodbine Ave

St. Louis, MO 63122